HOLOGRAPHY FOR THE PRACTICAL PERSON

BY

BRANDON W. LANGLEY

DISSERTATION

Submitted in partial fulfillment of the requirements
for the degree of Doctor of Philosophy in Physics
in the Graduate College of the
University of Illinois at Urbana-Champaign, 2019

Urbana, Illinois

Doctoral Committee:

Assistant Professor Thomas Faulkner, Committee Chair
Professor Philip W. Phillips, Director of Research
Professor Peter Abbamonte
Professor Lance Cooper

Abstract

This article opens with a pedagogical discussion of holography aimed at calculating the thermodynamics and transport coefficients in condensed matter systems. Therein, we will discuss the duality of thermodynamics to classical field theory, construct the associated dual action at the field theory's boundary, and divulge the numerical techniques of the Einstein-DeTurck equations. The latter allows a numerical treatment of linear response theory in highly nontrivial gravitational backgrounds. We will use these techniques in the analysis of two major problems. In the first, we will discuss the specific implementation of the numerical methodology in the exploration of holographic lattices. Particularly, we construct generalizations of AdS-Reissner-Nordström that interpolate between those used in two previous studies — one that reports power-law scaling for the mid-frequency regime of the optical conductivity and one that does not. We find no evidence for power-law scaling of the conductivity, thereby corroborating the previous negative result that gravitational crystals are insufficient to generate the power-law mid-infrared conductivity observed in cuprate superconductors. In the second problem, we present the full charge and energy diffusion coefficients for the Einstein-Maxwell dilaton (EMD) action for Lifshitz spacetime characterized by a dynamical critical exponent z. We compute the fully renormalized static Lifshitz thermodynamic potential explicitly, which confirms the forms of all thermodynamic quantities including the Bekenstein-Hawking and Smarr-like relationships. For transport, we target our analysis at finite chemical potential and include axion fields to generate momentum dissipation. Beyond analysis of the bounds, we find deviation from universal transport obtains when either the chemical potential or momentum dissipation are large relative to temperature, an echo of strong thermoelectric interactions. We also find that regardless of what is diffusing, energy or charge, the diffusion constant is independent of matter content when $z = 2$. This state of affairs obtains because the diffusion equation is scale invariant when $z = 2$.

For my mother Marcy Schafler and in memory of my father Scott Langley

Acknowledgements

So begins a voluminous list of people who have made my excursion through graduate school manageable. Unyielding, unbridled love, first and foremost, to my mother Marcy for the endless and unconditional support and love throughout my life. And to my brother Zach, for we have so much to share with each other that our conversations might never end if the world allowed it. To my cousins Matt and Sarah, who are basically my siblings, and my aunt Lorie, for I always look forward to Thanksgiving when you can berate me about still being in grad school. To my late grandparents Joseph and Myrna Schafler, who passed away at the start of my graduate journey but were so unconditionally proud of me.

Incalculable gratitude to my colleagues. To my advisor Philip Phillips, who I wanted to work for the moment I met him. His unorthodox thinking and research directions have allowed me to explore a truly wondrous world of physics that somehow incorporates condensed matter, general relativity, field theory, and string theory if you *really* push it. We may be as disparate as personalities come, and my time in your tutelage has pushed me to grow beyond my comfort zone and I know you are always in my corner. Gratitude to my pseudo-twin Garrett Vanacore, who has served as my brother-in-arms during the most trying times. And to all my past and present groupmates and collaborators Mark Schubel, Zhidong Leong, Kridsanaphong Limtragool, Chandan Setty, Christian Boyd, Luke Yeo, Matteo Baggioli, Gabriele La Nave, and many more.

Immeasurable, unbounded thanks to my friends Carolyn Kan, Zack Dell, Vikyath Rao, Farshid Jafarpour, Judy Chiu, Barbara Stekas, Tanya Perlova, Rezvan Shahoei, Anne Gilot and innumerable others for indulging me and my parasitic interests for half an eternity. And the same to my college friends Rajen Dutta, Stephen Crouch, and Chris Merck; I am extremely grateful we were able to reunite at Raj's wedding. And the same to my long-lasting high school friend Saswato Roy, who checks up on my existence on a (somewhat) regular basis. And to my local Super Smash Bros. community for providing an outlet for me to embarrass my students and introducing me to the world of competitive gaming.

And to thank you to anyone, anywhere who assisted me in my life's journey.

Table of Contents

Notations

- Einstein notation where indices are repeated denote summed contractions, *e.g.*

$$F_{ac}F_b{}^c = \sum_c F_{ac}F_b{}^c$$

- Symmetrized indices: $A_{(a}B_{b)} = \frac{1}{2}\left(A_aB_b + A_bB_a\right)$

- Antisymmetrized indices: $A_{[a}B_{b]} = \frac{1}{2}\left(A_aB_b - A_bB_a\right)$

- p-form[1]: $\omega = \frac{1}{p!}\omega_{a_1\cdots a_p}dx^{a_1}\wedge\cdots\wedge dx^{a_p}$

- Exterior derivative: $d\omega = \frac{1}{p!}\nabla_b\omega_{a_1\cdots a_p}dx^bdx^{a_1}\cdots dx^{a_p}$

- Interior product: $i_\xi\omega = \frac{1}{p!}\xi^b\omega_{ba_1\ldots a_{p-1}}dx^{a_1}\cdots dx^{a_{p-1}}$ fix maybe

- Lie derivative: $\mathcal{L}_\xi\omega = (di_\xi + i_\xi d)\omega$

[1] In general wedge products are presumed and not written.

1 Holography for the Practical Person

1.1 Duality of Semi-classical Field Theory and Thermodynamic Potentials

Holgraphy is a technique borne of string theory and a high-browed conjecture [1], but its skeleton is classical field theory. Holography is generally implemented as a duality in the sense of the AdS/CFT correspondence: a duality between a specific bulk geometry (anti-de Sitter spacetime) to a conformal field theory that exists at the boundary of said bulk [2]. However, this is only a specific implementation of a universal feature of semi-classical field theories. Any field theory where a saddle point approximation is applicable allows a duality between a bulk field theory and an interpretation of a boundary thermodynamic potential. All we really need is to define an action and follow the holographic program, and any features that we choose to include have nontrivial effects in the dual theory than can depend on many details of the bulk geometry.

Consider the partition function for a general field theory,

$$\mathcal{Z} = \int \prod_n \mathcal{D}\phi_n e^{-I[\{\phi_n\}]}, \tag{1.1}$$

where $I[\{\phi_n\}]$ is a (local) action and $\{\phi_n\}$ refers to some collection of fields and their relevant derivatives. Here $\mathcal{M}$ is a $(d_s + 2)$-dimensional Lorentzian manifold which we will define in the next section[1]. Throughout this work we will always assume $\mathcal{M}$ is a Lorentzian manifold. Implicit in Eq. (1.1) is that we have performed a Wick rotation to a Euclidean time.

For the saddle point approximation, consider that all fields in the system take the form

$$\phi_n = \overline{\phi}_n + \delta\phi_n, \tag{1.2}$$

where $\{\overline{\phi}_n\}$ is the set of classical solutions that solve the Euler-Lagrange equations and $\{\delta\phi_n\}$ are small variations about them. A generic variation of

[1] Typically it is convenient in holographic problems to have d_s be the number of spatial dimensions, with the extra two as the time and radial dimensions.

I can be expressed

$$\delta I = \int_{\mathcal{M}} (\text{EOMs}) + \int_{\partial\mathcal{M}} \sum_n \Pi_n^{(\phi)} \delta\phi_n. \tag{1.3}$$

where $\partial\mathcal{M}$ is the (d_s+1)-dimensional boundary of the bulk manifold and $\{\Pi_n^{(\phi)}\}$ the conjugate momenta to $\{\phi_n\}$. By definition, the variation in the bulk action vanishes on-shell where the equations of motion are satisfied, and the only piece to survive is the boundary contribution. This is the "hologram," where a classical approximation to a field theory amounts to a projection onto a one-lower dimensional spacetime.

For a thermodynamic system, the partition function is directly related to the free energy W:

$$\mathcal{Z} = e^{-W/T}. \tag{1.4}$$

If we are working in the saddle point approximation, we arrive at the essential statement of holography:

$$\delta I^{(\text{o.s.})} = \frac{\delta W}{T}. \tag{1.5}$$

As we established, the variation of the action only contributes to the boundary, and thus the surviving boundary term has the interpretation of a fundamental thermodynamic relation,

$$\frac{\delta W}{T} \leftrightarrow \int_{\partial\mathcal{M}} \sum_n \Pi^{(\phi)_n} \delta\phi_n. \tag{1.6}$$

Thus we can establish a *holographic dictionary* between the bulk field quantities $\{\phi_n\}$ and $\{\Pi_n^{(\phi)}\}$ and thermodynamic quantities in W. The variation of W will take on a quite literal description of a fundamental thermodynamic relation like

$$dW = -\mathcal{S}dT - \mathcal{Q}d\mu - JdE + \cdots \tag{1.7}$$

where we have "source" quantities like temperature T, chemical potential μ, electric field E, and so on, and respective "responses" like entropy $\mathcal{S}$, charge $\mathcal{Q}$, current J, and so on. In the most general sense, we will think of the relations

$$\phi_n \leftrightarrow \text{sources}, \quad \Pi_n^{(\phi)} \leftrightarrow \text{responses} \tag{1.8}$$

where the information about the thermodynamic potential is all contained within the classical field solutions. At its core, this is the program of holography. The game is to construct your personal choice of action I and see what thermodynamic potential it generates! In this way, thermodynamic systems

can be constructed that ostensibly can deal with strongly-interacting systems without ever touching a microscopic model; we have all the tools we need to solve for macroscopic quantities. Holographic models exist for a host of condensed matter systems including strange metals [3], superconductors [4], Josephson junctions [5], Mott insulators [6], graphene [7] and innumerable others. Generally, we are looking to observe qualitatively similar features in excitations and phases to map these holographics models by hand to their corresponding condensed matter system.

1.2 General Relativity: a Brief Refresher

Holographic methods are underpinned by general relativity so it is important to keep track of some of the objects and ideas we'll frequently refer to. For a complete overview of general relativity, we refer to Wald [8]. Imagine we have a *Lorentzian manifold* $(\mathcal{M}, g_{ab})$, which is a real, smooth manifold $\mathcal{M}$ which possesses a metric (tensor) g_{ab}. The metric is a fundamental measure of infinitesimal length scales in a spacetime,

$$ds^2 = g_{ab} dx^a \otimes dx^b. \tag{1.9}$$

The distinction of Lorentzian indicates a $(1, D-1)$ signature; one timelike coordinate and $D-1$ spacelike coordinates, such that is locally similar to Minkowski spacetime.[2] As always, we lazy physicists will drop the tensor product $\otimes$ from the notation hereon.

The coordinates x^a in Eq. (1.9) are, of course, arbitrary. They are merely a nonphysical naming scheme to help us keep track of where we are. Coordinates can be freely changed with a transformation matrix of partial derivatives,

$$dx^a = \frac{\partial x^a}{\partial y^b} dy^b. \tag{1.10}$$

Such a transformation is called a *diffeomorphism*. How objects change under diffomorphisms is paramount in general relativity. Essentially, objects that transform "nicely" are known as *tensors*, which merely transform through successive applications of the transformation matrix in Eq. 1.10 or its inverse.[3]

Speaking of a tangled mess, the friendly old partial derivative ∂_a is not so friendly in a curved spacetime. It is not a tensor. It behooves us to introduce

[2]Such manifolds are also called pseudo-Riemannian, reflecting that not all metric components are positive-definite as in a Riemannian manifold.

[3]The official statement is that all indices in a tensor must transform covariantly or contravariantly with a change of basis.

the *covariant derivative*,

$$\begin{aligned}\nabla_c T^{a_1\cdots a_q}_{b_1\cdots b_q} = \partial_c T^{a_1\cdots a_q}_{b_1\cdots b_q} + \Gamma^{a_1}_{cd} T^{d\cdots a_p}_{b_1\cdots b_q} + \cdots + \Gamma^{a_p}_{cd} T^{a_1\cdots d}_{b_1\cdots b_q} \\ - \Gamma^{d}_{cb_1} T^{a_1\cdots a_p}_{d\cdots b_q} - \cdots - \Gamma^{d}_{cb_q} T^{a_1\cdots a_p}_{b_1\cdots d},\end{aligned} \tag{1.11}$$

where the *Levi-Civita connection* Γ^a_{bc} is introduced to ensure (1.11) transforms like a tensor. The Levi-Civita connection is defined,

$$\Gamma^a_{bc} = \frac{1}{2} g^{ad} \left(\partial_b g_{dc} + \partial_c g_{bd} - \partial_d g_{bc} \right), \tag{1.12}$$

which follows if:

1. It is metric compatible: $\nabla_c g_{ab} = 0$,
2. It is torsion-free: $\Gamma^a_{bc} = \Gamma^a_{cb}$ (or $\Gamma^a_{[bc]} = 0$).

Metric compatibility ensures that raising and lowering indices is a tranquil process; raising and lowering operations can just phase through derivatives willy nilly.

Now that we have a usable derivative for curved spacetimes, let us examine the notion of curvature. In particular, we take a look at what happens if we commute covariant derivatives and find

$$[\nabla_b, \nabla_c] T^a = R^a{}_{bcd} T^d, \tag{1.13}$$

$$R^a{}_{bcd} = \partial_c \Gamma^a_{db} - \partial_d \Gamma^a_{cb} + \Gamma^a_{ce} \Gamma^e_{db} - \Gamma^a_{de} \Gamma^e_{cb}, \tag{1.14}$$

where $R^a{}_{bcd}$ is the *Riemann curvature tensor*. You can think of this commutation like taking an infinitesimal two-step stroll, then doubling back but reversing the order of your steps. If the spacetime is curved, in general you will not arrive back at your starting point, but instead some other point that is dependent on just how curved the spacetime you're wading through is. Two contractions of the Riemann tensor are also fundamentally important for us,

$$R_{ab} = R^c{}_{acb}, \quad R = R^a_a, \tag{1.15}$$

the *Ricci tensor* and *Ricci scalar*, respectively.

The Riemann tensor contains a host of symmetries and redundancies which we will not discuss here, except to note it follows a *Bianchi identity*,

$$\nabla_e R_{abcd} + \nabla_c R_{abde} + \nabla_d R_{abec} = 0, \tag{1.16}$$

which implies that the trace-reversed Ricci tensor is conserved,

$$\nabla^a \left(R_{ab} - \frac{1}{2} R g_{ab} \right) = 0. \tag{1.17}$$

This is the very relation that prompted Einstein to postulate his famous equation relating geometry and matter (reference),

$$R_{ab} - \frac{1}{2}Rg_{ab} + \Lambda g_{ab} \propto T_{ab} \tag{1.18}$$

due to the fact the *stress-energy tensor* T_{ab}, a tensor that describes the density and flux of energy and momentum in spacetime, is also conserved,

$$\nabla^a T_{ab} = 0. \tag{1.19}$$

This conservation law is really just the tensor-ized statement of conservation of energy and momentum. This fundamental proposal promotes the metric to being its own dynamical variable complete with its own equation of motion. Here Λ is an arbitrary additive constant called the *cosmological constant*. Einstein considered the necessity of this arbitrary addition a failure of the theory, but it is actually quite a useful quantity as we will later see! These conservation laws will be important for more than a historical perspective and will be necessary for defining a stable and consistent numerical scheme.

The equation of motion Eq. (1.18) can be obtained from a principle of least action formulation, where

$$I = \int_{\mathcal{M}} \sqrt{-g}\,(R - 2\Lambda + \mathcal{L}_{\text{matter}}) \tag{1.20}$$

is the *Einstein-Hilbert action*. The piece $\sqrt{-g}$ is a volume factor where $g = \det g_{ab}$; the volume form $d^D x\sqrt{-g}$ measures an infinitesimal volume of the spacetime and is invariant under diffeomorphisms. This action contains the scalar curvature R as a measure of the kinetics of the geometry and $\mathcal{L}$ for all the matter contained within the system. The stress energy tensor is defined as

$$T_{ab} \equiv -\frac{2}{\sqrt{-g}}\frac{\delta\left(\sqrt{-g}\mathcal{L}_{\text{matter}}\right)}{\delta g^{ab}}. \tag{1.21}$$

For convenience I have done away with the usual Newton constant that defines the proportionality in Eq. (1.18) ($G_N = 1/16\pi$). The conservation of the stress-energy tensor is a consequence that the action I is invariant under diffeomorphisms, hereunto saying a theory is diffeomorphism invariant. This is a property of all constructions because coordinate choices are always arbitrary and should have no physical consequence. A variation of the action under a diffeomorphism is

$$\begin{aligned}\delta_\xi I = 0 &= \int_{\mathcal{M}} \sqrt{-g}\left(R_{ab} - \frac{1}{2}Rg_{ab} + \Lambda g_{ab} - T_{ab}\right)\nabla^a \xi^b \\ &= \int_{\mathcal{M}} \sqrt{-g}\xi^b \nabla^a T_{ab}\end{aligned} \tag{1.22}$$

up to boundary terms. Because ξ^b is arbitrary, T_{ab} is conserved in the bulk.

That concludes our review! Contained herein are most of the tools you'll need to approach holographic problems, with one exception to cover: how to define a boundary.

1.3 Defining a Boundary

Suppose one of our coordinates is oh-so-special. Call it r, for radial. Let us foliate our bulk spacetime into hypersurfaces Σ_r of constant r along this radial direction. The bulk metric can be divvied up through the ADM formalism[4] as

$$ds^2 = N^2 dr^2 + \gamma_{ij}\left(dx^i + N^i dr\right)\left(dx^j + N^j dr\right) \tag{1.23}$$

where γ_{ij} is the intrinsic metric on Σ_r, and the parameters N and N^i are called the *lapse* and *shift*, respectively. The metric g_{ab} is then codified by the parameters $\{N, N^i, \gamma_{ij}\}$ with the inverse

$$g^{ab}\nabla_a \otimes \nabla_b = \frac{1}{N^2}\left(\nabla_r - N^i\nabla_i\right)\otimes\left(\nabla_r - N^j\nabla_j\right) + \gamma^{ij}\nabla_i\otimes\nabla_j. \tag{1.24}$$

Be aware that γ^{ij} is the inverse of the intrinsic metric, which is *not* the same thing as raising the indices of γ_{ij} with the bulk metric! We will use the indices $(i, j, k, \dots)$ to denote non-radial components and the contractions of such objects use the intrinsic metric. The Ricci scalar can then be reexpressed as

$$R[g] = R[\gamma] + K^2 - K_{ij}K^{ij} + \nabla_a\left(-2Kn^a + 2n^b\nabla_b n^a\right) \tag{1.25}$$

where $R[g]$ and $R[\gamma]$ are the Ricci scalars for the bulk metric and intrinsic metric, respectively, and the vector $n^a = (1/N, -N^i/N)$ is the outward unit normal vector to Σ_r. The extrinsic curvature K_{ij} is defined

$$\begin{aligned} K_{ij} &\equiv \nabla_{(i}n_{j)} \\ &= \frac{1}{2N}\left(\dot{\gamma}_{ij} - 2\nabla^{(\gamma)}_{(i}N_{j)}\right) \end{aligned} \tag{1.26}$$

where $\nabla^{(\gamma)}_i$ is the covariant derviative defined for the intrinsic curvature γ_{ij} and $K = K^i_i$. The dot denotes a radial derivative ∂_r.

Let us examine a generic action

$$I = -\int_{\mathcal{M}}\sqrt{-g}\left(R - \frac{1}{2}\left(\nabla\phi\right)^2 - V(\phi) - \frac{1}{4}Z(\phi)F^2\right) - \int_{\partial\mathcal{M}}\sqrt{-\gamma}2K \tag{1.27}$$

[4]Named for Richard Arnowitt, Stanley Deser and Charles W. Misner.

which features a $U(1)$ field strength $F = dA$ for a 1-form A and a scalar field ϕ. These types of objects are the general stuff of field theory so it is important that we understand how to handle them! The K-dependent boundary term added is the *Gibbons-Hawking term*, added to cancel the boundary contribution from the total derivative term in Eq. (1.25). This is required to have a well-defined variational problem. A generic variation of this action yields

$$\delta I = \int_{\mathcal{M}} \sqrt{-g}\,(\text{EOMs}) + \int_{\partial\mathcal{M}} \left(\frac{1}{2}T^{ab}\delta\gamma_{ab} - J^a\delta A_a + \mathcal{O}_\phi\delta\phi\right), \tag{1.28}$$

which as we have discussed, leaves only a boundary term on-shell. The boundary stress-energy tensor T_{ab}, current J^a and scalar operator $\mathcal{O}_\phi$ are given by

$$T^{ab} = 2\sqrt{-\gamma}\left(K^{ab} - K\gamma^{ab}\right), \quad J^a = \sqrt{-\gamma}n_b Z(\phi)F^{ab}, \quad \mathcal{O}_\phi = -\sqrt{-\gamma}n_a\nabla^a\phi. \tag{1.29}$$

These bare responses are not guaranteed to be stable at the boundary and will in general require renormalization! This is performed with the addition of boundary action counter-terms $I_{\text{c.t.}}$, which we demand to depend only upon intrinsic fields in Σ_r.

The action of Eq. (1.27) can be formulated in the language of radial evolution [9, 10] as $I = \int dr L$ with a Lagrangian

$$\begin{aligned} L = -\int_{\Sigma_r} \sqrt{-\gamma}N\Bigg(&R[\gamma] + K^2 - K_{ij}K^{ij} \\ &- \frac{\gamma^{ij}}{2N^2}Z(\phi)\left(\dot{A}_i - \partial_i A_r + N^k F_{ki}\right)\left(\dot{A}_j - \partial_j A_r + N^l F_{lj}\right) \\ &- \frac{1}{4}Z(\phi)\gamma^{ij}\gamma^{kl}F_{ik}F_{jl} - \frac{1}{2N^2}\left(\dot{\phi}^2 - N^i\partial_i\phi\right)^2 - \frac{1}{2}\gamma^{ij}\partial_i\phi\partial_j\phi - V(\phi)\Bigg), \end{aligned} \tag{1.30}$$

where the Gibbons-Hawking term has already canceled out the boundary contribution from R. Note that N, N^i and A_r have no kinetic terms and are therefore Lagrange multipliers which will yield some first-order constraints. The constraints from N and N^i are a consequence of diffeomorphism invariance; that is, we have exactly D first-order constraints, removing the dynamics of the D free reparameterizations. The constaint from A_r is one from $U(1)$ invariance. The conjugate momenta are defined

$$\Pi^{(\gamma)ij} \equiv \frac{\delta L}{\delta\dot{\gamma}_{ij}} = \sqrt{-\gamma}\left(K^{ij} - K\gamma^{ij}\right), \tag{1.31a}$$

$$\Pi^{(A)i} \equiv \frac{\delta L}{\delta\dot{A}_i} = \frac{\sqrt{-\gamma}}{N}\gamma^{ij}Z(\phi)\left(\dot{A}_j - \partial_j A_r + N^k F_{kj}\right) \tag{1.31b}$$

$$\Pi^{(\phi)} \equiv \frac{\delta L}{\delta\dot{\phi}} = \frac{\sqrt{-\gamma}}{N}\left(\dot{\phi} - N^i\partial_i\phi\right) \tag{1.31c}$$

which are exactly the same as the responses in Eq. (1.28). As stated previously, these are in general *not* well-defined in the boundary limit $r \to \infty$. However, counter-terms can be generated in a controlled way. The general mechanism solves the radial Hamilton-Jacobi equations with a recursive solution involving a functional series expansion [9, 10].

The Hamiltonian is

$$H = \int_{\Sigma_r} \left(\Pi^{(\gamma)ij} \dot{\gamma}_{ij} + \Pi^{(A)i} \dot{A}_i + \Pi^{(\phi)} \dot{\phi} \right) - L \tag{1.32}$$

$$= \int_{\Sigma_r} \left(N\mathcal{H} + N^i \mathcal{H}_i - A_r \partial_i \Pi^{(A)i} \right) \tag{1.33}$$

where

$$\mathcal{H} = \frac{1}{\sqrt{-\gamma}} \left(\Pi^{(\gamma)ij} \Pi^{(\gamma)}_{ij} - \frac{1}{D-2} \Pi^{(\gamma)2} + \frac{1}{2Z(\phi)} \Pi^{(A)i} \Pi^{(A)}_i + \frac{1}{2} \Pi^{(\phi)2} \right)$$
$$+ \sqrt{-\gamma} \left(R[\gamma] - \frac{1}{4} Z(\phi) F_{ij} F^{ij} - \frac{1}{2} \partial_i \phi \partial^i \phi - V(\phi) \right), \tag{1.34}$$

$$\mathcal{H}_i = -2\nabla^{(\gamma)j} \Pi^{(\gamma)}_{ji} + \Pi^{(A)j} F_{ji} + \Pi^{(\phi)} \partial_i \phi \tag{1.35}$$

Thus, the first-order constraints imposed by the variations of N, N^i and A_r are

$$\mathcal{H} = 0, \quad \mathcal{H}_i = 0, \quad \partial_i \Pi^{(A)i} = 0. \tag{1.36}$$

As expected, N and N^i yield Hamiltonian and momentum constraints, respectively, and A_r yields a continuity equation for the current $\Pi^{(A)i}$ within Σ_r. The last feature is crucially important: we have established a mechanism to encode a locally conserved boundary current.

1.4 Example to Live By: The AdS Reissner-Nordström Black Hole

Paramount to all our discussion is the fundamental solution of the AdS Reissner-Nordström black hole. In general relativity nomenclature, Reissner-Nordström refers to a black hole with electric charge. We take a bulk action which contains only features of geometry and electromagnetism, the Einstein-Maxwell action[5]

$$I_{\text{bulk}} = -\int_{\mathcal{M}} \sqrt{-g} \left(R - 2\Lambda - \frac{1}{4} F^2 \right) \tag{1.37}$$

[5]The astute reader will notice the minus sign in front of the action, which is necessary to prescribe the dual thermodynamics. If it's more comfortable, you might think this minus sign is meant to be there in a spacetime with negative curvature!

where $F = dA$ is the exterior derivative of a $U(1)$ field and $\mathcal{M}$ is a $(d_s + 2)$-dimensional Lorentzian manifold. The metric ansatz

$$ds^2 = \frac{L^2}{r^2 f(r)} dr^2 - \frac{r^2}{L^2} f(r) dt^2 + \frac{r^2}{L^2} d\vec{x}_{d_s}^2, \tag{1.38}$$

is a possible solution to the Einstein equations, where L is the AdS length. The *emblackening factor* f is taken such that $\lim_{r\to\infty} f(r) = 1$ and $f(r_+) = 0$, where r_+ is the largest root of f. These conditions imply that our metric is asymptotically AdS as $r \to \infty$ and that there is an event horizon at $r = r_+$. Thus, r is a radial coordinate that takes us from a black hole horizon to a conformal boundary. As $r \to \infty$, the scaling symmetry

$$r \to \lambda^{-1} r, \quad t \to \lambda t, \quad x^i \to \lambda x^i \tag{1.39}$$

obtains.[6]

This action yields the bulk equations of motion, the Einstein-Maxwell equations:

$$E_{ab} = R_{ab} - \frac{2\Lambda}{d_s} g_{ab} - \frac{1}{2}\left(F_{ac}F_b{}^c - \frac{1}{2d_s} F^2 g_{ab}\right) = 0, \tag{1.40a}$$

$$M^a = \nabla_b F^{ab} = 0 \tag{1.40b}$$

Here we have removed the Ricci scalar from the Einstein-Maxwell equations using

$$R = \left(2 + \frac{4}{d_s}\right)\Lambda + \left(\frac{1}{4} - \frac{1}{2d_s}\right) F^2, \tag{1.41}$$

which can be acquired by taking the trace of the Einstein equations. It is convenient to do this both for compactifying the equations of motion and, more importantly later on, to define a stable numerical solution scheme.

The Einstein-Maxwell equations allow an enormous class of solutions. In fact, a general set of solutions to the equations does not exist and there only a handful of nontrivial analytic solutions. One possible such solution is the AdS Reissner-Nordström black hole,

$$\Lambda = -\frac{d_s(d_s+1)}{2L^2}, \tag{1.42}$$

$$A = \mu\left(1 - \left(\frac{r_+}{r}\right)^{d_s - 1}\right) dt, \tag{1.43}$$

$$f(r) = 1 + q^2\left(\frac{r_+}{r}\right)^{2d_s} - M\left(\frac{r_+}{r}\right)^{d_s+1}, \tag{1.44}$$

$$q = \sqrt{\frac{d_s - 1}{2d_s}}\frac{\mu L}{r_+}, \quad M = 1 + q^2 \tag{1.45}$$

[6]Often, scale invariance is close enough to conformal invariance that most people don't segregate the two.

Let us take some time to dissect the features of this solution. The nature of the AdS hyperbolic geometry is encoded by the negative cosmological constant Λ. The boundary conditions imposed on A_t are a Dirichlet condition at the boundary, $\lim_{r\to\infty} A_t(r) = \mu$, and a regularity condition at the horizon, $A_t(r_+) = 0$. For convenience, we often set $L = 1$, noting that it can be restored through dimensional analysis.

Why black holes? We will demonstrate how a black hole naturally imparts the properties of a thermodynamic system. Near the horizon

$$ds^2 \approx \frac{L^2}{r_+^2 f'(r_+)} \frac{dr^2}{r - r_+} - \frac{r_+^2 f'(r_+)}{L^2} (r - r_+)\, dt^2 + \frac{r_+^2}{L^2} d\vec{x}_{d_s}^2, \tag{1.46}$$

which with a change of variables $\varrho^2 = r - r_+$ and Wick rotation $\tau = -it$ obtains

$$ds^2 \approx \frac{4L^2}{r_+^2 f'(r_+)} \left[d\varrho^2 + \left(\frac{r_+^2 f'(r_+)}{2L^2} \right)^2 \varrho^2 d\tau^2 \right] + \frac{r_+^2}{L^2} d\vec{x}_{d_s}^2. \tag{1.47}$$

We see the radial coordinate and Euclidean time take the form of simple polar coordinates near the horizon. For a suitable dual theory, the Euclidean time τ must have a period of $1/T$ where T is the temperature of the thermodynamic ensemble. To avoid a conical singularity, the constraint

$$\begin{aligned} T &= \frac{r_+^2 f'(r_+)}{4\pi L^2}, \\ &= \frac{r_+}{4\pi L^2} \left(d_s + 1 - \frac{(d_s - 1)^2}{2d_s} \frac{\mu^2 L^2}{r_+^2} \right), \end{aligned} \tag{1.48}$$

is forced, and is dubbed the Hawking temperature. This singularity, in essence, is a guarantee that the near-horizon polar coordinates $\{\varrho, \frac{r_+^2 f'(r_+)}{2L^2}\tau\}$ function appropriately; that is, the dimensionless polar angle has a period of 2π. Anything else and the polar system could be visualized as a cone (more or less than 2π to loop around) and a singularity emerges at $\varrho = 0$, the cone's tip.

The temperature of our theory is entirely determined by the near-horizon geometry. The mere presence of a black hole both turns on and completely determines the temperature, and its absence guarantees $T = 0$. Of course, $T = 0$ can be achieved despite the presence of the black hole when $f'(r_+) = 0$, or $q^2 = d_s + 1$. Such a black is dubbed *extremal* and results in a double root of f at the horizon, giving a completely different near-horizon geometry of the form $AdS_2 \times \mathbb{R}^{d_s}$.[7]

Instead of viewing the horizon radius as constraining the temperature, we will visualize T and μ as the independent variables that determine $r_+(T, \mu)$.

[7]This $T = 0$ horizon structure imparts unique features which aid in the computation of response functions, as seen in [11].

Inverting (1.48),

$$\frac{r_+(T,\mu)}{L} = \frac{2\pi TL}{d_s+1}\left(1+\sqrt{1+\frac{2}{d_s}(d_s+1)(d_s-1)^2\left(\frac{\mu}{2\pi TL}\right)^2}\right), \tag{1.49}$$

and the thermodynamic potential can be expressed explicitly as a function of T and μ.

The free energy can be computed from the on-shell action. In order to evaluate a stable boundary action we will integrate over the interval $[r_+, r_\infty]$, where r_∞ is a placeholder radial cutoff to signify $r \to \infty$. We demand that all our symplectic form is stable in this limit and nothing is ultimately a function of the cutoff r_∞. The Ricci scalar (1.41) can be plugged in to yield the on-shell action:

$$I^{(\text{o.s.})} = -\int_{\mathcal{M}} \sqrt{-g}\left(\frac{4\Lambda}{d_s} - \frac{1}{2d_s}F^2\right) - \int_{\partial\mathcal{M}} \sqrt{-\gamma}2K. \tag{1.50}$$

The bulk contribution can be expressly integrated, and the Gibbons-Hawking term for our ansatz is easily computed We arrive at

$$I^{(\text{o.s.})} = \frac{\text{vol}_{d_s}}{TL}\left[-2d_s\left(\frac{r_\infty}{L}\right)^{d_s+1} + (d_s-1)M\left(\frac{r_+}{L}\right)^{d_s+1}\right] \tag{1.51}$$

after removing all vanishing contributions from the boundary limit. The parameter vol_{d_s} is a d_s-dimensional spatial volume.

Presently, our boundary action diverges and is not well-defined. As it happens, the only term required to stabilize our theory is a volume term,

$$I_{\text{c.t.}} = \int_{\partial\mathcal{M}} \sqrt{-\gamma}\frac{2d_s}{L}. \tag{1.52}$$

This modification affects only the stress-energy tensor in Eq. (1.28), which is now

$$\mathbb{T}^a{}_b = 2\sqrt{-\gamma}\left(K^{ab} - K\delta^a{}_b + \frac{d_s}{L}\delta^a{}_b\right). \tag{1.53}$$

The stress-energy tensor is now stable in the $r \to \infty$ limit, and obtains

$$\mathbb{T}^t{}_t = d_s\frac{M}{L}\left(\frac{r_+}{L}\right)^{d_s+1}, \quad \mathbb{T}^{x^i}{}_{x^j} = -\frac{M}{L}\left(\frac{r_+}{L}\right)^{d_s+1}\delta^i{}_j. \tag{1.54}$$

We first notice that the stress-energy tensor is traceless, $\mathbb{T}^a{}_a = 0$. This is a standard property of a conformally invariant theory, which emerges as the Ward identity for Weyl invariance; namely, the consequence of the action being invariant under the Weyl transformation

$$\gamma_{ab} \to e^{-2\Omega(x)}\gamma_{ab}. \tag{1.55}$$

Now, the full on-shell boundary action is

$$I^{(\text{o.s.})} = \frac{W}{T} = -\text{vol}_{d_s} \frac{M}{TL} \left(\frac{r_+}{L}\right)^{d_s+1}, \tag{1.56}$$

and W is the free energy. This is it! We have computed the thermodynamic potential for our theory. Let us check that the response it computes are intuitive! Armed with (1.49), all partial derivatives and expressions can be computed explicitly. First, the entropy,

$$\begin{aligned} \mathcal{S} &= -\frac{\partial W}{\partial T}, \\ &= \text{vol}_{d_s} 4\pi \left(\frac{r_+}{L}\right)^{d_s}, \end{aligned} \tag{1.57}$$

where $\text{vol}_{d_s}(r_+/L)^{d_s}$ is exactly the surface area of the black hole. This is the celebrated Bekenstein-Hawking relation (where we have chosen $G_N = \frac{1}{16\pi}$).

Next, the charge associated with the chemical potential μ is

$$\begin{aligned} \mathcal{Q} &= -\frac{\partial W}{\partial \mu}, \\ &= \text{vol}_{d_s}(d_s - 1)\frac{\mu}{L}\left(\frac{r_+}{L}\right)^{d_s-1} = \text{vol}_{d_s} J^t, \end{aligned} \tag{1.58}$$

which is exactly the predicted charge density. Now we can compute the system's internal energy,

$$\begin{aligned} \mathcal{E} &= W + T\mathcal{S} + \mu\mathcal{Q}, \\ &= \text{vol}_{d_s} d_s \frac{M}{L}\left(\frac{r_+}{L}\right)^{d_s+1} = \text{vol}_{d_s} \mathbb{T}^t{}_t \end{aligned} \tag{1.59}$$

which is in fact directly represented by the tt-component of the stress energy tensor.

The final quantity we will check is the system pressure p. Our system's volume dependence is trival, so the pressure is just

$$\begin{aligned} p &= -\frac{W}{\text{vol}_{d_s}}, \\ &= \frac{M}{L}\left(\frac{r_+}{L}\right)^{d_s+1} = -\mathbb{T}^{x^1}{}_{x^1}. \end{aligned} \tag{1.60}$$

In a system with translational invariance, the pressure is simply related to the system's stress! What's more, the pressure's relation to the thermodynamic potential guarantees the satisfaction of a Smarr-like relation

$$\epsilon + p = Ts + \mu\rho, \tag{1.61}$$

where ϵ, s and ρ are the energy, entropy and charge densities respectively.

1.4.1 Kubo Formula for Conductivities

As a quick aside, let us discuss the effect of a time-dependent perturbation on a system of the form

$$H_{\text{source}} = \sum_A \mathcal{O}_A(t)\phi_A(t) \tag{1.62}$$

where ϕ_A are small potentials sourcing responses $\mathcal{O}_A$. Mathematically, any such linear response can expressed with a Green function via

$$\delta\langle\mathcal{O}_A(t)\rangle = \int dt' \mathcal{G}_{AB}(t-t')\phi_A(t'). \tag{1.63}$$

In a traditional problem, ϕ_A may be something like an electric or thermal potential. However, we are often interested not in the response to a potential but to its corresponding "force," i.e. an electric field or temperature gradient. Mathematically, we use a generalized force $\mathcal{F}_A = -\partial_t\phi_A$. Then, in frequency space

$$\tilde{\mathcal{F}}_A(\omega) = i\omega\tilde{\phi}_A(\omega). \tag{1.64}$$

We can define a conductivity as accumulated response of the force throughout history,

$$\delta\langle\mathcal{O}_A(t)\rangle = \int dt' \sigma_{AB}(t-t')\mathcal{F}_A(t'). \tag{1.65}$$

The relation of the Green function to conductivity is then simply

$$\tilde{\sigma}_{AB}(\omega) = \frac{\tilde{\mathcal{G}}_{AB}(\omega)}{i\omega}, \tag{1.66}$$

which is the Kubo formula for conductivities. Importantly, we note that a source of frequency ω generates a response at exactly the same frequency. Thus, it is fruitful to only work in Fourier space for conductivities, so we will drop the tildes in the future.

1.4.2 Transport Properties of the AdS Reissner-Nordström Black Hole

Thus far we have established the AdS-RN black hole *static background*: a spacetime with a massive charged black hole that is asymptotically anti-de Sitter. Now that everything's settled, the best way to learn more is to prod it! We'll now consider how to compute dynamical quantities, namely linear transport. For further details on this treatment, see [12, 13].

To observe the character of charge and thermal transport in this theory, let us implement a linear response mechanism. We will consider both that

the temperature and chemical potential will be modified to be have a *slight* and perturbatively treatable gradient,

$$T \to T + x^1 \nabla_{x^1} T, \qquad \mu \to \mu + x^1 \nabla_{x^1} \mu, \tag{1.67}$$

which without loss of generality we can choose to be along x^1 by rotational symmetry. The effect of a chemical potential gradient is exactly the same as an applied electric field; it generates motion of its conjugate charge. And of course, a thermal gradient will generate a flow of heat. Calling the charge and heat currents $j^{(\rho)x^1}$ and $j^{(q)x^1}$ respectively, these gradients will define a conductivity matrix

$$\begin{pmatrix} j^{(\rho)x^1} \\ j^{(q)x^1} \end{pmatrix} = \begin{pmatrix} \sigma & T\alpha \\ T\alpha & T\overline{\kappa} \end{pmatrix} \begin{pmatrix} -\nabla_{x^1}\mu \\ -\left(\nabla_{x^1} T\right)/T \end{pmatrix} \tag{1.68}$$

where σ is the optical condutivity, $\overline{\kappa}$ is the closed-circuit thermal conductivity, and α is the Seebeck coefficient. The charge and heat currents can inform us a great deal about material behavior. For instance, in a metal they are directly proportional to each other! This is because the only carriers of energy in the system are effectively free electrons, so the charge and thermal carriers have a total overlap. This is the Wiedemann-Franz Law, and it breaks down in the converse: any other interactions in the material mean that these currents will *not* overlap.

Let us take a moment to examine *how* the temperature gradient is implemented. In our theory, it is expressly included by measuring the period of Euclidean time. Thus, we can rescale the time coordinate $t = \bar{t}/T$ and the new coordinate $\bar{t}$ has a period independent of temperature. Then perturbing with a gradient, all tensors in our theory are adjusted using

$$dt = \frac{d\bar{t}}{T} \to \frac{d\bar{t}}{T}\left(1 - x^1 \frac{\nabla_{x^1} T}{T}\right) = dt\left(1 - x^1 \frac{\nabla_{x^1} T}{T}\right). \tag{1.69}$$

Then overall, we formulate the gradient perturbation on our background fields near the boundary like

$$\delta ds^2 \approx 2x^1 \frac{\nabla_{x^1} T}{T}\left(\frac{r}{L}\right)^2 dt^2, \tag{1.70}$$

$$\delta A \approx x^1 \left(\nabla_{x^1}\mu - \mu \frac{\nabla_{x^1} T}{T}\right) dt. \tag{1.71}$$

Before we take the next step, let us bestow time-dependence upon our gradients as well,

$$\nabla_{x^1} T \to e^{-i\omega t} \nabla_{x^1} T, \qquad \nabla_{x^1}\mu \to e^{-i\omega t}\nabla_{x^1}\mu, \tag{1.72}$$

Of course, because we are working to linear order it is salubrious to immediately work in the Fourier basis.

It will prove convenient to modify our perturbations with a set of gauge transformations to shift all our sources onto transverse modes. Consider a small diffeomorphism $x^a \to x^a + \xi^a$ and $U(1)$ transformation λ given by

$$\xi = -e^{-i\omega t}\frac{x^1}{i\omega}\frac{\nabla_{x^1}T}{T}\nabla_t, \qquad \lambda = e^{-i\omega t}\frac{x^1}{i\omega}\nabla_{x^1}\mu. \tag{1.73}$$

This choice leaves the perturbation as

$$\delta ds^2 \approx e^{-i\omega t}\frac{2}{i\omega}\frac{\nabla_{x^1}T}{T}\left(\frac{r}{L}\right)^2 dtdx^1, \tag{1.74}$$

$$\delta A \approx e^{-i\omega t}\frac{1}{i\omega}\left(\nabla_{x^1}\mu - \mu\frac{\nabla_{x^1}T}{T}\right)dx^1 \tag{1.75}$$

where we have used

$$\delta g_{ab} = \mathcal{L}_\xi g_{ab} = 2\nabla_{(a}\xi_{b)}, \tag{1.76}$$

$$\delta A_a = \mathcal{L}_\xi A_a + \nabla_a\lambda = \xi^b\nabla_b A_a + A_b\nabla_a\xi^b + \nabla_a\lambda \tag{1.77}$$

where $\mathcal{L}_\xi$ denotes the Lie derivative.

This formulation is very convenient: not only has the x^1-dependence dropped completely, but the equations of motion for the transverse modes

$$\delta A = e^{-i\omega t}\delta\tilde{A}_{x^1}(r)dx^1, \quad \delta ds^2 = e^{-i\omega t}2\left(\frac{r}{L}\right)^2\delta\tilde{g}_{tx^1}(r)dtdx^1 \tag{1.78}$$

are

$$\left(\frac{L}{r}\right)^{d_s}\left[\left(\frac{r}{L}\right)^{d_s} f\delta\tilde{A}'_{x^1} + \rho\delta\tilde{g}_{tx^1}\right]' + \frac{\omega^2}{f}\left(\frac{L}{r}\right)^4\delta\tilde{A}_{x^1} = 0, \tag{1.79a}$$

$$\delta\tilde{g}'_{tx^1} + \left(\frac{L}{r}\right)^{d_s+2}\rho\delta\tilde{A}_{x^1} = 0, \tag{1.79b}$$

which completely decouple from all other modes. Thus, the dynamics of the system need only be described by these two fields. The second of these, Eq. (1.4.2), is a first-order constraint that effectively implements momentum conservation. Actually, the constraint readily compacts all our dynamics to a single equation of motion:

$$\left(\frac{L}{r}\right)^{d_s}\left[\left(\frac{r}{L}\right)^{d_s} f\delta\tilde{A}'_{x^1}\right]' - \left(\frac{L}{r}\right)^{2d_s+2}\rho^2\delta\tilde{A}_{x^1} + \frac{\omega^2}{f}\left(\frac{L}{r}\right)^4\delta\tilde{A}_{x^1} = 0, \tag{1.80}$$

and thus the entirety of the transport problem has reduced to a single ordinary differential equation!

In general, the asymptotic series at the boundary is

$$\delta\tilde{A}_{x^1} = \delta\tilde{A}^{(0)}_{x^1} - \frac{1}{d_s-1}\left(\frac{L}{r}\right)^{d_s-1}\delta\tilde{A}^{(J)}_{x^1} + \cdots, \tag{1.81}$$

$$\delta\tilde{g}_{tx^1} = \delta\tilde{g}^{(0)}_{tx^1} - \frac{1}{d_s+1}\left(\frac{L}{r}\right)^{d_s+1}\delta\tilde{g}^{(J)}_{tx^1} + \cdots, \tag{1.82}$$

and thus the source gradients are implemented as boundary conditions on $\delta\tilde{g}^{(0)}_{tx^1}$ and $\delta\tilde{A}^{(0)}_{x^1}$ via Eq. (1.75). Then the boundary action at quadratic order in the perturbations is

$$\delta I = \int_{\partial\mathcal{M}} \left[\left(\gamma_{tt}\mathbb{T}^{tx^1} - \mu J^{x^1} \right) \left(-\frac{1}{i\omega}\frac{\nabla_{x^1} T}{T} \right) + J^{x^1} \left(-\frac{1}{i\omega}\nabla_{x^1}\mu \right) \right]. \quad (1.83)$$

As advertised, the role of $-\nabla_{x^1}\mu$ is exactly the same as an applied electric field sourcing an electric current $j^{(\rho)x^1} = J^{x^1}$. The temperature gradient sources a heat current defined by

$$j^{(q)x^1} \equiv \gamma_{tt}\mathbb{T}^{tx^1} - \mu J^{x^1}, \quad (1.84)$$

which is exactly what we wanted: a measure of how much energy flows in excess of charge transport.

Dual-wielding our boundary expansion (1.81) and renormalized responses we can express

$$\gamma_{tt}\tilde{\mathbb{T}}^{tx^1} = L^{-1}\delta\tilde{g}^{(J)}_{tx^1} - \epsilon\delta\tilde{g}^{(0)}_{tx^1} + \cdots, \quad (1.85)$$

$$\tilde{J}^{x^1} = -\delta\tilde{A}^{(J)}_{x^1} - \rho\delta\tilde{g}^{(0)}_{tx^1} + \cdots, \quad (1.86)$$

where the remaining terms will not contribute to the finite action. At this point, we note that the constraint guarantees

$$\delta\tilde{g}^{(J)}_{tx^1} = -L\rho\delta\tilde{A}^{(0)}_{x^1}. \quad (1.87)$$

This constraint is straightforward there is momentum dissipation, but in general the response is not so simple! Now, the whole of the response is determined to be

$$\begin{pmatrix} J^{x^1} \\ \gamma_{tt}T^{tx^1} \end{pmatrix} = \begin{pmatrix} -\frac{1}{L^{d_s-1}}\frac{\delta\tilde{A}^{(J)}_{x^1}}{\delta\tilde{A}^{(0)}_{x^1}} & -\rho \\ -\rho & -\epsilon \end{pmatrix} \begin{pmatrix} \delta\tilde{A}^{(0)}_{x^1} \\ \delta\tilde{g}^{(0)}_{tx^1} \end{pmatrix}. \quad (1.88)$$

This is all the information we need and with one final swift substitution, the conductivity matrix is established[8][9]:

$$\sigma(\omega) = \frac{1}{i\omega L^{d_s-1}}\frac{\delta\tilde{A}^{(J)}_{x^1}}{\delta\tilde{A}^{(0)}_{x^1}}, \quad (1.89)$$

$$T\alpha(\omega) = \frac{\rho}{i\omega} - \mu\sigma, \quad (1.90)$$

$$T\overline{\kappa}(\omega) = \frac{\epsilon + p - 2\mu\rho}{i\omega} - \mu^2\sigma. \quad (1.91)$$

[8]For diffusive properties, the open-circuit thermal conductivity $T\kappa = \frac{\epsilon}{i\omega} + \frac{\rho^2}{\sigma\omega^2}$ is the one of importance instead of $\overline{\kappa}$.

[9]In general, the pressure term contained in $\overline{\kappa}$ should emerge from translation invariance though it is not manifest from our consideration.

We know every quantity here except for σ, which must be determined by solving (1.80). This procedure must be done numerically.

The only thing that remains is to establish the boundary conditions for the differential equation (1.80). At the boundary, we simply choose the Dirichlet condition

$$\delta A^{(0)}_{x^1} = 1. \tag{1.92}$$

For the second condition, let us examine the form of $\delta \tilde{A}_{x^1}$ near the horizon. In the vicinity, it is easy to see

$$\delta \tilde{A}_{x^1} \sim (r - r_+)^{\pm \frac{i\omega}{4\pi T}} \tag{1.93}$$

This near-horizon wave-like solution is a universal feature, with the plus and minus signs corresponding to out-going and in-falling waves, respectively. We demand that all waves near a black hole horizon will be in-falling, which will correspond to causal response functions. A wave is leaving the event horizon is the signature of a white hole and oppositely corresponds to anti-causal response functions. Thus, the horizon boundary condition is

$$\delta \tilde{A}_{x^1} = \left(1 - \frac{r_+}{r}\right)^{-\frac{i\omega}{4\pi T}} \delta \breve{A}_{x^1} \tag{1.94}$$

with $\delta \breve{A}_{x^1}$ analytic near $r = r_+$. In practice, we substitute[10] into (1.80) and solve for $\delta \breve{A}_{x^1}$.

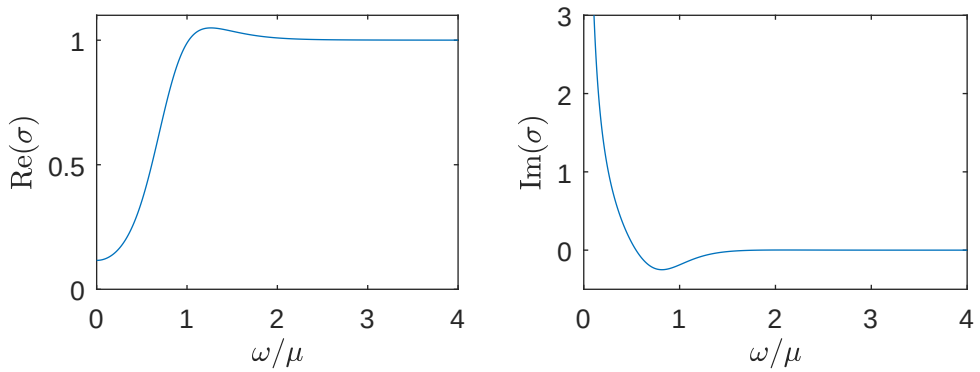

Figure 1.1: Plots of real and imaginary parts of σ for $d_s = 2$, $\mu = 1.4\sqrt{2}$ and $T/\mu = 0.115$. $L = 1$ is used for convenience.

In Fig. 1.1 we display a typical solution for σ in the AdS-Reissner-Nordström black hole. These forms actually match quite well to low-energy graphene, which is described by a 2+1-dimensional relativistic theory [12,14]. Let us examine the high and low frequency behavior. Firstly, we notice that

[10] Often, it is wise to substitute some other factors as well, which we discuss in the numerics chapter.

$\lim_{\omega\to\infty}\sigma = 1$ in $d_s = 2$. In general, σ will follow a power law behavior for high-frequency which is dependent upon d_s:

$$\sigma \sim (-i\omega)^{d_s-2}. \tag{1.95}$$

The power law can be extracted by examining (1.80). If we rescale $r \to -i\omega r$ and send $\omega \to \infty$, the equation of motion becomes independent of ω and thus the power law of the current is just given by its scaling dimension in r. It is quite common for high-frequency behavior in holographic system to behave in this manner! Once the energy scale of ω vastly exceeds all others (T and μ, in this case), it is the only thing the response functions can see.

For the low frequency behavior, we observe $\mathrm{Im}(\sigma) \sim 1/\omega$ as $\omega \to 0$. It would easy to mistakenly think that $\mathrm{Re}(\sigma)$ tends to a finite value, but by the Kramers-Kronig relations, the imaginary divergence indicates $\mathrm{Re}(\sigma) \sim \delta(\omega)$. Thus the real part diverges as well, despite the lack of direct indication in the finite frequency numerics. The DC conductivity completely diverging is an expected feature of a system that does not have any momentum dissipation.

Here is a thought experiment to help understand. Our system possesses a nonzero charge density and a boost symmetry from Lorentz invariance. Therefore, if we boost the system, it appears we have a current without ever having to apply an electric field! By breaking translational symmetry, *i.e.* inserting momentum dissipation, we can no longer freely boost and the DC conductivity will be finite.[11]

This calculation has hopefully elucidated the holographic program. We can clearly see how bulk fields contain information within that is imprinted on the boundary as sources and responses.

[11] Momentum dissipation is not strictly required to obtain a finite DC conductivity, as we will see in Lifshitz holography.

2 Numerics

Analytics are beautiful, sometimes. Perhaps less so after a few hundred counter-term calculations and asymptotic expansions. But frankly, at some point, analytics will fail you. It really doesn't take much in the way of complicating your model to push analytic solutions well out of reach. This is when we must turn our attention to an incredibly important and deep set of tools that are often brushed under the rug for the cardinal sin of being "boring": numerics. It should be noted that numerics is not the easy way out. It will be just as tedious and frustrating as the analytics, except that some of the procedure may take place in a computational black box.

This chapter is meant to lay out a procedure in detail to assist in the computations of a particular set of gravitational problems. Namely, we will work through the Einstein-DeTurck formalism [15], which is a way of handling time-independent solutions to the Einstein equations. Time dependence can be included at the level of linear response, where a static system is jolted by small time-dependent sources, just as we've done previously in the AdS-RN solution. The first step of our numerical prep is to understand how in the world the Einstein equations can be handled by a computer.

2.1 The DeTurck Term

The Einstein equations must be among some of the most awful equations us feeble humans could envision solving. Second-order, coupled, highly non-linear partial differential equations complete with gauge invariance. A real nightmare beyond the scope of a select few analytic solutions. The question begs, how can such a thing be fed to a computer? We must carefully sculpt a procedure that our computer can stomach.

Broadly, we can categorize the Eintstein equations into either elliptic or hyperbolic partial differential equations. Our equations can be formatted into (weakly) elliptic operators in the absence of time-dependence, which are generalizations of the Laplace equation. This type of equation can naturally be solved supplied only with boundary data. This class of solutions is what we will examine in this work and is sufficient for all of linear response theory. Some problems, such as turbulence [16], require full time-dependent treatment from the hyperbolic class of solutions, which is beyond the scope of this work.

The proposed scheme is then to solve for a nonlinear static background, and then compute the time-depdendent fluctuations around this background. By linearizing the time dependence, we are able to simply Fourier transform away the once problematic minus sign and keep our solutions all confined into elliptic operators. That said, the treatment of each of these two sections is quite different and demand different schemes.

We now modify the Einstein equations to the Einstein-DeTurck equations,

$$E^H_{ab} \equiv E_{ab} - \nabla_{(a}\xi_{b)} = 0, \tag{2.1}$$

where the additional piece is call the DeTurck term. By identically fixing the constraint $\xi^a = 0$, the gauge of the problem can be sufficiently fixed. We reiterate the conserved quantities

$$\nabla^a \left(R_{ab} - \frac{1}{2} R g_{ab} \right) = 0, \quad \nabla^a T_{ab} = 0, \tag{2.2}$$

and demanding the Einstein-DeTurck equations are solved in conjunction with the always-true conservation laws gives us

$$\Box \xi^a + R^a{}_b \xi^b = 0. \tag{2.3}$$

Thus, hidden in these expressions is the fact that ξ^a itself solves an elliptic equation. If we implement $\xi^a = 0$ as boundary data, we will inherently fix $\xi^a = 0$ globally a posteriori! Thus the gauge will be fixed and the original Einstein equations are satisfied.

The vector ξ^a thus far has been a free choice, but now we will hone in on a specific one, one that will afford us a controlled iteration scheme. Let's examine the Ricci tensor R_{ab} under the perturbation $g_{ab} \to \overline{g}_{ab} + \delta g_{ab}$,

$$\delta R_{ab} = -\frac{1}{2}\overline{\Box}\delta g_{ab} - \overline{R}_{acbd}\delta g^{cd} + \overline{R}_{(a}{}^{c}\delta g_{b)c} + \overline{\nabla}_{(a}\overline{\nabla}^{c}\delta \hat{g}_{b)c}, \tag{2.4}$$

where the overline denotes operations dependent only upon the background metric and the hat denotes the trace-reversed metric, $\delta \hat{g}_{ab} = g_{ab} - \frac{1}{2} g^{ab}\delta g$. The character of this linearized equation is determined by its second-order derivatives. If we choose

$$\xi^a = g^{bc}\Gamma^a_{bc}, \tag{2.5}$$

then the Einstein-DeTurck equations will grant us a weakly elliptic operator in the iteration by eliminating the last term in (δR_{ab} eqn), as demonstrated:

$$\delta R^H_{ab} = -\frac{1}{2}\overline{\Box}\delta g_{ab} - \overline{R}_{acbd}\delta g^{cd} + \overline{R}_{(a}{}^{c}\delta g_{b)c} - \delta\Gamma^c_{ab}\overline{\xi}_c. \tag{2.6}$$

For the actual numerical implementation, we attenuate the DeTurck term by introducing a *reference metric* $\tilde{g}_{ab}$, with associated Christoffel symbol $\tilde{\Gamma}^a_{bc}$

and covariant derivative $\tilde{\nabla}_a$, such that

$$\xi^a = g^{bc}\left(\Gamma^a_{bc} - \tilde{\Gamma}^a_{bc}\right) = -\left(\frac{g}{\tilde{g}}\right)^{-1/2}\tilde{\nabla}_b\left(\left(\frac{g}{\tilde{g}}\right)^{1/2} g^{ab}\right), \tag{2.7}$$

$$\xi_a = g^{bc}\left(\tilde{\nabla}_b g_{ca} - \frac{1}{2}\tilde{\nabla}_a g_{cb}\right). \tag{2.8}$$

(tension field map Riemannian manifold identity map is harmonic) In the iteration scheme, the reference metric can just be taken to be the initial solution guess; for our systems, this is usually Reissner-Nordström. Thus, $\xi^a = 0$ is satisfied initially and the numerical scheme is more stable.

We see this scheme both fixes our gauge and gives a controlled iteration. To actually solve the Einstein-DeTurck equations we employ the Newton-Raphson method. This method may be familiar from elementary calculus, where it is used to iteratively compute a root of a function $f(x)$. We begin with an initial guess x_0 for the root and add a small correction δx. Using the Taylor series expansion for f about x_0, we may use $f(x_0)$ and $f'(x_0)$ to estimate the correction δx that takes us towards the root, namely

$$f(x_0 + \delta x) = 0 \quad \Rightarrow \quad \delta x \approx -\frac{f(x_0)}{f'(x_0)}. \tag{2.9}$$

To find the true root we may iterate this process until the corrections ϵ converge to zero. In a similar fashion, we may make an initial guess for a metric $\overline{g}$ satisfying the Einstein-DeTurck equations then use the linearized equations to solve for a correction. Viewing the equations as a nonlinear functional of the metric components (using the notation $L[g]$), we would write

$$L[\overline{g}] + \frac{\delta L}{\delta g}\Big|_{\overline{g}}\delta g = 0. \tag{2.10}$$

In our implementation $L[\overline{g}]$ is a numerical vector obtained by plugging the guess into the full equations, while $\delta L[\overline{g}]/\delta g$ is a numerical matrix obtained from plugging the guess into the linearized equations. The vector of corrections δg is obtained by solving the system of equations, and successive iterations ideally (but not necessarily) converge to a complete solution. Our code typically converges to about ten digits of precision in seven iterations or less for the holographic lattice models discussed in chapter 3 using double precision numbers. It is ill-advised to try to invert the matrix operation in Eq. (2.10) directly. Some examples of more advanced programs for linear solutions are LU or SVD decomposition, which organize the matrices into easy-to-manage submatrices. Most modern day mathematics software like MATLAB and Mathematica have numerous optimized solvers for linear systems with these methods built-in, so we will not detail them.

2.2 Differentiation Matrices

Let us now explore in specifics how the discretization will work. There are two primary methods: finite difference and pseudospectral. These are two possible ways to choose a grid and accompanying differentiation matrix, each with their advantages and disadvantages. For a thorough look into spectral methods, see Trefethen [17].

2.2.1 Finite Difference

Finite difference is the tried and true method for approximating derivatives. In the vicinity of a point, any differentiable function $f(x)$ can be expanded as

$$f'(x) = \frac{1}{2\Delta x}\left[f(x+\Delta x) - f(x-\Delta x)\right] + O\left(\Delta x^2\right), \tag{2.11}$$

$$f''(x) = \frac{1}{\Delta x^2}\left[f(x+\Delta x) - 2f(x) + f(x-\Delta x)\right] + O\left(\Delta x^2\right). \tag{2.12}$$

To increase the precision, a larger locus of points can be used. The higher order the scheme, the more accurate our approximation. Generally, we select a centralized differentiation scheme as in Eq. (2.12), but we will need to use an asymmetric form near the boundary. We can expand to whatever order we like, though we typically use sixth-order in for our purposes, whose sizable differentiation matrices look like

$$D^{(1)} = \frac{1}{60\Delta x}\begin{pmatrix} 147 & -360 & 450 & -400 & 225 & -72 & 10 & 0 & \cdots \\ 10 & 77 & -150 & 100 & -50 & 15 & -2 & 0 & \cdots \\ -2 & 24 & 35 & -80 & 30 & -8 & 1 & 0 & \cdots \\ \ddots & & \ddots & & \ddots & & \ddots & & \ddots \\ \ddots & 1 & -9 & 45 & 0 & -45 & 9 & -1 & \ddots \\ \ddots & & \ddots & & \ddots & & \ddots & & \ddots \\ \cdots & 0 & -1 & 8 & -30 & 80 & -35 & -24 & 2 \\ \cdots & 0 & 2 & -15 & 50 & -100 & 150 & -77 & -10 \\ \cdots & 0 & -10 & 72 & -225 & 400 & -450 & 360 & -147 \end{pmatrix}, \tag{2.13}$$

$$D^{(2)} = \frac{1}{180\Delta x^2}\begin{pmatrix} 938 & -4014 & 7911 & -9490 & 7380 & -3618 & 1019 & -126 & \cdots \\ 126 & -70 & -486 & 855 & -670 & 324 & -90 & 11 & \cdots \\ -11 & 214 & -378 & 130 & 85 & -54 & 16 & -2 & \cdots \\ \ddots & & \ddots & & \ddots & & \ddots & & \ddots \\ \ddots & 2 & -27 & 270 & -490 & 270 & -27 & 2 & \ddots \\ \ddots & & \ddots & & \ddots & & \ddots & & \ddots \\ \cdots & -2 & 16 & -54 & 85 & 130 & -378 & 214 & -11 \\ \cdots & 11 & -90 & 324 & -670 & 855 & -486 & -70 & 126 \\ \cdots & -126 & 1019 & -3618 & 7380 & -9490 & 7911 & -4014 & 938 \end{pmatrix}, \tag{2.14}$$

where all the unfilled entires are zeros and the middle rows are always centered on the diagonal. Hence, the finite difference matrices will be sparse matrices and should be stored accordingly. Finite difference is the simple and safe way to implement numerical differentiation, though perhaps somewhat crude. Being such a safe bet is a bonus though! It is recommended that prior to attempting a fancier pseudospectral method, to check that your system works with finite difference.

2.2.2 Pseudospectral

Periodic Functions

In the world of periodic functions, there is a generally superior method for implementing a differentiation matrix over finite difference to take advantage of periodicity. Periodic functions emerge in physics in a multitude of places; any periodic structure or symmetry present will impart wavelike properties upon a system. In holography, "lattices" can be imprinted, and by extension disorder, using periodic functions.

Suppose a periodic function on the interval $(0, 2\pi]$ is evenly divided into N points,

$$x_n = \frac{2\pi n}{N}, \quad n = 1, \ldots, N, \tag{2.15}$$

and the points $f_n = f(x_n)$ are the respective discretized values for some function $f(x)$ at those points. The discrete Fourier transform can be represented,

$$\tilde{f}_k = \frac{2\pi}{N}\sum_{n=1}^{N} e^{-ikx_n} f_n, \quad k = \begin{cases} -\frac{N-1}{2}, \ldots, \frac{N-1}{2}, & N \text{ odd} \\ -\frac{N}{2}, \ldots, \frac{N}{2}+1, & N \text{ even} \end{cases} \tag{2.16}$$

and the inverse,

$$f_n = \frac{1}{2\pi}\sum_{k} e^{ikx_n}\tilde{f}_k, \tag{2.17}$$

is summed over the aforementioned k values. The form of the eventual differentiation matrices varies depending on N being odd or even, and I will list both. Suppose we have an interpolating function $p(x)$ on this interval,

$$p(x) = \frac{1}{2\pi} \sum_k e^{ikx} \tilde{f}_k, \tag{2.18}$$

$$= \sum_{n=1}^{N} f_n S_N(x - x_n), \tag{2.19}$$

where $S_N(x_m - x_n) = \delta_{mn}$ such that $p(x_n) = f_n$. The kernel can then be expressed,

$$S_N(x) = \begin{cases} \frac{1}{N} \sin\left(\frac{Nx}{2}\right) \csc\left(\frac{x}{2}\right), & N \text{ odd} \\ \frac{1}{N} \sin\left(\frac{Nx}{2}\right) \cot\left(\frac{x}{2}\right), & N \text{ even} \end{cases}. \tag{2.20}$$

Now, the derivatives of the original function can be approximated by taking derivatives on $p(x)$ and evaluating at the grid points. We will call these the Fourier differentiation matrices. The first-order differentiation matrices are, for N odd,

$$D^{(1)}_{mn} = \begin{cases} 0, & m = n \\ \frac{(-1)^{m-n}}{2} \csc\left(\frac{\pi(m-n)}{N}\right), & m \neq n \end{cases}, \tag{2.21}$$

and N even,

$$D^{(1)}_{mn} = \begin{cases} 0, & m = n \\ \frac{(-1)^{m-n}}{2} \cot\left(\frac{\pi(m-n)}{N}\right), & m \neq n \end{cases}. \tag{2.22}$$

The second-order differentiation matrices are, for N odd,

$$D^{(2)}_{mn} = \begin{cases} -\frac{N^2}{12} + \frac{1}{12}, & m = n \\ -\frac{(-1)^{m-n}}{2} \csc\left(\frac{\pi(m-n)}{N}\right) \cot\left(\frac{\pi(m-n)}{N}\right), & m \neq n \end{cases}, \tag{2.23}$$

and N even,

$$D^{(2)}_{mn} = \begin{cases} -\frac{N^2}{12} - \frac{1}{6}, & m = n \\ -\frac{(-1)^{m-n}}{2} \csc^2\left(\frac{\pi(m-n)}{N}\right), & m \neq n \end{cases}. \tag{2.24}$$

Notably, $D^{(2)} \neq \left(D^{(1)}\right)^2$, so it is important to define the second-order differentiation matrix separately.

Contrary to finite difference, this spectral method yields full matrices, not sparse ones. Appropriately, its rate of convergence is much faster: exponential instead of polynomial as the grid size shrinks. A dozen points in the

spectral method may do the job of hundreds in finite difference. Whenever a periodic function rears its head, it is worthwhile to utilize. However, these methods can be extended to non-periodic functions.

A quick note on a possible error than can crop up when implementing these Fourier differentiation matrices: we generally recommend using an odd number of points. The even matrices actually possess a zero mode, and when inverted for solving a set of linear differential equations can potentially introduce a numerical artifact into the solutions. This does in fact happen in holographic problems when it comes time to consider fluctuations for linear response theory. Using an odd number of points tempers this artifact and will give much more agreeable solutions, and it is unfortunate that the even definition is almost always the only one listed.

Non-Periodic Functions: the Chebyshev Grid

In the case of periodic functions, the functions were approximated through a "trigonometric polynomial," a sum of phase factors. For a generic non-periodic function, instead the sensible interpolation function will be an algebraic polynomial. However, once again using an evenly spaced grid often results in the disastrous Runge phenomenon. The approximation not only fails to converge as $N \to \infty$, but the error in the interpolated points diverges at the potentially exponential rate of 2^N.

The countermeasure is simple enough: instead of using an evenly spaced grid, use an uneven one. There is no unique choice of an approriate grid, but to counteract the Runge phenomenon we require a grid whose density goes

$$\text{density} \sim \frac{N}{\pi\sqrt{1-x^2}} \tag{2.25}$$

as $N \to \infty$. A nearly ubiquitous choice that should cover almost anything but very special cases is the Chebyshev grid, given by

$$x_n = \cos\left(\frac{\pi n}{N}\right), \quad n = 0, 1, \ldots, N, \tag{2.26}$$

which we might consider recommended to us by the form of the density (the derivative of $\cos^{-1} x$). This grid ranges over $[-1, 1]$ (backwards) and has a higher clustering of points near the boundary than the center (this can of course be easily extended to any domain size).

As in the Fourier case, we'll define a so-called *cardinal function*,

$$p_n(x) = \frac{\prod_{l\neq n}^{N}(x - x_l)}{\prod_{l\neq n}^{N}(x_n - x_l)}, \tag{2.27}$$

which on this go-around is a polynomial that follows $p_n(x_m) = \delta_{mn}$ at the grid points, and thus serves to interpolate the Kronecker delta. Once again, by

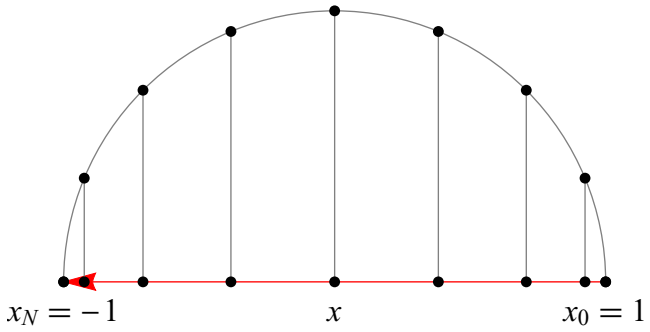

Figure 2.1: The Chebyshev grid is evenly spaced on the semicircle arc which increases the endpoint density once projected onto the x-axis.

taking derivatives on this function and evaluating at the grid points, we can express a differentiation matrix. The first-order Chebyshev differentiation matrix entires are

$$D_{00}^{(1)} = -D_{NN}^{(1)} = \frac{2N^2+1}{6}, \tag{2.28}$$

$$D_{nn}^{(1)} = -\frac{x_n}{2\left(1-x_n^2\right)}, \qquad 1 \le n \le N-1, \tag{2.29}$$

$$D_{mn}^{(1)} = \frac{c_m}{c_n}\frac{(-1)^{m+n}}{x_m - x_n}, \qquad 0 \le m,n \le N, \quad m \ne n \tag{2.30}$$

where

$$c_n = \begin{cases} 2, & n = 0, N \\ 1, & n \ne 0, N. \end{cases} \tag{2.31}$$

The second-order matrix entries are

$$D_{00}^{(2)} = D_{NN}^{(2)} = \frac{N^4-1}{15}, \tag{2.32a}$$

$$D_{0n}^{(2)} = \frac{2}{3}\frac{(-1)^n}{c_n}\frac{\left(2N^2+1\right)(1-x_n)-6}{(1-x_n)^2}, \qquad 1 \le n \le N, \tag{2.32b}$$

$$D_{n0}^{(2)} = \frac{2}{3}\frac{(-1)^{n+N}}{c_n}\frac{\left(2N^2+1\right)(1+x_n)-6}{(1+x_n)^2}, \qquad 1 \le n \le N, \tag{2.32c}$$

$$D_{nn}^{(2)} = \frac{\left(N^2-1\right)\left(1-x_n^2\right)+3}{3\left(1-x_n^2\right)^2}, \qquad 1 \le n \le N-1, \tag{2.32d}$$

$$D_{mn}^{(2)} = \frac{(-1)^{m+n}}{c_n}\frac{x_m^2 + x_m x_n - 2}{\left(1-x_m^2\right)(x_m-x_n)^2}, \qquad 1 \le m,n \le N-1, \quad m \ne n \tag{2.32e}$$

which unlike the Fourier case we do in fact have $D^{(2)} = \left(D^{(1)}\right)^2$. While it is edifying to write out these expressions, as listed they are perhaps not terribly useful. There is potentially an enormous disparity in magnitudes of elements given here, so the best bet is to express $D^{(1)}$ as tamely as possible using some trigonometric relations:

$$D_{00}^{(1)} = -D_{NN}^{(1)} = \frac{2N^2+1}{6}, \tag{2.33a}$$

$$D_{nn}^{(1)} = -\frac{1}{2}\csc\left(\frac{\pi n}{N}\right)\cot\left(\frac{\pi n}{N}\right), \qquad 1 \leq n \leq N-1, \tag{2.33b}$$

$$D_{mn}^{(1)} = \frac{(-1)^{m+n}}{2}\frac{c_m}{c_n}\csc\left(\frac{\pi(m+n)}{2N}\right)\csc\left(\frac{\pi(m-n)}{2N}\right), \quad 0 \leq m,n \leq N, \quad m \neq n, \tag{2.33c}$$

and simply use $\left(D^{(1)}\right)^n$ for n-th order differentiation matrices. This procedure should help to avoid round-off error by computing a product of numbers for each element rather than subtracting large numbers from one another.

Pseudospectral methods do meet some limitations; they do not behave well for non-analytic functions. If there exists a region where a function becomes non-analytic, this method is not trustworthy in the region's vicinity (for example, if a function contains logarithmic components, as happens often in holography). For such cases, finite difference methods are recommended. If you are adamant about using pseudospectral methods insofar as they can be applied, you can patch Chebyshev and finite difference grids together, using finite difference only when the pseudospectral methods begin to fail.

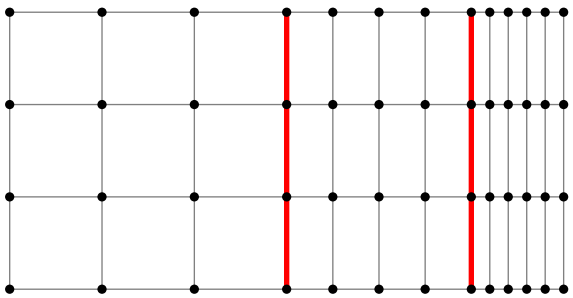

Figure 2.2: Example of a patched grid where the red lines mark the overlap.

Generally, finite difference is sufficient for the job can be used exclusively. It is often salubrious to knit patches of different densities together even in just the finite difference case; in holographic systems with conformal boundaries, increasing the grid density in the boundary region can increase precision in

the answer without resorting to going beyond machine precision using 16-bit numbers. For an nth-order differential equation, the only requirement for patching is that all derivatives of orders $\{0, \ldots, n-1\}$ are continuous where they meet. Thus, each patch is merely implemented with the continuity conditions as boundary conditions.

2.2.3 Multivariate Problems

If we aim to solve the Einstein equations, we should level-up to handle functions of more than one variable. Consider a function $f(x, y)$, that we will discretize as $f_{mn} = f(x_m, y_n)$ on a grid of $N_x \times N_y$ points. The setup is very much the same: we will turn f into a vector and differentiate it with matrix multiplication, but we must specify how to organize multiple coordinates.

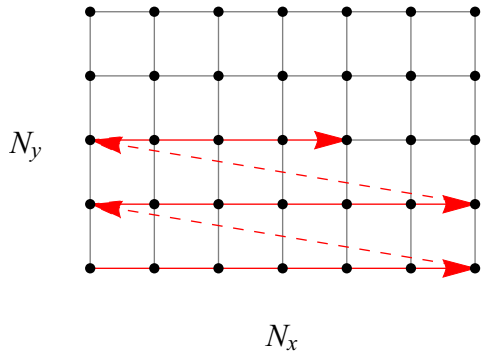

Figure 2.3: A sample grid where we elect to trace over the x-coordinate first and increment in the y-direction.

The straightforward way to parameterize the discretization is to begin at the corner (x_1, y_1) and trace over the entirety of x for this y-value, then increment y and repeat. The tracing of the grid is displayed in figure 2.3 and f's discretized form is

$$f(x,y) \Rightarrow \begin{pmatrix} f_{11} & \cdots & f_{N_x 1} & f_{12} & \cdots & f_{N_x 2} & \cdots & \cdots & f_{1N_y} & \cdots & f_{N_x N_y} \end{pmatrix}^T. \tag{2.34}$$

For matrices, the extension can made with the Kronecker product. Given some matrix A of dimension $m \times n$ and a matrix B of dimension $p \times q$, the Kronecker product between the two gives a $mp \times nq$ matrix defined by[1]

$$A \otimes B \equiv \begin{pmatrix} a_{11}B & \cdots & a_{1n}B \\ \vdots & \ddots & \vdots \\ a_{m1}B & \cdots & a_{mn}B \end{pmatrix} \tag{2.35}$$

[1]As the notation might indicate, the Kronecker product is a special case of the tensor product.

Thus, we can express all coombindations of partial dervatives:

$$\partial_x^i \partial_y^j \Rightarrow D_{N_y}^{(i)} \otimes D_{N_x}^{(j)}. \tag{2.36}$$

All coefficients in front of derivatives will merely become diagonal matrices.

The application of boundary conditions works exactly like it does in the one-dimensional problem. Each row of the differential operator returns the value of the differential equation at that ponit. If we wish to implement a boundary condition at that point, we merely replace that row with the boundary condition.

Naturally, this process can be extended for as many coordinates as desired. However, if for each of D dimensions we were to use, say, a Chebyshev grid of N points then the system we are working with requires full matrices of size $N^D \times N^D$. This exponential growth rate means that memory allocation becomes a problem very quickly for higher dimensions. Even $D = 3$ often takes a supercomputer to handle a system requiring high precision. For this reason, we manage to keep ourselves limited to $D \leq 2$ in the scope of this work.

3 Holographic Lattices

3.1 Introduction

In holography, one of our features is that we have completely avoided a microscopic description of a theory. Instead, we describe smeared thermodynamic objects like entropy, charge, currents and the like. However, our ultimate goal is to encapsulate features of actual condensed matter systems and match results onto experiments, and one important ubiquitous feature is a lattice. Our central aim in these lattice models is to understand how the lattice will affect the optical conductivity; that is, how a lattice will dissipate electric charge transport.

Superficially, a lattice is a material structure present in solids. Atoms arrange themselves in some discrete pattern, and this has a host of physical consequences. The most obvious and notable effect of a lattice is that it breaks continuous translation invariance and thus causes momentum dissipation. One of the earliest attempts to capture this behavior in holography was the holographic lattice introduced by Horowitz, Santos, and Tong [18]. Their model takes a minimal holographic description of charged matter, namely a Einstein-Maxwell formulation in AdS, and deform the solution with a scalar field with a periodic source. The periodicity of the scalar is imprinted upon the charged matter, and thus provides a means of breaking translation invariance and dissipating momentum. For this series of lattice models, we begin with a usual Einstein-Maxwell action in $d_s + 2 = 4$ bulk dimensions, but add a scalar field component

$$I_{\text{bulk}} = -\int_{\mathcal{M}} \sqrt{-g}\left(R - 2\Lambda - \frac{1}{4}F^2\right) + I_\phi, \tag{3.1}$$

where $F = dA$ is the usual exterior derivative of a $U(1)$ field. I_ϕ is a scalar field contribution to the action that will imprint a lattice through gravitational interactions. We will dicuss the findings of these models, then divulge how to actually solve them.

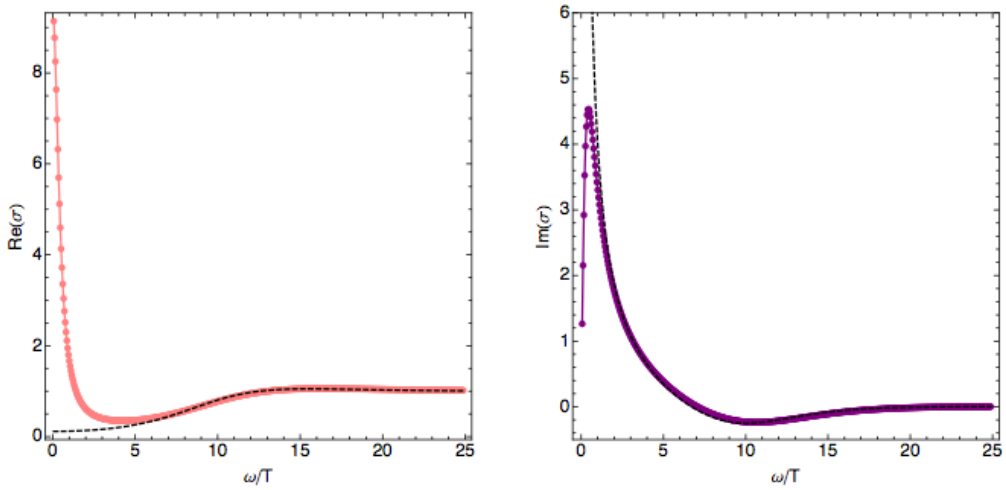

Figure 3.1: From [18]. Real and imaginary parts of the optical conductivity in the holographic lattice (red and purple) and RN-AdS$_4$ (black dashed lines). The holographic lattice displays a broadened Drude peak in its real part that is absent from RN-AdS. Destruction of the $1/\omega$ divergence in Im σ by the holographic lattice further supports interpretation of the rise in Re σ as a broadened Drude peak.

3.1.1 The Horowitz-Santos-Tong Holographic Lattice

The original holographic lattice endeavor of Horowitz, Santos and Tong (HST) used a single scalar field with an action like

$$I_\phi = -\int_{\mathcal{M}} \left[\frac{1}{2}\left(\nabla\phi\right)^2 + V(\phi)\right] \tag{3.2}$$

where for simplicity the scalar potential is just a mass term, $V(\phi) =$. This scalar field, like all bulk fields, generate a dual source and response in the boundary theory. To imprint a lattice, HST chose to use a scalar source of the form

$$\phi_{\text{source}} \sim A_0 \cos kx. \tag{3.3}$$

This term will *explicitly* impart x-dependence throughout all of the bulk fields, and requires an extensive numerical treatment.

Fig. 3.1 is a plot from the original HST lattice paper [18], clearly demonstrating the impact of the lattice in the low-frequency behavior of the conductivity. In particular, the Drude peak divergence of the DC conductivity has disappeared now that $\lim_{\omega\to 0} \text{Im}(\sigma) = 0$. One might consider that the peak in Re(σ) has broadened and imparted a host of nontrivial features to the low-frequency regime. Indeed, the low frequency behavior now follows a

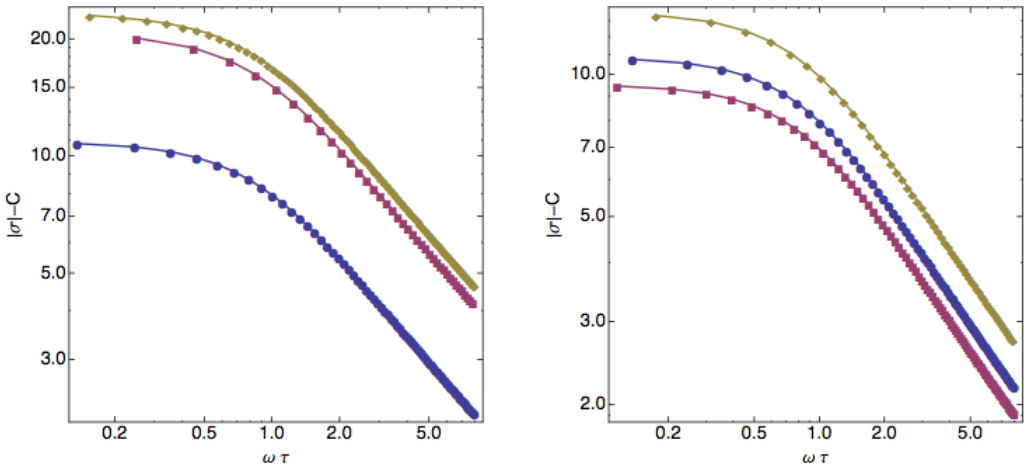

Figure 3.2: From [18]. Magnitude of the optical conductivity minus the offset C, displayed as log-log plots. Left: $T/\mu = 0.115$ and wavenumber of $k_0 = 3$ (diamonds), $k_0 = 1$ (squares), and $k_0 = 2$ (circles). Right: $k_0 = 2$ with $T/\mu = 0.98$ (diamonds), $T/\mu = 0.115$ (circles), and $T/\mu = 0.13$ (squares). Both plots take $A_0/k_0 = 3/4$ exhibit a power law falloff with exponent $-2/3$ (indicated by the slope of the linear part).

Drude-like form for simple hydrodynamic momentum dissipation [19],

$$\sigma(\omega) = \frac{K\tau}{1 - i\omega\tau} \tag{3.4}$$

where τ is a characteristic relaxation time for the fluid's momentum. The Drude form captures the behavior of any quantum field theories described by hydrodynamic models, and this includes the low-frequency behavior in strange metals [20].

Beyond these intuitive results, the HST treatment claimed a very surprising feature: that in the mid-frequency regime, the optical conductivity follows a power law

$$|\sigma(\omega)| \sim \omega^{-2/3}. \tag{3.5}$$

This is *precisely* the power law observed in the mid-infrared frequency range of the optical conductivity [20–23] for optimally doped copper-oxide superconductors! On the face of it, this is a stupendously unexpected result. If true, the power law is perhaps a fundamental feature that can occur irrespective of the microscopic behavior of the materials it occurs in. Thus, the holographic lattice must offer some tunable parameter to control a mid-frequency scaling regime. In Fig. 3.2 is the log-log plot from [18] used to demonstrate the power law. Over a short band in frequency, it seems the power law is present due to the $-2/3$ slope.

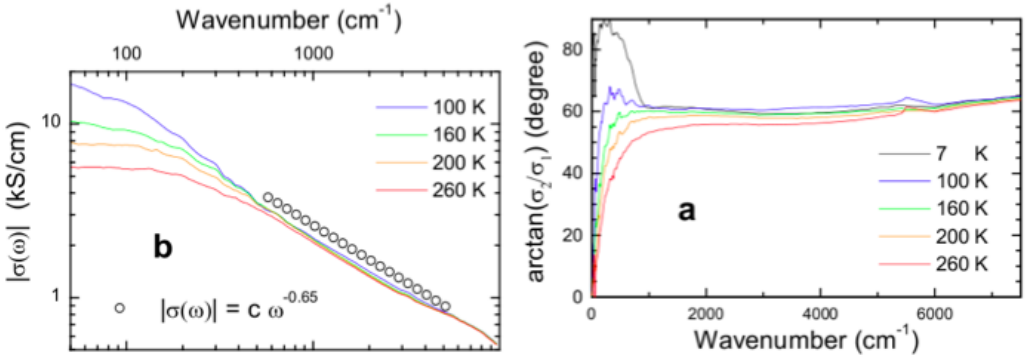

Figure 3.3: From [20]. On the left, the optical conductivity of optimally doped $Bi_2Sr_2Ca_{0.92}Y_{0.08}Cu_2O_{8+\delta}$ in its normal state. There is a universal $\omega^{-2/3}$ scaling over a wide range of temperatures. On the right, the phase angle between the real and imaginary parts of the conductivity.

Power laws are ubiquitous in critical phenomena as they are the fingerprint of scale invariant correlations. To no surprise then, quantum criticality is the most commonly proffered explanation [24–26] for the power-law scaling. However, we currently have no microscopic understanding of how quantum criticality emerges from the strong correlations that mediate the normal state near optimal doping. Such an understanding requires precise knowledge of the low-energy degrees of freedom in the strongly coupled regime. Ascertaining these degrees of freedom has proven difficult because the integral of the optical conductivity [27, 28] up to the optical gap exceeds the number of doped holes. Consequently, no one-to-one mapping [29] exists between the number of doped holes and the actual propagating degrees of freedom at low energy.

An early spoiler: we will go through a lot of analysis and model comparisons to arrive the conclusion that the result is false. There is no power law to speak of. The true lesson after the rigamarole of numerical holography is this: beware the log-log plot! This type of plot is useful precisely for analyzing data over several orders of magnitude, and nothing less!

3.1.2 The Q-lattice

However, the key claim that Einsteinian gravity, a Maxwell field and an inhomogeneous charge density encode the mid-infrared conductivity of the cuprates has been called into question [30, 31]. In reference [30] Donos and Gauntlett (DG) studied a model inspired by the Q-ball potential of Coleman [32] which has the added simplification that only ordinary rather than partial differential equations need be solved to obtain the conductivity. Their scalar

field contribution is of the form

$$I_\phi = -\int_{\mathcal{M}} \frac{1}{2}\left[|\nabla\phi|^2 + V\left(|\phi|^2\right)\right], \tag{3.6}$$

where the complex scalar field uses a plane wave formulation,

$$\phi(r,x) = \varphi(r)e^{ikx}. \tag{3.7}$$

This clever choice imparts x-dependence on the model *implicitly*, but will leave all Einsteinian background fields independent of x, bypassing the need for PDEs. Inherently, this consideration leads to a uniform charge density. Added differences with the work of HST is the use of a scalar mass of $m^2 = -3/2$[1] and the radial gauge as opposed to the de Donder gauge and Lorenz gauges. Their optical conductivity results are displayed in Fig. 3.4, which captures the low-frequency Drude form we expect for a dissipative system. In addition, rather than using a log-log plot to discern the presence of a power law, they plotted

$$\alpha = 1 + \omega\frac{|\sigma|''}{|\sigma|'}. \tag{3.8}$$

A value of $\alpha = -2/3$ would correspond to the mid-infrared power-law conductivity of the cuprates. None was found. In fact, α was found to vary fairly widely as a function of frequency precisely where the power law was reported by HST, as observed in Fig. 3.5. Similar results from a slightly different model have also been reported in [31].

3.1.3 The Two-Scalar Model

If we presume both results are correct, then the only resolution to the problem must lie somewhere in the explicit x-dependence of the background fields! In order to investigate the discrepancy, we introduced the two-scalar model to parameterize a smooth transformation between the two models [33]. Consider the action

$$I_\phi = -\int_{\mathcal{M}} \sum_{I=1}^{2}\left[\frac{1}{2}\left(\nabla\phi_I\right)^2 + V(\phi_I)\right] \tag{3.9}$$

with the usual mass potential $V(\phi) = \frac{m^2}{2L^2}\phi^2$. For our scalar field sources, we demand

$$\begin{aligned}\phi_{1,\text{source}} &\sim A_1\cos\left(k_1 x + \frac{\theta}{2}\right),\\ \phi_{2,\text{source}} &\sim A_2\cos\left(k_2 x - \frac{\theta}{2}\right),\end{aligned} \tag{3.10}$$

[1]Extremal RN-AdS$_4$ has an emergent $AdS_2 \times \mathbb{R}^2$ geometry near the horizon, which hosts a quantum dual with a Breitenlohner-Freedman (BF) bound higher than that of the boundary theory. Donos et al. argue that the HST results may be unstable because their chosen scalar field mass violates the BF bound in the near-horizon CFT.

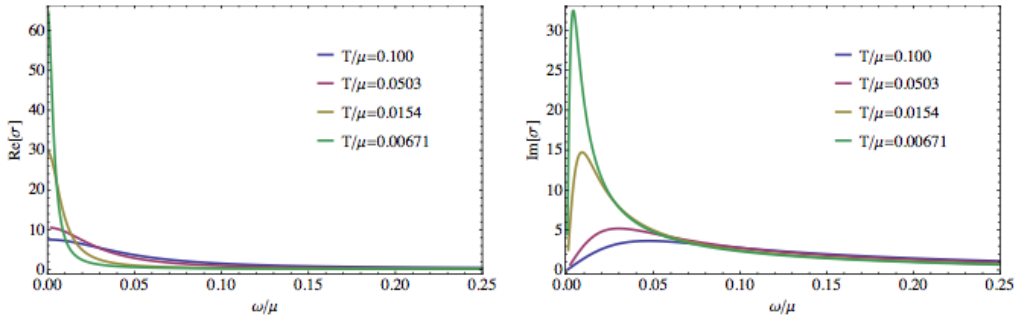

Figure 3.4: Real and imaginary parts of the optical conductivity in the Q-lattice model with $\lambda/\mu = 1/2$ and $k/\mu = 1/\sqrt{2}$. The falloff of Im σ and the broad peak in Re σ in the zero frequency limit are indicative of a broadened Drude peak stemming from breaking of translational invariance.

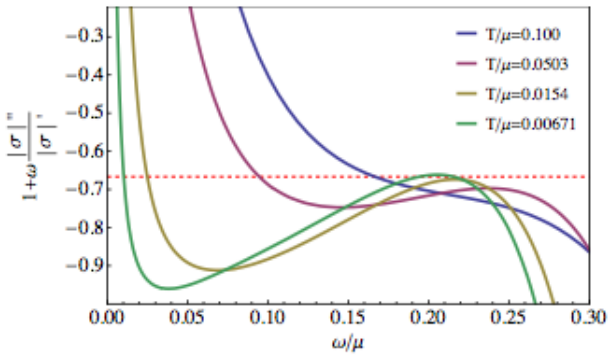

Figure 3.5: An $\omega^{-2/3}$ falloff of $|\sigma(\omega)|$ is reflected in a constant value of $-2/3$ for $1 + \omega(|\sigma|''/|\sigma|')$ (red dashed line). The Q-lattice does not exhibit universal scaling of this form for $\lambda/\mu = 1/2$ and $k/\mu = 1/\sqrt{2}$.

For the selection $A_1 = A_2$ and $k_1 = k_2$, the phase θ smoothly shifts between the two lattice solutions. Specifically, for $\theta = 0$ the HST lattice obtains, and for $\theta = \pi/2$ the Q-lattice obtains, with the two scalar fields functioning identically to the real and imaginary parts of a complex scalar field.

The equations of motion for this model are

$$E_{ab} \equiv R_{ab} - \frac{2\Lambda}{d_s} g_{ab} + \sum_{I=1}^{2} \left(\frac{1}{2} \nabla_a \phi_I \nabla_b \phi_I + \frac{1}{d_s} V(\phi_I) g_{ab} \right) - \frac{1}{2} \left(F_{ac} F_b^{\ c} - \frac{1}{2d_s} F^2 g_{ab} \right) = 0, \tag{3.11a}$$

$$M_a \equiv \nabla_b F^b_{\ a} = 0, \tag{3.11b}$$

$$\Xi_I \equiv \Box \phi_I - V'(\phi_I) = 0. \tag{3.11c}$$

Here we have written the metric's equation of motion E_{ab} only in terms of

the Ricci tensor and not the Ricci scalar, which can always be eliminated by taking the trace of the equation.

3.2 Static Solution with Spatial Dependence

The first objective is to find a static solution to (3.11), which requires a numerical approach. We will assume that, in addition to the usual radial dependence in AdS solutions, there is also some non-trivial x-dependence for one of our spatial coordinates and invariant in y, the other. First, we must make an ansatz that will be computer-friendly. Our line element takes the form

$$ds^2 = \frac{L^2}{u^2}\Bigg[\frac{Q_{uu}}{(1-u)P(u)}du^2 - (1-u)P(u)Q_{tt}dt^2 + Q_{xx}(dx + Q_{ux}du)^2 + Q_{yy}dy^2\Bigg]. \tag{3.12}$$

In addition, we format the $U(1)$ and scalar fields as

$$A = (1-u)a(u,x)dt, \tag{3.13}$$

$$\phi_I = u^{\Delta_-}\varphi_I(u,x), \tag{3.14}$$

where Δ_- is the smallest (*i.e.*, leading) power in ϕ_I as $u \to 0$. The functions Q_{ab}, a and φ_I will be determined numerically by solving Eq. (3.11). We have previously worked with the radial coordinate r to measure from horizon at r_+ to boundary at $r \to \infty$. For the purposes of numerical computation, we would like to compactify this coordinate. We have made the transformation to Poincaré coordinates with

$$u = \frac{r_+}{r} \tag{3.15}$$

so the entire radial spacetime is collapsed onto $u \in [0,1]$, with $u = 0$ the boundary and $u = 1$ the horizon. To appropriate the numerical formatting, we have taken out factors of u and $(1-u)$ in our ansatz. Then, we ensure that the remaining functions all follow boundary conditions to guarantee the asymptotic forms we desire. The function $P(u)$ is a remnant from the emblackening factor, which for AdS-RN$_4$ we take to be

$$P(u) = 1 + u + u^2 - \frac{\mu_0^2}{2}u^3. \tag{3.16}$$

This ansatz clearly reduces to the planar Reissner-Nordström black hole when $Q_{uu} = Q_{tt} = Q_{xx} = Q_{yy} = 1$, $Q_{ux} = 0$, $a = \mu = \mu_0$ and $\varphi = 0$. We will also note that the boundary line element is easily interpreted as a 2+1 Minkowski metric,

$$ds^2_{\text{bdy}} = -dt^2 + dx^2 + dy^2. \tag{3.17}$$

The lattice will be imposed via the scalar field sources. Asymptotically, the scalar fields takes the form

$$\phi_I = u^{\Delta_-}\phi_I^{(-)}(x) + u^{\Delta_+}\phi_I^{(+)}(x) + \cdots \tag{3.18}$$

where $\phi_I^{(-)}$ and $\phi_I^{(+)}$ are the source and response of some dual scalar operator $\mathcal{O}$ in the boundary, respectively.[2] The asymptotic powers $\Delta_\pm$ are given by

$$\Delta_\pm = \frac{d_s+1}{2} \pm \sqrt{\frac{(d_s+1)^2}{4} + m^2L^2}, \tag{3.19}$$

and thus the scalar field mass determines the asymptotic scaling forms. In our calculations, we consider for convenience $m^2L^2 = -2$ which generates the amiable leading powers $\Delta_- = 1$ and $\Delta_+ = 2$.

To imprint the lattice, match our sources as in Eq. (3.10)

$$\begin{aligned}\phi_1^{(-)}(x) &= A_1 \cos\left(k_1 x + \frac{\theta}{2}\right), \\ \phi_2^{(-)}(x) &= A_2 \cos\left(k_2 x - \frac{\theta}{2}\right)\end{aligned} \tag{3.20}$$

These simple boundary conditions will be imprinted throughout every function. The amplitude of the lattice(s) can be tuned through the amplitudes A_I and the wavenumbers $k_I = 2\pi/l_I$ set length scales l_I that can be interpreted as lattice spacings. For simplicity, we have limited ourselves to a one-dimensional lattice, but the effects can be generalized to higher dimensions at a great cost to numerical complexity.

Instead of solving $E_{ab} = 0$, we modify our equations with the DeTurck term discussed in section such and such,

$$E^H_{ab} = E_{ab} - \nabla_{(a}\xi_{b)}, \tag{3.21}$$

where the vector

$$\xi^a = g^{bc}\left(\Gamma^a_{bc} - \breve{\Gamma}^a_{bc}\right) \tag{3.22}$$

is defined with respect to a reference metric $\breve{g}_{ab}$. For the reference metric, we use exactly the ansatz (3.12) with the aforementioned RN-ADS$_4$ solution. It is paramount that we use a reference metric with a similar structure to our eventual solution; that is, one with the same poles.

Holography is fundamentally about boundary conditions and it is time to define ours. At the boundary, we will impose Dirichlet conditions

$$\begin{aligned}&Q_{uu}(0,x) = Q_{tt}(0,x) = Q_{xx}(0,x) = Q_{yy}(0,x) = 1, \\ &Q_{ux}(0,x) = 0, \quad a(0,x) = \mu, \quad \varphi_I(0,x) = \phi_I^{(-)}(x).\end{aligned} \tag{3.23}$$

[2]It is also possible to consider the reverse where ϕ_+ serves as the source and ϕ_- the response, which is known as *alternative quantization*.

At the horizon we specify regularity conditions. We assume that all our functions follow a Taylor expansion about the horizon,

$$Q_{ab}(u,x) = Q_{ab}(1,x) - (1-u)\partial_u Q_{ab}(1,x) + \cdots \tag{3.24a}$$
$$a(u,x) = a(1,x) - (1-u)\partial_u a(1,x) + \cdots \tag{3.24b}$$
$$\varphi_I(u,x) = \varphi_I(1,x) - (1-u)\partial_u \varphi_I(1,x) + \cdots \tag{3.24c}$$

and plug these expansions into the equations of motion (3.11) and demand they are solved order-by-order at $u = 1$. This will in general fix relationships among the (0) and (1) coefficients giving Robin-type boundary conditions. One such condition is $Q_{uu}(1,x) = Q_{tt}(1,x)$, and thus the corresponding temperature of the black hole is

$$T = \frac{P(1)}{4\pi L} = \frac{6-\mu_0^2}{8\pi L}. \tag{3.25}$$

Finally, along the x-direction we will take periodic boundary conditions on all functions,

$$Q_{ab}(u,x) = Q_{ab}(u,x+l), \tag{3.26a}$$
$$a(u,x) = a(u,x+l), \tag{3.26b}$$
$$\varphi_I(u,x) = \varphi_I(u,x+l), \tag{3.26c}$$

which we can automatically achieve by utilizing a Fourier differentiation matrix. For simplicity we choose $l = 2\pi$, with the option to have periodicity of higher harmonics.

Here we present some numerical results for the static background. In Fig. 3.6 we demonstrate the shift between a uniform and x-dependent charge density for our two models. In Fig. 3.7 we use the decreasing magnitude of $\max(\xi^2)$ to demonstrate convergence for higher grid density in u. Convergence in x proceeds in avalanches, thanks to effective Nyquist sampling. The u convergence is plotted for a uniform grid. We notice saturation occurring at $N_u \gtrsim 50$ points, which is merely due to machine precision! This result can be improved without increase to precision by patching together higher density grids near the boundary. We have used higher precision results for all our numerics, and use this plot to demonstrate both the convergence of our scheme and the importance of careful grid formulation. In Fig. 3.8 we provide a sample static solution for all of our background fields.

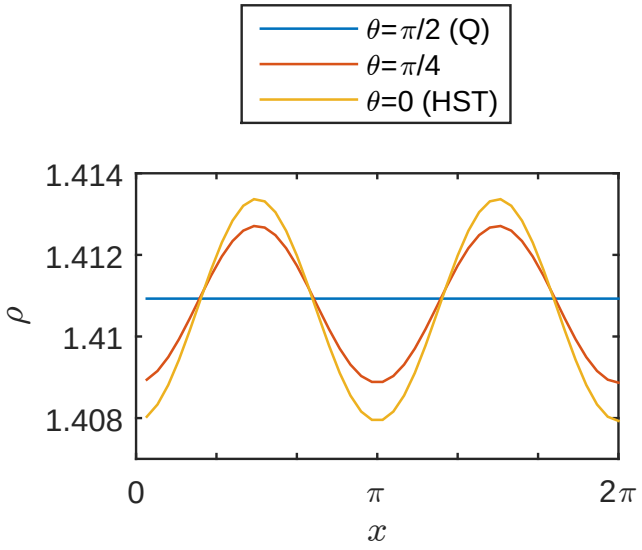

Figure 3.6: Plot of the charge density $\rho = \lim_{u\to 0} \sqrt{-g} F^{tu}$ for same parameters as Fig. 3.8.

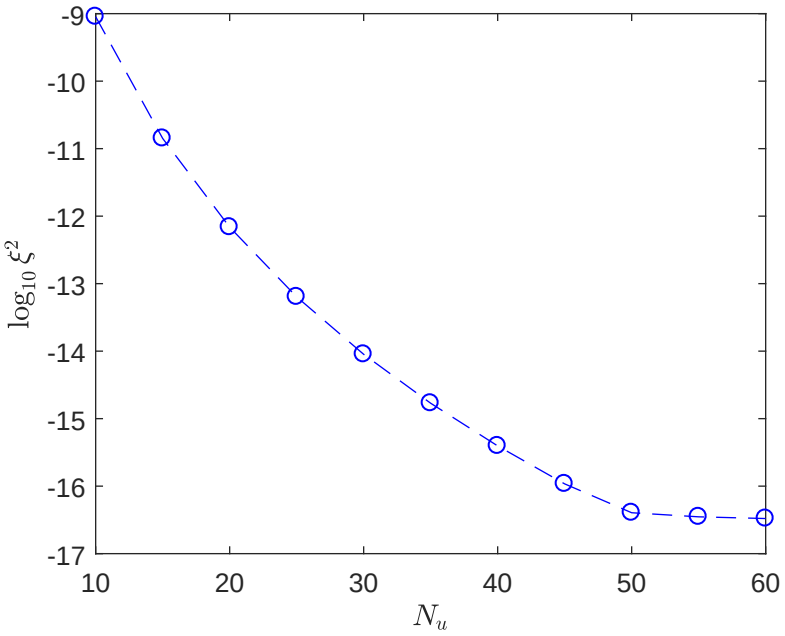

Figure 3.7: Plot demonstrating convergence for increasing grid density in u with N_u grid points. Model is calculated at double precision with $N_x = 35$ with a uniform grid, $k_1 = k_2 = 2$ and $\theta = \frac{\pi}{4}$ (other parameters: $\mu = 1.4\sqrt{2}$, $T/\mu = 0.115$, and $A_1 = A_2 = 2$).

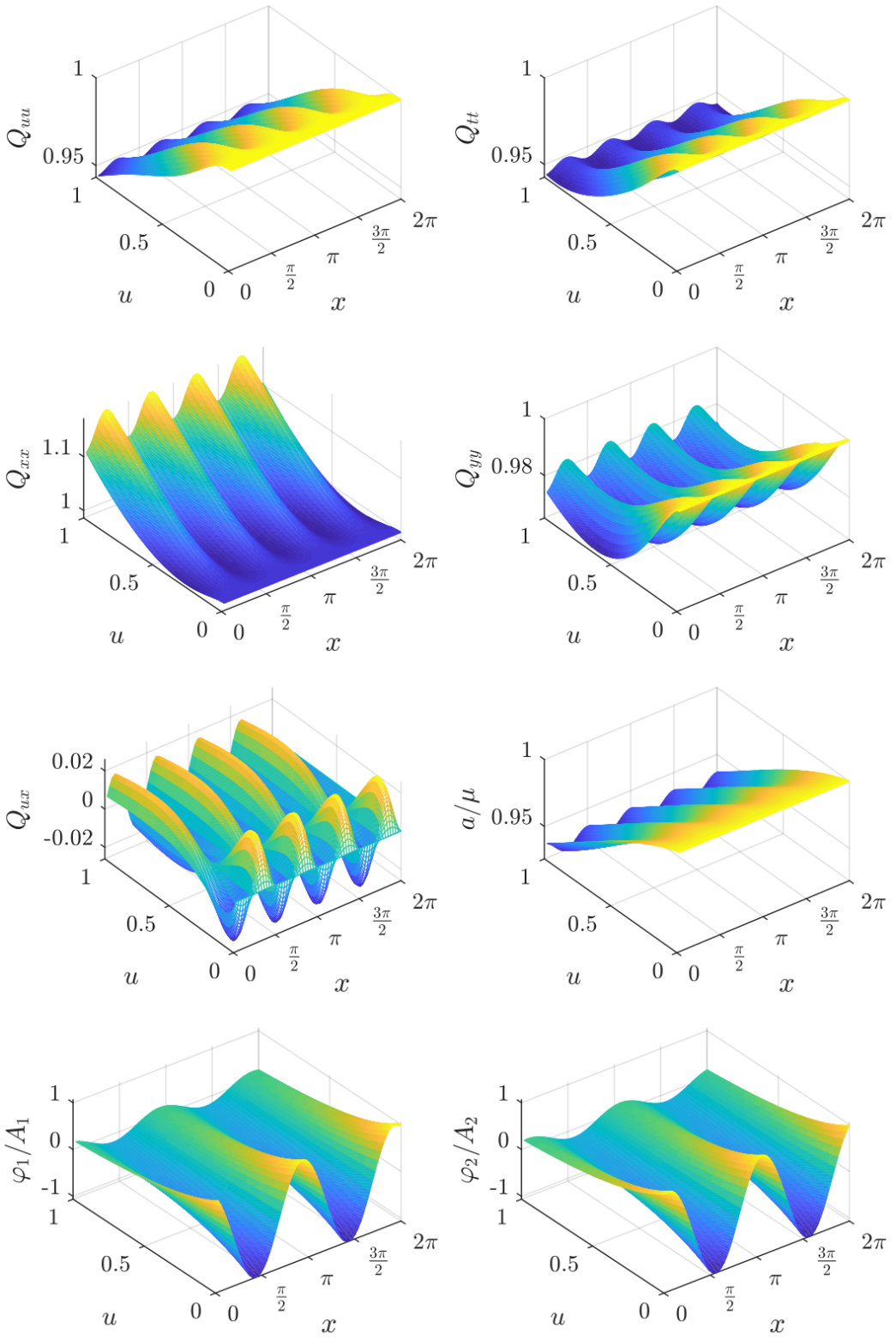

Figure 3.8: The full static solution for $k_1 = k_2 = 2$ and $\theta = \frac{\pi}{4}$ (other parameters: $\mu = 1.4\sqrt{2}$, $T/\mu = 0.115$, and $A_1 = A_2 = 2$). This data is taken for $N_x = 65$ and $N_u = 200$ and has $\xi^2 \lesssim 10^{-23}$.

3.3 Conductivity of the Holographic Lattice

3.3.1 Fluctuation Ansatz

Upon constructing the static background with broken translation invariance, we can now poke and prod it to obtain time-dependent response functions at the linear response level. Such response functions can be obtained by considering linear time-dependent fluctuations about the static background. In particular we aim to extract the AC conductivity $\sigma(\omega)$ by supplying a uniform time-dependent electric field $e^{-i\omega t}E$ in the x-direction. Denoting the background fields with bars, we write

$$g_{ab} = \overline{g}_{ab} + \delta g_{ab}, \quad A_a = \overline{A}_a + \delta A_a, \quad \phi_I = \overline{\phi}_I + \delta\phi_I, \tag{3.27}$$

where δg_{ab}, δA_a and $\delta\phi_I$ are fluctuations small compared to the static background. The linearized equations of motion (3.11) governing the fluctuations are given by

$$\begin{aligned}
&-\frac{1}{2}\overline{\Box}\delta g_{ab} - \overline{R}_{acbd}\delta g^{cd} + \overline{R}_{(a}{}^{c}\delta g_{b)c} + \overline{\nabla}_{(a}\overline{\nabla}^{c}\delta\hat{g}_{b)c} = \Lambda\delta g_{ab} \\
&\qquad + \sum_{I=1}^{2}\left[\overline{\nabla}_{(a}\overline{\phi}_I\overline{\nabla}_{b)}\delta\phi_I + \frac{1}{4}V'\left(\overline{\phi}_I\right)\right]\overline{g}_{ab}\delta\phi + \frac{1}{2}V\left(\overline{\phi}\right)\delta g_{ab} + \overline{F}_{(a}{}^{c}\delta F_{b)c} \\
&\qquad - \frac{1}{2}\overline{F}_{ac}\overline{F}_{bd}\delta g^{cd} - \frac{\delta g_{ab}}{8}\overline{F}^2 - \frac{\overline{g}_{ab}}{4}\overline{F}^{cd}\delta F_{cd} + \frac{\overline{g}_{ab}}{4}\overline{F}_{cd}\overline{F}_{e}{}^{d}\delta g^{ce} \qquad (3.28a) \\
&\overline{\Box}\delta A_a - \overline{R}_{a}{}^{b}\delta A_b - \overline{\nabla}_a\overline{\nabla}^{b}\delta A_b - \overline{F}_{ca}\overline{\nabla}_b\delta\hat{g}^{bc} - \delta g^{bc}\overline{\nabla}_b\overline{F}_{ca} - \overline{F}^{bc}\overline{\nabla}_b\delta g_{ca} = 0, \qquad (3.28b) \\
&\overline{\Box}\delta\phi_I - \overline{\nabla}_a\delta\hat{g}^{ab}\overline{\nabla}_b\overline{\phi}_I - \delta g^{ab}\overline{\nabla}_a\overline{\nabla}_b\overline{\phi}_I - V''\left(\overline{\phi}\right)\delta\phi_I = 0, \qquad (3.28c)
\end{aligned}$$

where $\delta F = d(\delta A)$ is the field strength perturbation and $\delta\hat{g}_{ab} \equiv \delta g_{ab} - (\delta g/2)\overline{g}_{ab}$ is the usual trace-reversed metric perturbation. Note that $\delta g^{ab} = -\delta(g^{ab})$, which is to say that the metric perturbation with raised indices is not the same as the perturbation of the metric's inverse.

The background is static, so a Fourier transform in time is salubrious. All the fluctuations can be expressed

$$\delta g_{ab}(u,t,x) \sim e^{-i\omega t}\delta\tilde{g}_{ab}(u,x), \tag{3.29a}$$

$$\delta A_a(u,t,x) \sim e^{-i\omega t}\delta\tilde{A}_a(u,x), \tag{3.29b}$$

$$\delta\phi_I(u,t,x) \sim e^{-i\omega t}\delta\tilde{\phi}_I(u,x), \tag{3.29c}$$

and in the Fourier basis the problem is once again reduced to a two-dimensional (u,x) grid.

The electric field will be generated by δA_x, which then feeds back into the equations of motion and turns on various fluctuations. In general, this can turn on 12 fluctuations:

$$\{\delta g_{uu}, \delta g_{ut}, \delta g_{ux}, \delta g_{tt}, \delta g_{tx}, \delta g_{xx}, \delta g_{yy}, \delta A_u, \delta A_t, \delta A_x, \delta\phi_1, \delta\phi_2\}, \tag{3.30}$$

where all the terms with odd y-parity can be turned off by symmetry. The fluctuation equations possess the gauge symmetries of diffeomorphism invariance and $U(1)$ invariance. One common choice is to pick the de Donder and Lorenz gauges, respectively given by

$$\overline{\nabla}^a \delta\hat{g}_{ab} = 0, \quad \overline{\nabla}^a \delta A_a = 0. \tag{3.31}$$

Such a choice would leave only d'Alembertians as second derivative terms in our fluctuation equations (3.28) . Notably, these gauges are *not* sufficient in general to fix a unique solution and further choices (for example, the Coulomb gauge) are required. HST chose this gauge and would go on to solve the 11 coupled PDEs (one scalar field turned off). There is a more convenient choice that will reduce the number of equations we have to work with.

Instead, the number of fluctuations to work with can be cleanly reduced with a radial gauge,

$$\delta g^{ua} = 0, \quad \delta A^u = 0. \tag{3.32}$$

We can take the ansatz

$$\begin{aligned}
\delta ds^2 = \frac{1}{u^2}[&-fQ_{tt}h_{tt}dt^2 + Q_{xx}h_{xx}\left(dx + Q_{ux}du\right)^2 + Q_{yy}dy^2 \\
&+ 2fQ_{tt}h_{tx}dt\left(dx + Q_{ux}du\right)], && \text{(3.33a)} \\
\delta A = (1-u)b_t dt &+ b_x\left(dx + Q_{ux}du\right), && \text{(3.33b)} \\
\delta\phi_I = u^{\Delta_-}&\psi_I, && \text{(3.33c)}
\end{aligned}$$

This has reduced our pool of functions to 8: $\{h_{tt}, h_{tx}, h_{xx}, h_{yy}, b_t, b_x, \varphi_1, \varphi_2\}$. Note that all 12 equations of motion still need to be solved!

Regularity will imply that $h_{tt} \sim O(1-u)$, which is to say the horizon structure is unmodified, maintaining the same location and the same temperature.[3] It is convenient to define

$$h_{xx} = (1-u)h_+ + h_-, \qquad h_{yy} = (1-u)h_+ - h_-, \tag{3.34}$$

which is also implied by the horion structure. This reveals that the trace of the metric fluctuations vanishes at the horizon.

3.3.2 Fluctuation Boundary Conditions

As with the static background, we will specify Dirichlet conditions at the boundary and regularity conditions at the horizon. In the radial gauge, there are 7 second-order differential equations to solve, giving 14 conditions to fix. However, the 4 remaining radial equations of motion must *also* be solved. Fortunately, this can be swiftly accomplished with a choice of boundary

[3]This fall-off is of course guaranteed by the radial gauge.

conditions (as we might expect, seeing how this is a gauge theory). To see this, remember that everywhere the Einstein-Maxwell equations of motion obey a set of continuity equations,

$$\nabla_a E^{ab} = 0, \quad \nabla_a M^a = 0. \tag{3.35}$$

(define these things) By construction, we suppose that our non-radial equations of motion will be solved everywhere. Then if the radial equations are solved at a single point, $E^{ua} = 0$ and $M^u = 0$, the continuity equation requires that $\partial_u E^{ua} = 0$ and $\partial_u M^u = 0$ at that point as well. Hence, the radial equations would not just be solved at that point but in the locus of all nearby points in the radial direction. And on it goes. Therefore, the requirement that the radial equations are solved to lowest order at a single point in u is sufficient to fix them everywhere. Thus, we can fix the radial equations to be solved at the horizon and simultaneously solve all 11 equations.

Near the black hole horizon, all time-dependent functions take infalling boundary conditions. This is the statement that in tortoise coordinates, all fluctuations take the form of waves near the horizon, with infalling waves corresponding to causal response functions and outgoing waves to anticausal ones.[4] The singularity present at $u = 1$ is not a physical singularity; it can be removed with a coordinate transformation. If we switch over to infalling Eddington-Finkelstein coordinates, defined by a time coordinate shift of the form

$$dt_+ = dt + \frac{du}{f}, \tag{3.36}$$

then the coordinate singularity at $u = 1$ is no longer present. Because the singularity can removed with a gauge choice, this is not a physical singularity. Additionally, near the horizon,

$$e^{-i\omega t} \to e^{-i\omega t_+}(1-u)^{\frac{i\omega}{4\pi T}}, \tag{3.37}$$

which itself is the form of an infalling wave.Thus, we demand our functions take the form

$$h_{ab} = e^{-i\omega t}\left(1-u^3\right)^{\frac{i\omega}{4\pi T}}\tilde{h}_{ab}, \tag{3.38}$$

$$b_a = e^{-i\omega t}\left(1-u^3\right)^{\frac{i\omega}{4\pi T}}\tilde{b}_a, \tag{3.39}$$

$$\psi_I = e^{-i\omega t}\left(1-u^3\right)^{\frac{i\omega}{4\pi T}}\tilde{\psi}_I \tag{3.40}$$

and that the functions $\{\tilde{h}_{ab}, \tilde{b}_a, \tilde{\psi}_I\}$ are regular at the horizon, infalling boundary conditions are guaranteed.[5] In this way, the horizon conditions are reduced to the very same type of Robin boundary conditions that the static

[4] Anticausal boundary conditions correspond to a white hole.

[5] The factor u^3 is only chosen for convenience.

background was constructed with. It is convention for physicists to be lazy in notation, so in keeping with tradition we will from hereon just t instead of t_+, which will surely never be confusing.

Now let us look toward the boundary at $u = 0$. The functions take the asmyptotic form

$$\tilde{h}_{ab}(u,x) = \tilde{h}^{(0)}_{ab}(x) + \cdots + u^3\tilde{h}^{(3)}_{ab}(x) + \cdots , \tag{3.41a}$$

$$\tilde{b}_a(u,x) = \tilde{b}^{(0)}_a(x) + u\tilde{b}^{(1)}_a(x) + \cdots , \tag{3.41b}$$

$$\tilde{\psi}_I(u,x) = \tilde{\psi}^{(0)}_I(x) + \cdots + u^{3-2\Delta}\tilde{\psi}^{(3-2\Delta)}_I(x) + \cdots , \tag{3.41c}$$

where the listed components are the non-normalizable and normalizable modes to be fixed with boundary data. If we use 11 regularity conditions, one for each equation of motion, then only three conditions remain to be specified at the boundary. However, still seven Dirichlet conditions must be enforced and we must avoid overconstraint.

The number of boundary conditions can be reduced with a clever gauge choice [34]. Combined with gauge invariance, the boundary conditions as $u \to 0$ are asymptotically constrained to be

$$u^2\left(\delta g_{ab} + \mathcal{L}_\xi \overline{g}_{ab}\right) \to 0, \tag{3.42a}$$

$$\delta A_a + \mathcal{L}_\xi \overline{A}_a + \overline{\nabla}_a \lambda \to e^{-i\omega t} E dx, \tag{3.42b}$$

$$u^{-\Delta}\left(\delta\phi_I + \mathcal{L}_\xi \overline{\phi}_I\right) \to 0, \tag{3.42c}$$

where the vector ξ^a encodes an infinitesimal diffeomorphism $x^a \to x^a + \xi^a$ via a Lie derivative $\mathcal{L}$ and the scalar field λ an infinitesimal $U(1)$ transformation. These conditions demand that both (1) the asymptotic forms of the metric, chemical potential, and scalar source are unchanged from the static background, and (2) a uniform electric field is sourced in the x-direction. The gauge transformations take the specific form

$$\xi = e^{-i\omega t}\left(\tilde{\xi}^u(x)u\partial_u + \tilde{\xi}^t(x)\partial_t + \tilde{\xi}^x(x)\partial_x\right) + \cdots \tag{3.43a}$$

$$\lambda = e^{-i\omega t}\tilde{\lambda}(x) + \cdots . \tag{3.43b}$$

These four functions $\{\tilde{\xi}^u, \tilde{\xi}^t, \tilde{\xi}^x, \tilde{\lambda}\}$ absolve four of the boundary conditions, leaving exactly three conditions to be imposed on the fluctuations, which is exactly the number of remaining conditions. Then (3.42) becomes

$$\tilde{\xi}^u = \frac{1}{2}\left(\tilde{h}^{(0)}_+ - \tilde{h}^{(0)}_-\right), \qquad \tilde{\xi}^t = \frac{i}{2\omega}\left(\tilde{h}^{(0)}_{tt} + \tilde{h}^{(0)}_+ - \tilde{h}^{(0)}_-\right)$$

$$\tilde{\xi}^{x\prime} = -\tilde{h}^{(0)}_-, \qquad \tilde{\xi}^x = \frac{i}{\omega}\left(-\tilde{h}^{(0)}_{tx} + \tilde{\xi}^{t\prime}\right), \tag{3.44a}$$

$$\tilde{\lambda} = -\frac{i}{\omega}\tilde{b}^{(0)}_t - \mu\tilde{\xi}^t, \qquad \tilde{b}^{(0)}_x = E - \mu\tilde{\xi}^{t\prime} - \tilde{\lambda}', \tag{3.44b}$$

$$\tilde{\psi}^{(0)}_I = -\tilde{\xi}^x\phi^{(-)\prime}_i - \frac{\Delta_-}{2}\left(\tilde{h}^{(0)}_+ - \tilde{h}^{(0)}_-\right)\phi^{(-)}_i. \tag{3.44c}$$

Now, the set of four gauge conditions can be eliminated, yielding

$$\tilde{h}_{-}^{(0)} - \frac{i}{\omega}\tilde{h}_{tx}^{(0)\prime} - \frac{1}{2\omega^2}\left(\tilde{h}_{tt}^{(0)\prime\prime} + \tilde{h}_{+}^{(0)\prime\prime} - \tilde{h}_{-}^{(0)\prime\prime}\right) = 0, \tag{3.45a}$$

$$\tilde{b}_{x}^{(0)} - \frac{i}{\omega}\tilde{b}_{t}^{(0)\prime} = E, \tag{3.45b}$$

$$\tilde{\psi}_{I}^{(0)} + \frac{\Delta_{-}}{2}\left(\tilde{h}_{+}^{(0)} - \tilde{h}_{-}^{(0)}\right)\phi_{I}^{(-)\prime} - \frac{i}{\omega}\tilde{h}_{tx}^{(0)}\phi_{I}^{(-)} - \frac{1}{2\omega^2}\left(\tilde{h}_{tt}^{(0)\prime} + \tilde{h}_{+}^{(0)\prime} - \tilde{h}_{-}^{(0)\prime}\right)\phi_{I}^{(-)} = 0. \tag{3.45c}$$

All the gauge artifacts introduced in the radial components of the metric are subleading; our boundary conditions are self-consistent and sufficient.

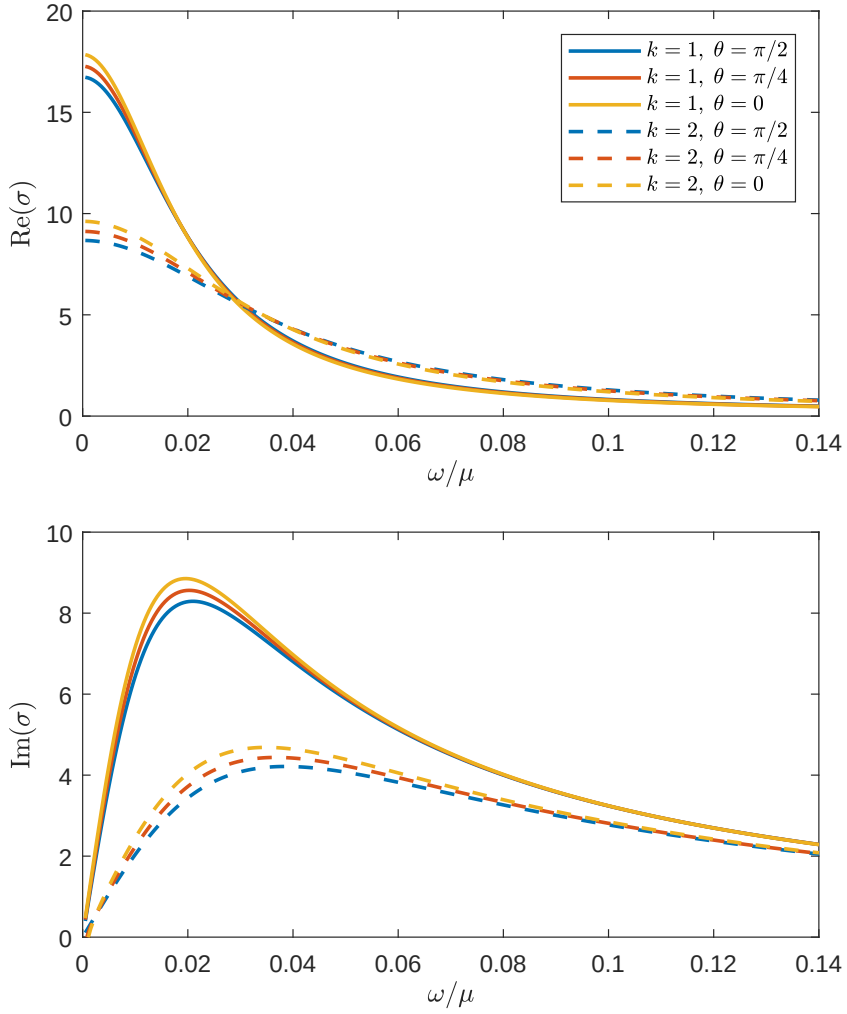

Figure 3.9: Low frequenecy plots of real and imaginary parts of the conductivity for various parameters. In each plot $A_0/k = 3/(2\sqrt{2})$, $\mu = 1.4\sqrt{2}$ and $T/\mu = 0.115/\sqrt{2}$.

This gauge choice modifies all boundary quantities, including the current

response, whose x-component is now given by

$$j^{(\rho)} = \tilde{b}_x^{(1)} - \frac{i}{2\omega}\left(\tilde{h}_{tt}^{(0)\prime} + \tilde{h}_{+}^{(0)\prime} - \tilde{h}_{-}^{(0)\prime}\right)\rho. \tag{3.46}$$

Then we can compute the average current,

$$\left\langle j^{(\rho)} \right\rangle = \frac{1}{l}\int_0^l dx j^{(\rho)} \tag{3.47}$$

and the AC conductivity will be given by the Kubo formula,

$$\sigma = \frac{\left\langle j^{(\rho)} \right\rangle}{i\omega\mathcal{E}}. \tag{3.48}$$

Because E sources all the perturbations, without loss of generality we can set $E = 1$. In Figs. 3.13 and 3.14 we display a full sample solution for the fluctuations.

Using this method, we computed the conductivity as a function of the interpolating parameter θ. Shown in Fig. 3.9 are the real and the imaginary parts of the conductivity for two different values of k and three values of θ. For each choice of parameters the low frequency conductivity obeys the Drude form. Note, even though $\theta = \pi/2$ corresponds to a uniform charge density of DG, the conductivities are almost identical to those of HST ($\theta = 0$).

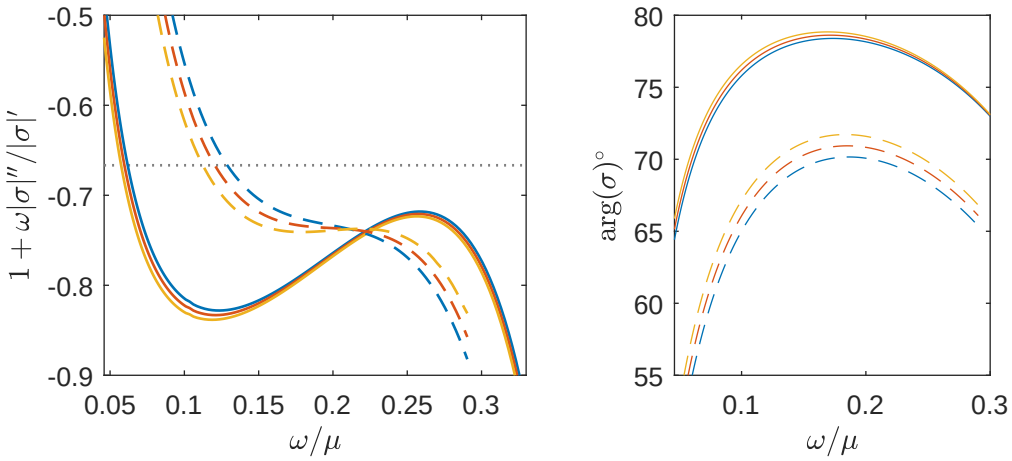

Figure 3.10: Plots of the power function and the argument of the conductivity for the same parameters as Fig. 3.9. The dotted line marks $-2/3$. Refer to Fig. 3.9 for legend.

Fig. 3.10 is the key test for the existence of the power-law conductivity. We show a couple of plots using the parameter choices of reference [18]. The dotted line on the left plot indicates a power law of $-2/3$. As is evident, regardless of the value of θ, no discernible power law exists even as k is

varied. Also of note is the fact that the DG ($\theta = \pi/2$) and HST ($\theta = 0$) models yield almost identical numerical results for the conductivity. The right figure presents the phase angle which also deviates from 60° and does not remain at any appreciable constant value over this frequency range.

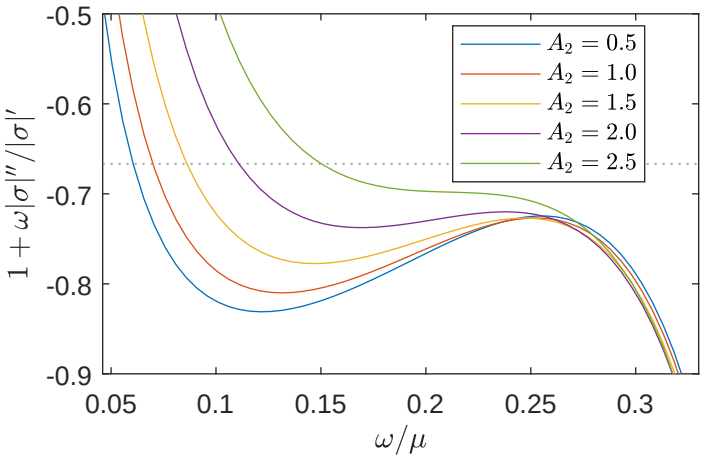

Figure 3.11: This plot was generated using $A_1 = 1.5$, $k_1 = 1$, $k_2 = 2$, $\theta = 0$, $\mu = 1.4\sqrt{2}$ and $T/\mu = 0.115/\sqrt{2}$. The amplitude A_2 of the higher harmonic lattice was adjusted.

As a final check we also varied the amplitude A_2 for a dichromatic lattice in Fig. 3.11, as this could introduce a mix of higher harmonics. In this case as well, no evident power law exists. In fact, for any range of parameters including temperature, no power law was found.

3.3.3 Conductivity Sum Rules

As part of our rigorous collection of checks we include sum rules for the optical conductivity. Our system has $\lim_{\omega\to\infty}\sigma(\omega) = 1$ for the $2+1$-dimensional boundary, and thus we define the integrated spectral weight

$$\Sigma(\omega/\mu) \equiv \int_0^{\omega/\mu} d\omega' \left[\mathrm{Re}(\sigma(\omega')) - 1\right]. \tag{3.49}$$

We here can swiftly prove that in fact, $\lim_{\omega\to\infty}\Sigma(\omega) = 0$. This fact is a consequence of the Kramers-Krönig relation. The statement of the relation begins with a complex analytic function $\chi(\omega)$ which vanishes as the real variable $\omega \to \infty$ at least as fast as $1/|\omega|$. This function must obey

$$\chi(\omega) = \frac{1}{i\pi}\mathcal{P}\int_{-\infty}^{\infty} d\omega' \frac{\chi(\omega')}{\omega' - \omega} \tag{3.50}$$

where $\mathcal{P}$ deneotes the principal part of the integral.

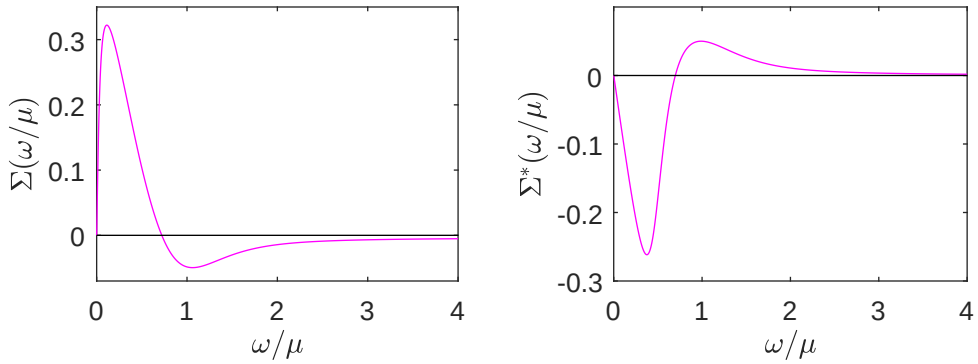

Figure 3.12: An example display of both sum rules for Σ and Σ^* satisfied within the numerical scheme.

Our conductivity is given in terms of the current-current Green function $G(\omega)$ by $\sigma(\omega) = G(\omega)/i\omega$. For the Kramers-Krönig relation to hold, we assume $G(\omega) - i\omega$ vanishes quickly enough as $\omega \to \infty$. If so, the relation merely reduces to

$$\begin{aligned} \lim_{\omega\to\infty} \Sigma(\omega) &= -\int_0^\infty d\omega' \frac{\mathrm{Im}(G(\omega') - i\omega')}{\omega'}, \\ &= \lim_{\omega\to 0^+} \frac{\pi}{2} \mathrm{Re}\left(G(\omega) - i\omega\right) = 0, \end{aligned} \tag{3.51}$$

which vanishes so long as $\mathrm{Re}(G(0)) = 0$ which is indeed true as we note $\mathrm{Im}(\sigma(0)) = 0$. The satisfaction of this sum rule is a robust feature of holographic lattices. The $D = 4$ Einstein-Maxwell theory also supports another sum rule, which defines a dual weight

$$\Sigma^*(\omega/\mu) \equiv \int_0^{\omega/\mu} d\omega' \left[\mathrm{Re}\left(\frac{1}{\sigma(\omega')}\right) - 1\right]. \tag{3.52}$$

This weight also obeys $\lim_{\omega\to\infty} \Sigma^*(\omega) = 0$ and emerges from an alternative quantization scheme [35–37]. In Fig. 3.12, we display a sample solution from our code satisfying these rules in the presence of a lattice.

3.4 Summary of Lattice Transport

Since we have introduced a model that is capable of interpolating between DG and HST and we find no power law in either case, we conclude that gravitational crystals, although adequate in describing Drude response, do not encode the power-law optical conductivity of the cuprates.

Regarding the origin of the power-law optical conductivity, the only study [38] to date that has successfully reproduced the $\omega^{-2/3}$ scaling relies on excitations which exist on all energy scales — namely scale-invariant matter or

unparticles. Given that the radial direction in AdS represents the running of coupling constants, in principle it contains the correct ingredients to capture unparticle excitations. Hence, we anticipate that some construction using gauge/gravity duality, other than the one presented here, should be able to reproduce the power law.

Beyond the specific results of the holographic lattice calculations, the numerical scheme presented in this chapter is a robust model that can handle systems vastly beyond the scope of analytic solutions; examples include Josephson junctions [5], superfluid vortices [39] and disorder [35].

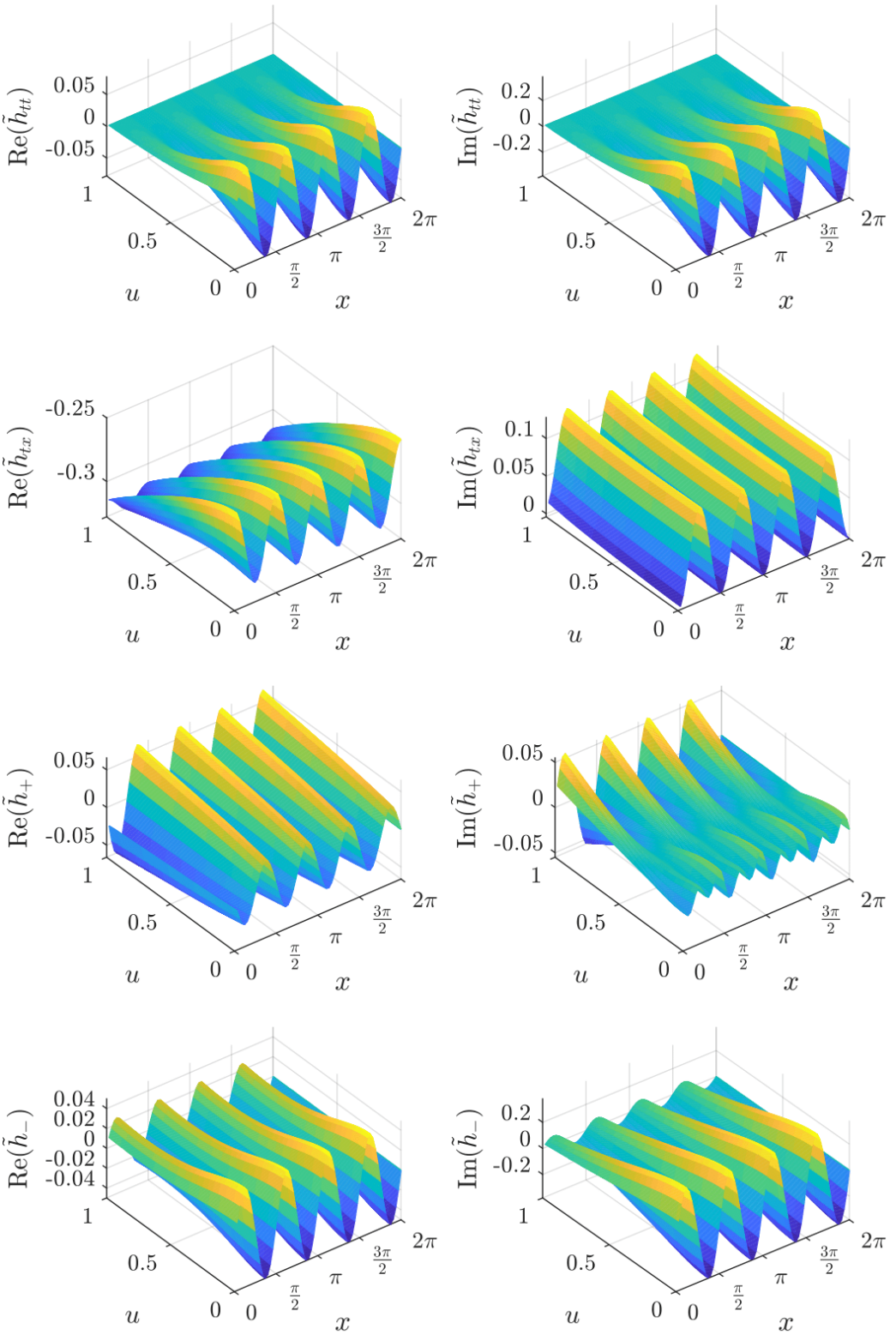

Figure 3.13: Metric fluctuations for $\omega/\mu = 0.09\sqrt{2}$ and same parameters as Fig. 3.8.

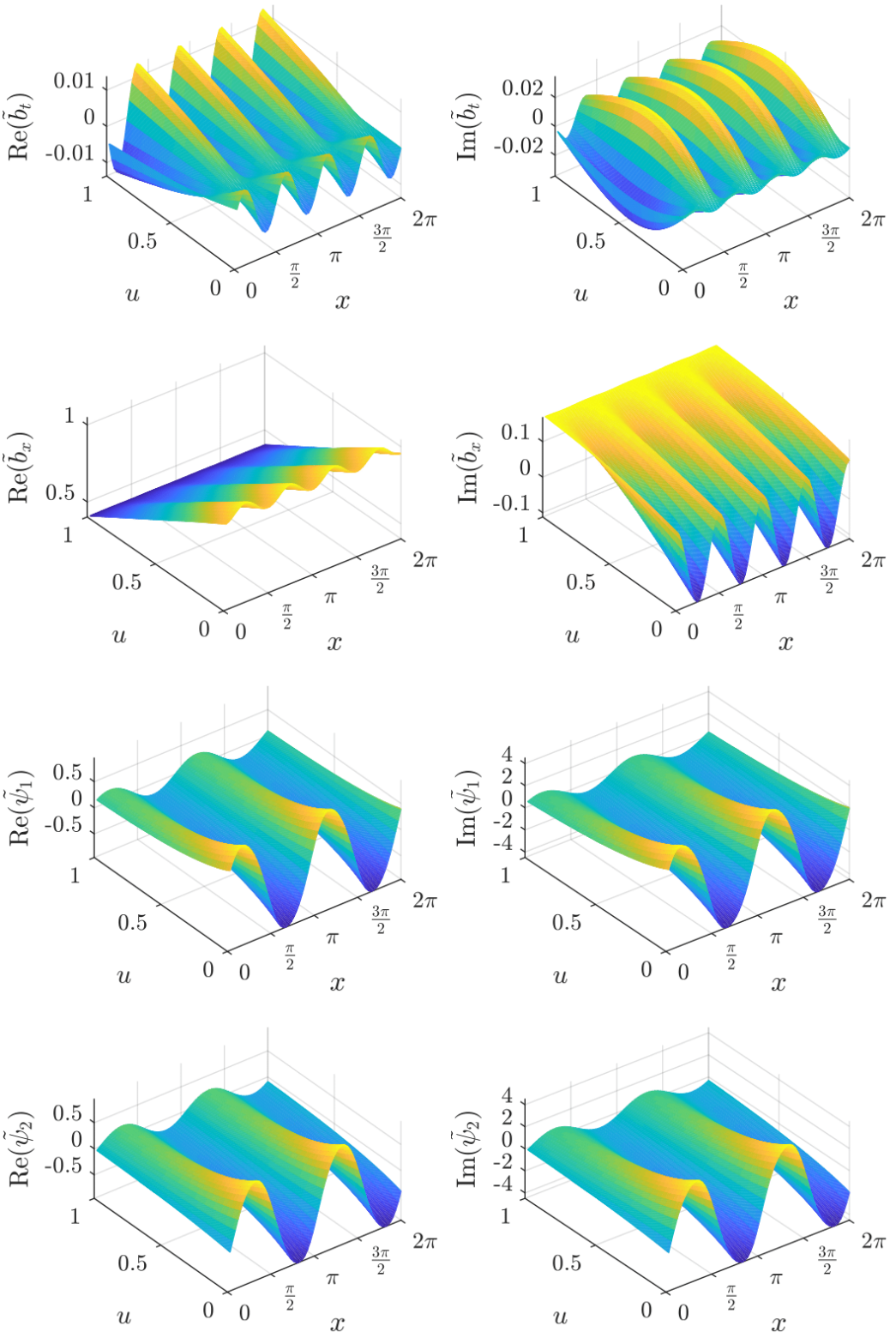

Figure 3.14: $U(1)$ and scalar field fluctuations for $\omega/\mu = 0.09\sqrt{2}$ and same parameters as Fig. 3.8.

4 Diffusive Transport and Thermodynamics in Lifshitz Holography

4.1 Introduction

Because most condensed matter systems do not conform to the full Lorentz symmetry and contain dynamical behavior characterized by Lifshitz transitions [40–43], tailoring the AdS/CFT program to condensed matter systems such as the cuprates requires a considerable extension. The simplest proffer to engineer such a non-relativistic setup is a Lifshitz geometry characterized by a dynamical critical exponent z [44–48]. A metric ansatz that encodes the features of both the dynamical exponent and a finite temperature is the form

$$ds^2 = \frac{dr^2}{r^2 f(r)} - r^{2z} f(r) dt^2 + r^2 d\vec{x}_{d_s}^2, \tag{4.1}$$

which defines a horizon by the largest root of $f(r_+) = 0$ and boundary at $r \to \infty$ where $f \to 1$. This ansatz encapsulates the scaling symmetry

$$r \to c^{-1} r, \quad t \to c^z t, \quad x^i \to c x^i. \tag{4.2}$$

at the boundary. For $z \neq 1$, this metric ansatz cannot be a vacuum solution to the Einstein equations. Indeed, such a Lifshitz geometry requires a nontrivial bulk stress-energy tensor. Herein lies the problem: there is no unique way of engineering the requisite stress-energy tensor.

A full analytic solution to an asymptotically Lifshitz geometry that features a black hole can be constructed via an Einstein-Maxwell-dilaton (EMD) action. This model is a direct extension of the AdS-Reissner-Nordström black hole to $z \neq 1$. This action is well-known in the literature as it has served as the workhorse for most of the Lifshitz papers [49–55].

In this work, we address a fully-renormalized solution to the EMD action that features both a chemical potential and a set of spatially-dependent axion fields that induce momentum dissipation for general z and dimensionality. The action is addressed completely at the level of the static background and DC transport. This range of analysis allows us to compute the set of both static susceptibilities and conductivities under a uniform "Lifshitz charge", which by the Einstein relations obtain the full set of thermoelectric diffusion constants. We are able to compare and contrast our results with universal features of diffusivity by Blake *et al.* [56, 57]. They consider the limits of

decoupled charge and thermal diffusion, and we find exact agreement in this limit. However, we find deviations from such behavior when matter interactions are cranked such that the thermoelectric coupling is significant.

A significant result we obtain once all the dust settles is that the length dependence of the transport properties, although they are governed by several independent scales ranging from the chemical potential to the strength of momentum dissipation, are ultimately controlled by the engineering dimension $[D]$ of the diffusion constants; by inspection of the diffusion equation, $[D] = 2 - z$. Consequently, the effective β-function [58],

$$\beta \equiv \frac{\partial}{\partial \ell} \frac{(\mathrm{tr}\boldsymbol{D})T}{v_B^2}, \tag{4.3}$$

should exhibit universal features as a function of the characteristic length scale ℓ. In Eq. (4.3), we measure the diffusion matrix $\boldsymbol{D}$ against the characteristic scale v_B^2/T, defined in terms of the butterfly velocity and the temperature [56]. We find that $\mathrm{sgn}(\beta) = \mathrm{sgn}(2 - z)$, indicating a fixed point at $z = 2$. At the scale-invariant point $z = 2$, diffusion is given exactly by the dimensionless number

$$D(z = 2) = \frac{1}{d_s}. \tag{4.4}$$

Our diffusion constants are strictly positive unlike the previous results with restricted range of validity for z [59, 60]. We find $z = 2$ corresponds to the fixed point associated with the length dependence of the diffusivities, in direct analogy with the β-function in Anderson localization [58]. Our conclusion here is made possible entirely because we have a regularizable boundary theory.

We find in general that diffusivity bounds [61, 62] do indeed exist for Lifshitz holography, with two possible violations. The first for $z = 1$, as is standard, has a divergent energy diffusion constant in the absence of momentum dissipation, caused by the inability of any sourced momentum to relax. The second occurs at $z \to \infty$, whereupon charge becomes completely localized and does not diffuse, manifest in the vanishing of the upper bound in the respective diffusion constant.

As a final important note, our exact treatment finds that the Ward identity associated with the Lifshitz symmetry in the EMD model. We find that the boundary stress-energy tensor $\mathbb{T}^a{}_b$ and dilaton response $\lambda_\phi \mathbb{O}_\phi$ obey

$$z\mathbb{T}^t{}_t + \mathbb{T}^{x^i}{}_{x^i} + \lambda_\phi \mathbb{O}_\phi = 0, \tag{4.5}$$

which aligns with the encoding of the Lifshitz symmetry via dilatation. This is a slight contrast to the usual identity which omits any contribution from the dilaton. In spite of this, these results are not contradictory in the context of [53, 54] for instance, due to an alternative construction of the boundary

theory and the dual stress-energy tensor. In fact, due to the nebulous nature of the interpretation of the boundary geometry, there is some leeway in the formulation.

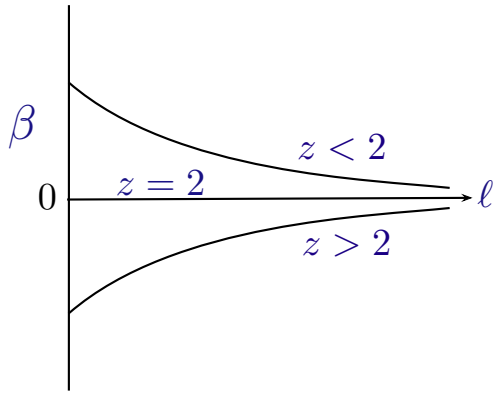

Figure 4.1: Heuristic plot of the $\beta-$function defined as the derivative of the trace of the diffusion matrix with respect to the system size. At $z = 2$, the diffusion coefficient is a universal dimensionless constant determined solely by the number of spatial dimensions. Away from $z = 2$, the diffusion constants (either charge or energy) have opposite slopes relative to an increase in the system size indicating a fixed point at $z = 2$. Regardless of z, β asymptotes to zero as the system size increases, indicating the bounded nature of the diffusivities. At $z = 2$, the diffusion equation is scale-invariant.

4.2 An Abridged History of Lifshitz Holography

The short history of Lifshitz holography is one of many fits and starts. The initial advance [44] in this context supplemented the standard bulk Lagrangian with two gauge fields, a 1-form and a 2-form both, coupled together via a topological term that controls the dynamical exponent z. Though a clean analytic construction, it is restricted to $d_s = 2$ spatial dimensions and is not amenable to emblackening factors which would encode a horizon.

Several other models have been proposed and analyzed [63], such as the Einstein-Proca model [64,65]. However the EMD model imbibes the most robust features for thermodynamics. One of the long-standing issues with this theory is the absence of a renormalization scheme for the boundary action, unlike AdS [66]. Without such a scheme, there is no real interpretation to the response functions and thermodynamics of the system. While some models could be worked out under specific conditions — the $z = 2$ Schrödinger symmetry [67] a case in point — or certain response functions obtained such as the specific heat [68], the general theory remained elusive [69]. One of

the culprits is the $U(1)$ field responsible for turning on $z \neq 1$ is poorly behaved at the boundary. There have been several proposals for dealing with this divergence. The original proposition for handling this divergence was to perform a Legendre transformation [52] to instead consider the stable dual $U(1)$ current as the fundamental variational instead of the electric field.

The Legendre transformation alone leaves the scheme incomplete. An alternative was proposed. Kiritsis and Matsuo's hydrodynamic ansatz, wherein the constant parameters controlling the static solution are promoted to slowly-varying functions of time and space, permits an analytic solution to the induced fluctuation equations. As its title suggests, this formulation allows all thermodynamic quantities to be expressed as components of a nonrelativistic fluid. The controlled expansion allows them to make contact with a renormalization scheme *without* performing a Legendre transformation. Their solution involves an infinite series of counter-terms involving the divergent $U(1)$ field and supports slowly varying transport properties.

The next stride was made by Cremonini *et al.* who examined the transverse modes of the EMD theory [70, 71]. Previous attempts on this model ignored the crucial coupling between the two $U(1)$ fields [72, 73], which must be present for a nontrivial solution. Cremonini *et al.* sought heat and charge transport response functions of the system at low frequencies. Therein, their program enabled a renormalization of specifically the transverse modes: they (1) perform the Legendre transformation for the divergent $U(1)$ field, (2) build a *second* ADM breakdown to separate time and space in the boundary with a timelike shift, and (3) renormalize the theory in terms of the corresponding $U(1)$ current and timelike shift. A feature of this scheme is that the counter-terms actually depend on both the non-normalizable and normalizable modes of the model. A renormalization scheme depending upon the theory's renormalizable modes is usually problematic, but in fact the counter-terms can be state-dependent for systems perturbed by irrelevant operators [74].

4.3 Action and Static Background

We suppose the Einstein-Maxwell-dilaton (EMD) action

$$I = -\int_{\mathcal{M}} \sqrt{-g}\left(R - \frac{1}{2}(\nabla\phi)^2 - V(\phi) - \frac{1}{4}\sum_{q=1}^{2} Z_q(\phi)F_q^2 - \frac{1}{2}X(\phi)\sum_{I=1}^{d_s}(\nabla\chi_I)^2\right) - \int_{\partial\mathcal{M}} \sqrt{-\gamma}2K + I_{\text{c.t.}}, \tag{4.6}$$

where $I_{\text{c.t.}}$ is a smattering of counter-terms to give us well-defined boundary action. Here, $\mathcal{M}$ is a $d_s + 2$-dimensional Lorentzian manifold and $\partial\mathcal{M}$ is its boundary. This action features two $U(1)$ fields, one which will serve to

assist turning on a nontrivial $z \neq 1$ solution and one which generates a standard chemical potential μ, a straight extension of the usual AdS-Reissner-Nordström black hole. The axion fields will generate momentum dissipation. This action yields the equations of motion

$$E_{ab} = R_{ab} - \frac{1}{2}\nabla_a\phi\nabla_b\phi - \frac{1}{d_s}V(\phi)g_{ab} - \frac{1}{2}\sum_{q=1}^{2} Z_q(\phi)\left(F_{q,ac}F_{q,b}{}^{c} - \frac{1}{2d_s}F_q^2 g_{ab}\right) - \frac{1}{2}X(\phi)\sum_{i=1}^{d_s}\nabla_a\chi_i\nabla_b\chi_I = 0, \tag{4.7a}$$

$$D_\phi = \Box\phi - V'(\phi) - \frac{1}{4}\sum_{q=1}^{2} Z_q'(\phi)F_q^2 - \frac{1}{2}X'(\phi)\sum_{I=1}^{d_s}(\nabla\chi_I)^2 = 0, \tag{4.7b}$$

$$M_q^a = \nabla_b\left(Z_q(\phi)F_q^{ab}\right) = 0, \tag{4.7c}$$

$$\Xi_I = \nabla_a\left(X(\phi)\nabla^a\chi_I\right) = 0. \tag{4.7d}$$

This system has a static solution, with matter fields given by

$$\begin{aligned}
&\phi = \lambda_\phi\left(\ln r + \phi_1\right), \quad \lambda_\phi = \sqrt{2d_s(z-1)},\\
&V(\phi) = -(z+d_s-1)(z+d_s), \quad Z_q(\phi) = e^{2\frac{\lambda_q}{\lambda_\phi}\phi}, \quad X(\phi) = e^{2\frac{\lambda_\chi}{\lambda_\phi}\phi},\\
&A_1 = \sqrt{\frac{2(z-1)}{z+d_s}}e^{d_s\phi_1}\left(r^{z+d_s} - r_+^{z+d_s}\right)dt, \quad \lambda_1 = -d_s,\\
&A_2 = \mu_2\left[1 - \left(\frac{r_+}{r}\right)^{z+d_s-2}\right]dt, \quad \lambda_2 = z-1,\\
&\chi_I = k\delta_{Ii}x^i, \quad \lambda_\chi = -(z-1),
\end{aligned} \tag{4.8}$$

and the emblackening factor

$$f(r) = 1 + \frac{z+d_s-2}{2d_s}\frac{\mu_2^2 e^{2(z-1)\phi_1}}{r_+^2}\left(\frac{r_+}{r}\right)^{2(z+d_s-1)} + \frac{1}{2(z-d_s)}\frac{k^2 e^{-2(z-1)\phi_1}}{r_+^{2z}}\left(\frac{r_+}{r}\right)^{2z} - M\left(\frac{r_+}{r}\right)^{z+d_s}, \tag{4.9}$$

where M is the mass of the black hole,

$$M = 1 + \frac{z+d_s-2}{2d_s}\frac{\mu_2^2 e^{2(z-1)\phi_1}}{r_+^2} + \frac{1}{2(z-d_s)}\frac{k^2 e^{-2(z-1)\phi_1}}{r_+^{2z}}. \tag{4.10}$$

Note that this solution demands $z \geq 1$ and forbids $k \neq 0$ for $z = d_s$. The temperature is

$$T = \frac{r_+^{z+1}f'(r_+)}{4\pi} = \frac{r_+^z}{4\pi}\left(z + d_s - \frac{(z+d_s-2)^2}{2d_s}\frac{\mu_2^2 e^{2(z-1)\phi_1}}{r_+^2} - \frac{1}{2}\frac{k^2 e^{-2(z-1)\phi_1}}{r_+^{2z}}\right), \tag{4.11}$$

derived by eliminating the conical singularity at the horizon.

4.4 Renormalization

In order to have a well-defined boundary action, and therefore dictionary, we must have a renormalization scheme to ensure all divergences are removed. If our action's variation can be expressed as

$$\delta I = \int_{\partial\mathcal{M}} \sum_n \Pi_n^{(\phi)} \delta\phi_n, \tag{4.12}$$

where we have symplectic data and the products of all the variations $\delta\phi_n$ and their radial conjugate momenta $\Pi_n^{(\phi)}$ are $O(1)$ as $r \to \infty$, then we have ascertained a renormalized boundary action. This scheme can be implemented not requiring a full, generalized solution but rather utilizing details of specific solutions only as necessary. The scheme for the low-frequency transverse transport properties was first laid out in [71]. If the reader seeks a more generalized approach beyond the scope of specific solutions, it is wise to turn to the radial Hamilton-Jacobi equations to define a boundary potential via a functional derivative expansion, as in [9, 10]. For our purposes, we need only examine the possible forms of nontrivial counter-terms to ascertain the renormalized action within the scope of our solution.

The variation of the action (4.6) yields

$$\delta I = \int_{\partial\mathcal{M}} \left(\frac{1}{2} T^{ab} \delta\gamma_{ab} - \sum_{q=1}^{2} J_q^a \delta A_{q,a} + \mathcal{O}_\phi \delta\phi \right), \tag{4.13}$$

$$T^{ab} = 2\sqrt{-\gamma}\left(K^{ab} - K\gamma^{ab}\right), \quad J_q^a = \sqrt{-\gamma} N_b Z_q(\phi) F_q^{ab}, \quad \mathcal{O}_\phi = \sqrt{-\gamma} N_a \nabla^a \phi, \tag{4.14}$$

where N^a is a unit vector normal to the boundary hypersurface foliating the bulk spacetime along the radial direction, and $K_{ab} \equiv \nabla_{(a} N_{b)}$. We have neglected the conjugate momenta for the axions as they vanish at the level of the static background and will not contribute to the DC currents. We absolutely do not have renormalized symplectic data, with the most glaring issue being that A_1 is divergent. However, its conjugate momentum is $O(1)$; hence we can switch to a stable scheme via a Legendre transformation. We select the counter-terms

$$I_{\text{c.t.}} = \int_{\partial\mathcal{M}} \left(A_{1,a} J_1^a + c_0^{(\text{vol})} \sqrt{-\gamma} + c_0^{(J_1^2)} \frac{J_1^2}{\sqrt{-\gamma} Z_1(\phi)} + \cdots \right), \tag{4.15}$$

where we can see the first term switches our potential to vary under J_1 instead of A_1, changing the boundary condition from Dirichlet to Neumann, as proposed in [52]. We will thusly refer to this action as I_N. While A_2 and J_2 already combine to yield an $O(1)$ boundary contribution, we must yet ensure the other responses are renormalized. Equipped with these counter-terms,

we define the new responses as

$$\mathbb{T}^a{}_b = 2\sqrt{-\gamma}\left(K^a{}_b - K\delta^a{}_b + \frac{1}{2}c_0^{(\mathrm{vol})}\delta^a_b\right) + \frac{2c_0^{(J_1^2)}}{\sqrt{-\gamma}Z_1(\phi)}\left(J_1^a J_{1,b} - \frac{1}{2}J_1^2\delta^a{}_b\right) + \cdots, \tag{4.16a}$$

$$\mathbb{A}_{1,a} = A_{1,a} + \frac{2c_0^{(J_1^2)}J_{1,a}}{\sqrt{-\gamma}Z_1(\phi)} + \cdots, \tag{4.16b}$$

$$\mathbb{O}_\phi = \sqrt{-\gamma}N_a\nabla^a\phi - c_0^{(J_1^2)}\frac{Z_1'(\phi)}{Z_1(\phi)^2}\frac{J_1^2}{\sqrt{-\gamma}} + \cdots. \tag{4.16c}$$

We find that

$$c_0^{(\mathrm{vol})} = z + 2d_s - 1, \quad c_0^{(J_1^2)} = \frac{1}{2(z+d_s)} \tag{4.17}$$

is sufficient. Note that implicit in the ellipses *are* remaining counter-terms, but the outlined contributions are the only terms that contribute to the finite action. All other terms will simply cancel divergences without contributing to the free energy and are worked out accordingly in Appendix A.1.

If we substitute in our static solution, we will find as $r \to \infty$,

$$\mathbb{T}^t{}_t = d_s M r_+^{z+d_s} + \cdots, \tag{4.18a}$$

$$\mathbb{T}^{x^i}{}_{x^j} = -M r_+^{z+d_s}\delta^i{}_j + \cdots, \tag{4.18b}$$

$$\mathbb{A}_{1,t} = \sqrt{\frac{2(z-1)}{z+d_s}}e^{d_s\phi_1}\left(\frac{M}{2} - 1\right)r_+^{z+d_s} + \cdots, \tag{4.18c}$$

$$\mathbb{O}_\phi = -\sqrt{2d_s(z-1)}\frac{M}{2}r_+^{z+d_s} + \cdots. \tag{4.18d}$$

We can now define a chemical potential associated with J_1: $\mu_1 = \lim_{r\to\infty}\mathbb{A}_{1,t}$. If we would like to switch ensembles back to Dirichlet boundary conditions, we can now use our renormalized $\mathbb{A}_1$ to do so,

$$I_D = I_N - \int_{\partial\mathcal{M}}\mathbb{A}_{1,a}J_1^a. \tag{4.19}$$

Note that the stress-energy tensor is actually traceless, which is a bit surprising for a Lifshitz theory as this is usually indicative of a scale-invariant theory, though it is not a necessary condition. Regardless, the Lifshitz scaling symmetry is manifestly encoded as a dilatation. This is reflected in the new Ward identity,

$$z\mathbb{T}^t{}_t + \mathbb{T}^{x^i}{}_{x^i} + \lambda_\phi\mathbb{O}_\phi = 0. \tag{4.20}$$

This modification to the Ward identity for the anisotropic Weyl transformation [75] is perhaps not so strange. Unlike the pure AdS case, there is no

simple interpretation of the boundary metric. Under separate constructions such as the Newton-Cartan background, modifications are expected [76].

While this renormalization machinery is sufficient for the static background, when it comes to the currents we will find that $z \neq 1$ causes the scaling of the source terms to be divergent. We can remove the source terms from our boundary action with a simple reformulation of our intrinsic metric,

$$\gamma_{ab}dx^a dx^b = -n^2\left(dt - \frac{n_i}{n^2}dx^i\right)^2 + \sigma_{ij}dx^i dx^j, \tag{4.21}$$

which functions akin to an inverted ADM formalism, which we further discuss in Appendix A.3.

4.5 Free Energy

The free energy can be computed from the on-shell action. The Ricci scalar

$$\begin{aligned} R =& \frac{1}{2}(\nabla\phi)^2 + \left(1 + \frac{2}{d_s}\right)V(\phi) \\ &+ \left(\frac{1}{4} - \frac{1}{2d_s}\right)\sum_{q=1}^{2} Z_q(\phi)F_q^2 + \frac{1}{2}X(\phi)\sum_{I=1}^{d}(\nabla\chi_I)^2 \end{aligned} \tag{4.22}$$

can be plugged in to yield the on-shell bulk action

$$I_{\text{bulk}}^{(\text{o.s.})} = -\int_{\mathcal{M}}\sqrt{-g}\left(\frac{2}{d_s}V(\phi) - \frac{1}{2d_s}\sum_{q=1}^{2} Z_q(\phi)F_q^2\right), \tag{4.23}$$

which we can expressly integrate. Combining with our boundary terms, we find that the full on-shell boundary action is

$$\begin{aligned} I_N^{(\text{o.s.})} = \frac{W_N}{T} = \text{vol}_{d_s}\frac{r_+^{z+d_s}}{T}\Bigg(&- z + \frac{(z-2)(z+d_s-2)}{2d_s}\frac{\mu_2^2 e^{2(z-1)\phi_1}}{r_+^2} \\ &+ \frac{z}{2(z-d_s)}\frac{k^2 e^{-2(z-1)\phi_1}}{r_+^{2z}}\Bigg), \end{aligned} \tag{4.24}$$

where vol_{d_s} is a d_s-dimensional spatial volume and W_N is the "Neumann" free energy. We are working in an ensemble with $W_N(T, \phi_1, \mu_2, k)$, indicating our independent variables, with $r_+(T, \phi_1, \mu_2, k)$ are an implicit function that solves Eq. (4.11). A priori, we notice that the charge density $J_1^t = \sqrt{2(z-1)(z+d_s)}e^{-d\phi_1}$ is a function of only ϕ_1, meaning that the parameter ϕ_1 directly and single-handedly sources both the responses μ_1 and $\mathbb{O}_\phi$.

Let us compute (and verify) our thermodynamic quantities. First, the entropy,

$$\begin{aligned}\mathcal{S} &= -\frac{\partial W_N}{\partial T}, \\ &= \text{vol}_{d_s} 4\pi r_+^{d_s},\end{aligned} \tag{4.25}$$

where $\text{vol}_{d_s} r_+^{d_s}$ is exactly the surface area of the black hole. This is the celebrated Bekenstein-Hawking relation (where we have chosen $G_N = \frac{1}{16\pi}$). Second, the charge associated with the chemical potential μ_2 is

$$\begin{aligned}\mathcal{Q}_2 &= -\frac{\partial W_N}{\partial \mu_2}, \\ &= \text{vol}_{d_s}(z + d_s - 2)\mu e^{2(z-1)\phi_1} r_+^{z+d_s-2} = \text{vol}_{d_s} J_2^t,\end{aligned} \tag{4.26}$$

which lines up exactly with our expectations. From here, it is possible to compute the system's internal energy,

$$\begin{aligned}\mathcal{E} &= W_N + T\mathcal{S} + \mu_2 \mathcal{Q}_2, \\ &= \text{vol}_{d_s} d_s M r_+^{z+d_s} = \text{vol}_{d_s} \mathbb{T}^t{}_t,\end{aligned} \tag{4.27}$$

which again is self-consistent: the energy contained is proportional to the black hole's mass, and given by the tt-component of the stress-energy tensor.

Next, let us consider what happens under the variation of ϕ_1. This, of course, is an effect that exists only for $z \neq 1$ and couples the variation of the Lifshitz $U(1)$ field and the dilaton. We find

$$\begin{aligned}\frac{\partial W_N}{\partial \phi_1} &= -\text{vol}_{d_s} 2d_s(z-1)(M-1) r_+^{z+d_s}, \\ &= \mu_1 \frac{\partial \mathcal{Q}_1}{\partial \phi_1} + \text{vol}_{d_s} \lambda_\phi \mathbb{O}_\phi,\end{aligned} \tag{4.28}$$

where

$$\mathcal{Q}_1 = \text{vol}_{d_s} \sqrt{2(z-1)(z+d_s)} e^{-d_s \phi_1} = \text{vol}_{d_s} J_1^t. \tag{4.29}$$

As expected, the explicit response of both components is manifest and they are not independent of each other in the context of the static solution. Finally, we compute the pressure p. Our system's trivial volume dependence means the pressure is just the negated thermodynamical potential density in the grand canonical ensemble — namely the density of the "Dirichlet" free energy $W_D = W_N - \mu_1 \mathcal{Q}_1$ — and is given by

$$\begin{aligned}p &= -\frac{W_D}{\text{vol}_{d_s}}, \\ &= \left(M - \frac{1}{z - d_s} \frac{k^2 e^{-2(z-1)\phi_1}}{r_+^{2z}} \right) r_+^{z+d_s} = -\mathbb{T}^{x^1}{}_{x^1} + \frac{k\mathcal{O}_k}{\text{vol}_{d_s}}.\end{aligned} \tag{4.30}$$

Here we have introduced an operator dual to the impurity k,

$$\mathcal{O}_k \equiv -\frac{1}{d_s}\frac{\partial W_N}{\partial k} = -\text{vol}_{d_s}\frac{ke^{-2(z-1)\phi_1}r_+^{-z+d_s}}{z-d_s}, \tag{4.31}$$

which functions analogously to a magnetization in response to an applied magnetic field [77]. The $1/d_s$ factor is chosen to normalize the response to one spatial coordinate. As expected, turning on impurities creates the disparity $p \neq -\mathbb{T}^{x^1}{}_{x^1}$. The simple form of the pressure guarantees the satisfaction of a Smarr-like relation,

$$\epsilon + p = Ts + \sum_{q=1}^{2}\mu_q\rho_q, \tag{4.32}$$

where ϵ, s, and ρ_q are the energy, entropy and charge densities respectively.

4.6 DC Conductivities

When we consider fluctuations of the bulk spacetime and fields at the level of slowly-varying gradients, the equations of motion decouple into three separate modes. A so-called sound mode from which susceptibilities can be derived, a tensor mode which expresses vorticity of the fluid, and a vector mode which contains the system's heat and charge currents [53, 54]. To acquire the DC conductivities, we can supply linear time sources for the vector mode and extract the current responses. We take the ansatz,

$$\delta ds^2 = 2r^2\delta g_{rx^1}drdx^1 + 2\left(-\frac{\nabla T}{T}r^{2z}ft + r^2\delta g_{tx^1}\right)dtdx^1, \tag{4.33a}$$

$$\delta A_q = \left(-\nabla\mu_q t + \frac{\nabla T}{T}A_{q,t}t + \delta A_{q,x^1}\right)dx^1, \tag{4.33b}$$

$$\delta\chi_I = \delta_{I1}\delta\chi_1, \tag{4.33c}$$

where the perturbations — without loss of generality due to rotational symmetry — are sourced along the x^1-direction. The equations of motion come in two batches,

$$-fr^{z-d_s+1}\left(r^{-z+d_s+3}\delta g'_{tx^1} + \sum_{q=1}^{2}\rho_q\delta A_{q,x^1}\right)' + k^2X(\phi)\delta g_{tx^1} = 0, \tag{4.34a}$$

$$j^{(\rho_q)\prime} = 0, \qquad j^{(\rho_q)} = -r^{z+d_s-1}fZ_q(\phi)\delta A'_{q,x^1} - \rho_q\delta g_{tx^1}, \tag{4.34b}$$

which are E_{tx^1} and $M_q^{x^1}$, and

$$\left[r_+^{z+d_s+1}f'(r_+) - \frac{1}{z-d_s}k^2X(\phi)r^{2(z-1)}\left(r^{-z+d_s} - r_+^{-z+d_s}\right)\right]\frac{\nabla T}{T} + \sum_{q=1}^{2}\rho_q\nabla\mu_q - kX(\phi)r^{z+d_s+1}f(\delta\chi_1' - k\delta g_{rx^1}) = 0, \tag{4.35a}$$

$$-k\frac{\nabla T}{T} + r^{z-d_s+1}\left[r^{-z+d_s+3}f\left(\delta\chi_1' - k\delta g_{rx^1}\right)\right]' = 0, \tag{4.35b}$$

which are E_{rx^1} and Ξ_1, respectively. We can see $\Xi_1 = 0$ follows from $E_{tx^1} = 0$. Thus, E_{rx^1} completely decouples from the other equations and acts as a first-order constraint.

The electric currents $j^{(\rho_q)} = J_q^{x^1}$ are conserved in the bulk, but we can construct another conserved current by considering a Killing vector as shown in Appendix A.2. The result is

$$j^{(q)\prime} = 0, \qquad j^{(q)} = r^{3z+d_s-1}f^2\left(r^{-2(z-1)}f^{-1}\delta g_{tx^1}\right)' - \sum_{q=1}^{2}A_{q,t}j^{(\rho_q)}, \tag{4.36}$$

and the conserved bulk quantity $j^{(q)}$ is the boundary heat current. We demand these functions are regular at the horizon in in-going Eddington-Finkelstein coordinates, given by the transformation

$$dt_+ = dt + \frac{dr}{r^{z+1}f}, \tag{4.37}$$

and thus near the horizon we obtain $t = t_+ - \frac{1}{4\pi T}\ln(r - r_+)$. Regularity yields the asymptotic relations

$$\delta g_{rx^1} \sim \frac{1}{k^2X(\phi_+)sT(r-r_+)}\left(s\nabla T + \sum_{q=1}\rho_q\nabla\mu_q\right), \tag{4.38a}$$

$$\delta g_{tx^1} \sim \frac{4\pi}{k^2X(\phi_+)s}\left(s\nabla T + \sum_{q=1}\rho_q\nabla\mu_q\right), \tag{4.38b}$$

$$\delta A_{q,x^1} \sim \frac{1}{4\pi T}\nabla\mu_q\ln(r-r_+), \tag{4.38c}$$

where we express our quantities in terms of the entropy and charge densities and defined $\phi_+ = \phi(r_+)$. Plugging into our currents, which are conserved in the bulk, we find

$$j^{(q)} = -\frac{4\pi T}{k^2X(\phi_+)}\left(s\nabla T + \sum_{q=1}^{2}\rho_q\nabla\mu_q\right), \tag{4.39a}$$

$$j^{(\rho_q)} = -r_+^{d_s-2}Z_q(\phi_+)\nabla\mu_q - \frac{4\pi\rho_q}{k^2X(\phi_+)s}\left(s\nabla T + \sum_{p=1}^{2}\rho_p\nabla\mu_p\right). \tag{4.39b}$$

The heat current is related to the energy current via

$$j^{(q)} = j^{(\epsilon)} - \sum_{q=1}^{2} \mu_q j^{(\rho_q)}, \tag{4.40}$$

which of course is a measure of energy flow in excess of the energy due to charge transfer. Thus, the energy current is given by

$$j^{(\epsilon)} = -r_+^{d_s-2} \sum_{q=1}^{2} Z_q(\phi_+)\mu_q \nabla\mu_q - \frac{4\pi\left(sT + \sum_{q=1}^{2}\mu_q\rho_q\right)}{k^2 X(\phi_+)s}\left(s\nabla T + \sum_{p=1}^{2}\rho_p\nabla\mu_p\right). \tag{4.41}$$

4.7 Energy and Charge Diffusion

Let us consider the diffusion of energy and charge in our system. From hereon we can simply work with densities. The energy and charges follow continuity equations,

$$\partial_t\epsilon + \nabla\cdot j^{(\epsilon)} = 0, \quad \partial_t\rho_q + \nabla\cdot j^{(\rho_q)} = 0. \tag{4.42}$$

In the Neumann ensemble, gradients of T, ϕ_1 and μ_2 source gradients of energy and charge density. We will examine the diffusion of the system's energy and electric charge under the constraint where the "Lifshitz charge" is completely fixed and uniform; that is, $j^{(\rho_1)} = 0$ and $\nabla\rho_1 = 0$. Under this constraint,

$$\nabla\epsilon = \left(c_{\mu_2} + \mu_2\zeta\right)\nabla T + \left(T\zeta + \mu_2\chi\right)\nabla\mu_2, \tag{4.43a}$$
$$\nabla\rho_2 = \zeta\nabla T + \chi\nabla\mu_2, \tag{4.43b}$$

where

$$c_{\mu_2} = T\left.\frac{\partial s}{\partial T}\right|_{\rho_1,\mu_2} = -T\frac{\partial^2 w_N}{\partial T^2}, \tag{4.44a}$$
$$\zeta = \left.\frac{\partial s}{\partial\mu_2}\right|_{T,\rho_1} = \left.\frac{\partial\rho_2}{\partial T}\right|_{\rho_1,\mu_2} = -\frac{\partial^2 w_N}{\partial T\partial\mu_2}, \tag{4.44b}$$
$$\chi = \left.\frac{\partial\rho_2}{\partial\mu_2}\right|_{T,\rho_1} = -\frac{\partial^2 w_N}{\partial\mu_2^2}, \tag{4.44c}$$

the susceptibilities are computable as second-order derivatives of the free energy density w_N.

The associated heat and charge currents,

$$j^{(q)} = -\overline{\kappa}\nabla T - T\alpha\nabla\mu_2, \qquad j^{(\rho_2)} = -\alpha\nabla T - \sigma\nabla\mu_2,$$
$$j^{(\epsilon)} = -\left(\overline{\kappa} + \mu_2\alpha\right)\nabla T - \left(T\alpha + \mu_2\sigma\right)\nabla\mu_2, \tag{4.45}$$

are given by, utilizing Eq. (4.39) and the constraint $j^{(\rho_1)} = 0$,

$$\overline{\kappa} = \frac{4\pi sT}{\Sigma_1 k^2 X(\phi_+)}, \tag{4.46a}$$

$$\alpha = \frac{4\pi\rho_2}{\Sigma_1 k^2 X(\phi_+)}, \tag{4.46b}$$

$$\sigma = r_+^{d_s-2} Z_2(\phi_+) + \frac{4\pi\rho_2^2}{\Sigma_1 k^2 X(\phi_+) s}, \tag{4.46c}$$

$$\Sigma_1 = 1 + \frac{\rho_1^2}{k^2 X(\phi_+) Z_1(\phi_+) r_+^{2d_s-2}}, \tag{4.46d}$$

where Σ_1 measures the response due to application of $\nabla\mu_1$ on the non-Lifshitz matter. The application of this gradient is what allows the conductivities to be finite even in the absence of momentum dissipation, *i.e.* $k \to 0$. This is an expected feature in a system with two species of $U(1)$ fields, first observed by Sonner [78] and later by Cremonini and Pope [70]. This conductivity feature is an instance of some of the more robust behavior a $U(1) \times U(1)$ model can afford.

The continuity equation (4.42) in concert with the conductivities (4.45) and susceptibilities (4.43) yields a diffusion equation for energy and charge:

$$\begin{pmatrix} \partial_t \rho_2 \\ \partial_t \epsilon \end{pmatrix} = \boldsymbol{D} \begin{pmatrix} \nabla^2 \rho_2 \\ \nabla^2 \epsilon \end{pmatrix}, \tag{4.47}$$

where the diffusion matrix $\boldsymbol{D}$ is determined from the conductivity matrix $\boldsymbol{\sigma}$ and susceptibility matrix $\boldsymbol{\chi}$ via the celebrated Einstein relation,

$$\boldsymbol{D} = \boldsymbol{\sigma}\boldsymbol{\chi}^{-1}. \tag{4.48}$$

The diffusion eigenvalues follow

$$D_+ D_- = \frac{\kappa}{c_{\rho_2}} \frac{\sigma}{\chi}, \tag{4.49a}$$

$$D_+ + D_- = \frac{\kappa}{c_{\rho_2}} + \frac{\sigma}{\chi} + \frac{T\sigma}{c_{\rho_2}} \left(\frac{\zeta}{\chi} - \frac{\alpha}{\sigma} \right)^2, \tag{4.49b}$$

where we define

$$c_{\rho_2} = c_{\mu_2} - \frac{T\zeta^2}{\chi} \tag{4.50}$$

as the specific heat for fixed electric charge — which follows from Maxwell relations — and

$$\begin{aligned} \kappa &= \overline{\kappa} - \frac{T\alpha^2}{\sigma}, \\ &= \frac{4\pi sT}{\Sigma_1 k^2 X(\phi_+) + \frac{4\pi\rho_2^2}{r_+^{d_s-2} Z_2(\phi_+) s}} \end{aligned} \tag{4.51}$$

to be the open-circuit thermal conductivity, where no electric charge can flow. We note that κ is explicitly dependent on both the metric and A_1, in contrast to traditional holographic systems where κ is explicitly dependent only upon the form of the metric [57]. This is a direct consequence of our fixed Lifshitz charge scenario.

4.7.1 The Butterfly Velocity

Computing the absolute diffusion constants is nice, but the size of quantities in physics that carry meaning must be dimensionless. To that end, the diffusion constants must be measured against the theory's characteristic velocity. In diffusion of non-interacting particles, the characteristic velocity is the speed of light c [61]. To discuss diffusion of anything in an absolute sense requires some kind of characteristic velocity that governs transport. In a metal, perhaps it is the Fermi velocity. What could it be in a Lifshitz geometry?

There is no direct speed of light analogue for a Lifshitz geometry. By design, any radial slice of our bulk geometry has a different "effective" speed of light, and as we approach the boundary the light cone diverges. We need a new idea. Here, we will review the butterfly velocity, a universal characteristic velocity for Lifshitz geometries [56].

To conjure our ethereal quantity, we begin by transforming the Lifshitz geometry into Kruskal shockwave coordinates. We start with the ansatz

$$ds^2 = \frac{d\varrho^2}{U(\varrho)} - U(\varrho)dt^2 + V(\varrho)d\vec{x}_{d_s}^2, \tag{4.52}$$

which can be acquired from (4.1) under the transformation $\varrho = r^z/z$. Under this transformation, the metric functions are

$$U(\varrho) = z^2\varrho^2 f, \quad V(\varrho) = (z\varrho)^{2/z}. \tag{4.53}$$

The tempearture in these coordinates is given simply by $T = U'(\varrho_+)/4\pi$. From this point we can transfer to the Krusal shockwave coordinates by defining

$$uv = -e^{U'(\varrho_+)\varrho_*(\varrho)}, \quad \frac{u}{v} = -e^{-U'(\varrho_+)t}, \tag{4.54}$$

where ϱ_* is defined as the usual tortoise coordinate via $d\varrho_* = d\varrho/U(\varrho)$. The metric is then given by

$$\begin{aligned} ds^2 &= A(uv)dudv + B(uv)d\vec{x}_{d_s}^2, \\ A(uv) &= \frac{4}{uv}\frac{U(\varrho(uv))}{U'(\varrho_+)^2}, \quad B(uv) = V(\varrho(uv)) \end{aligned} \tag{4.55}$$

The coordinates u and v are natural axes for the light cone. What's more, there are two event horizons: a "future" horizon at $u = 0$ and a "past" horizon at $v = 0$.

Consider a test particle launched from a distant time in the past t_w with energy E. As time runs forward, we watch this particle crash into the event horizon at $u = 0$. The particle's energy is then, of course, absorbed by the black hole and creates a shock.

The shock can be conceptualized as a kink $v \to v + h(x)$ occuring as the particle crosses the $u = 0$ horizon [79–81]. We rewrite the metric so that it takes the Kruskal form (4.55) for $u < 0$ and acquires the kink for $u \geq 0$:

$$\begin{aligned} ds^2 = A\left[u(v + \Theta(u)h(x)\right] du \left(dv + \Theta(u)\partial_i h(x) dx^i\right) \\ + B\left[u(v + \Theta(u)h(x)\right] d\vec{x}_{d_s}^2, \end{aligned} \tag{4.56}$$

where $\Theta(u)$ is the Heaviside step function. Then, let us transform *back* directly with $\hat{v} = v + \Theta(u)h(x)$, and the metric becomes

$$ds^2 = A(u\hat{v})du d\hat{v} + B(u\hat{v})d\vec{x}_{d_s}^2 - A(u\hat{v})\delta(u)h(x)du^2, \tag{4.57}$$

which is nearly identical to our starting metric. The kink is then encoded geometrically through the uu term in the metric and a delta function at the $u = 0$ horizon.

The evolution of our kink $h(x)$ is of course controlled through the Einstein equations. To match, the uu component of the stress-energy tensor for our test particle goes like

$$\delta T_{uu} \sim E e^{2\pi T t_w} \delta(u)\delta(\vec{x}), \tag{4.58}$$

where the particle's momentum $Ee^{2\pi T t_w}$ grows exponentially with time. This is the butterfly effect: regardless of a small initial perturbation, the contribution of back-reaction of the particle is not negligible after a sufficient scrambling time t_* [82]. If we retain only the terms proportional to $\delta(u)h(x)$, the dominant contributions at $u = 0$, we find the kink must obey

$$\left(\Box^{(x)} - m^2\right) h(x) \sim \frac{B(0)}{A(0)} E e^{2\pi T t_w} \delta(\vec{x}) \tag{4.59}$$

where $\Box^{(x)}$ is the spatial Laplacian and the screening length m is generally given by

$$m^2 = \frac{d_s}{A(0)} \frac{\partial B(u\hat{v})}{\partial(u\hat{v})}\bigg|_{u=0}. \tag{4.60}$$

$$= d_s \pi T V'(\varrho_+) = 2 d_s \pi T r_+^{2-z} \tag{4.61}$$

which is easily obtained from

$$A(0) = -\frac{1}{\pi T}, \qquad \frac{\partial B(u\hat{v})}{\partial(u\hat{v})}\bigg|_{u=0} = -V'(\varrho_+). \tag{4.62}$$

Eq. (4.59) utilizes that at $u = 0$

$$\left(\frac{1}{A(0)} \frac{\partial A(u\hat{v})}{\partial (u\hat{v})} + \frac{d_s}{2B(0)} \frac{\partial B(u\hat{v})}{\partial V(u\hat{v})} - \hat{T}_{u\hat{v}} \right) \Bigg|_{u=0} = 0 \tag{4.63}$$

where $\hat{T}_{ab}$ is the trace-reversed stress-energy tensor whose contribution is negligible. The key element is that (4.59) holds even for non-trivial background stress-energy tensors; that is, the kink's dynamics are only determined by the geometry components $A(u\hat{v})$ and $B(u\hat{v})$.

To understand the butterfly effect we need only solve Eq. (4.59). At long distances $x \gg m^{-1}$, we find

$$h(x) \sim \frac{E e^{2\pi T(t_w - t_*) - m|x|}}{|x|^{\frac{d_s - 1}{2}}}. \tag{4.64}$$

The Lyapunov exponent λ_L and butterfly velocity v_B can be read off as

$$\lambda_L = 2\pi T, \quad v_B = \frac{2\pi T}{m}. \tag{4.65}$$

Plugging in our calculated value for the screening length, we obtain

$$v_B^2 = \frac{2\pi}{d_s} T r_+^{z-2}. \tag{4.66}$$

It easy to see that v_B^2/T has the same scaling dimension as a diffusion constant! Thus, we have a characteristic velocity against which diffusion rates can be measured.

4.8 Lifshitz Diffusion Constants

Now that we are equipped with the Einstein relations and the characteristic velocity v_B, we are able to construct dimensionless measures of diffusion for the Lifshitz black hole. Rescaling Eq. (4.11) yields

$$1 = \frac{R^z}{4\pi} \left(z + d_s - \frac{(z + d_s - 2)^2}{2d_s} \tilde{\mu}_2^2 R^{-2} - \frac{1}{2} \tilde{k}^2 R^{-2z} \right), \tag{4.67}$$

$$r_+ = T^{1/z} R\left(\tilde{\mu}_2, \tilde{k}\right), \quad \tilde{\mu}_2 = \frac{\mu_2 e^{(z-1)\phi_1}}{T}, \quad \tilde{k} = \frac{k e^{-(z-1)\phi_1}}{T^z}, \tag{4.68}$$

and all pure numbers in our system will be functions of the two parameters $\tilde{\mu}_2$ and $\tilde{k}$. Written in scaling form, the determinant and trace of the diffusion

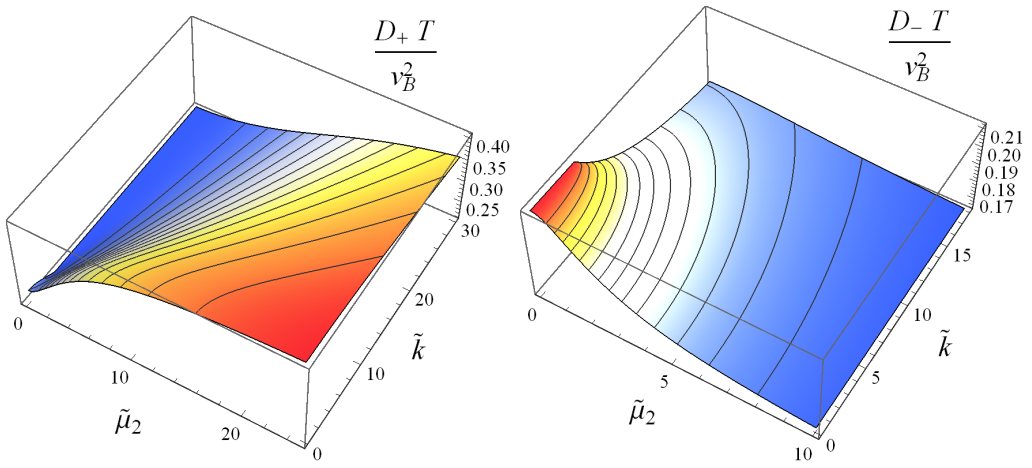

Figure 4.2: $D_\pm T/v_B^2$ for $d_s = 2$ and $z = 3/2$.

matrix are given, respectively, by

$$\frac{D_+ D_- T^2}{v_B^4} = \frac{z d_s \left[2(z+d_s) + \tilde{k}^2 R^{-2z}\right] - (z-2)(z+d_s-2)^2 \tilde{\mu}^2 R^{-2}}{8\pi^2 (z+d_s-2)\left[2(z-1)(z+d_s) + \tilde{k}^2 R^{-2z}\right]}, \tag{4.69a}$$

$$\begin{aligned}\frac{(D_+ + D_-)T}{v_B^2} &= \frac{d_s}{2\pi(z+d_s-2)} \\ &+ \frac{z d_s \left[2(z+d_s) + \tilde{k}^2 R^{-2z}\right] + (z-2)\left[(z-2)^2 - d_s^2\right]\tilde{\mu}_2^2 R^{-2}}{4\pi d_s \left[2(z-1)(z+d_s) + \tilde{k}^2 R^{-2z}\right]}.\end{aligned} \tag{4.69b}$$

We will always order the eigenvalues such that $D_+ \geq D_-$. We display a couple of solutions explicitly in Figs. 4.2 and 4.3. Notably, we find the diffusion eigenvalues are bounded. The bounds can be obtained analytically through various limits of $\tilde{\mu}_2$ and $\tilde{k}$ and are given by

$$\max\left(\frac{D_+ T}{v_B^2}\right) = \begin{cases} \frac{d_s}{2\pi(z-1)(z+d_s-2)} & z < 2 \\ \frac{1}{2\pi} & z \geq 2 \end{cases}, \tag{4.70a}$$

$$\min\left(\frac{D_+ T}{v_B^2}\right) = \begin{cases} \frac{z}{4\pi(z-1)} & z > 2 \text{ and } z > d_s \\ \frac{d_s}{2\pi(z+d_s-2)} & \text{else} \end{cases}, \tag{4.70b}$$

$$\max\left(\frac{D_- T}{v_B^2}\right) = \begin{cases} \frac{z}{4\pi(z-1)} & d_s < z < 2 \\ \frac{d_s}{2\pi(z+d_s-2)} & \text{else} \end{cases}, \tag{4.70c}$$

$$\min\left(\frac{D_- T}{v_B^2}\right) = \begin{cases} \frac{1}{2\pi} & z \leq 2 \\ \frac{d_s}{2\pi(z-1)(z+d_s-2)} & z > 2 \end{cases}, \tag{4.70d}$$

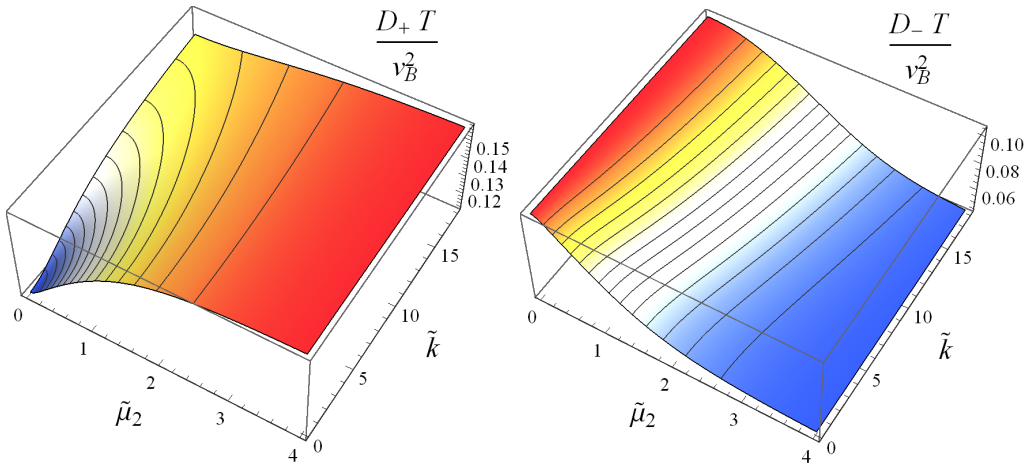

Figure 4.3: $D_\pm T/v_B^2$ for $d_s = 3$ and $z = 7/2$.

which are shown in Fig. 4.4 for $d_s = \{1, 2, 3\}$, in which the primacy of $z = 2$ as the scale-invariant point of the diffusion equation is evident. To illustrate this further, we plot Eq. (4.3) with the length defined as $\ell = 2\pi/\tilde{k}$ in Fig. 4.5.[1] This characteristic length functions as an effective lattice spacing. As is evident, there is a universal sign change at $z = 2$. At $z = 2$, the diffusion constants are equal and given by the universal value,

$$D_\pm = \frac{1}{d_s}, \tag{4.71}$$

as remarked in the introduction. The universal nature of the charge and energy diffusion constants stems from the underlying scale invariance of the diffusion equation when $z = 2$. The sign change of β signals a fixed point exists at $z = 2$ analogous to the scale-invariance that obtains for the conductance in the case of $d_s = 2$ in Anderson localization [58]. Necessarily, the diffusion scale v_B^2/T is also a pure number at this point, as seen in Eq. (4.66) where the horizon dependence vanishes. The marginality of $z = 2$ has been noted in other contexts such as a Lifshitz string [83] and the stability of scalar hair [84]. Note that we have allowed non-integer values of d_s in our solutions, which can effectively be obtained through the use of a hyperscaling violating parameter.

To put our results for the transport in the context of expected results, we first observe the universal features. In the decoupling limit where the chemical potential is turned off, we find the charge and energy diffusion constants follow

$$\lim_{\tilde{\mu}_2 \to 0} \frac{\sigma}{\chi} \frac{T}{v_B^2} = \frac{d_s}{2\pi(z + d_s - 2)}, \qquad \lim_{\tilde{\mu}_2, \tilde{k} \to 0} \frac{\kappa}{c_{\rho_2}} \frac{T}{v_B^2} = \frac{z}{4\pi(z-1)}, \tag{4.72}$$

[1] We could very well have used $\det \boldsymbol{D}$ instead of $\mathrm{tr}\, \boldsymbol{D}$, though the qualitative features are identical.

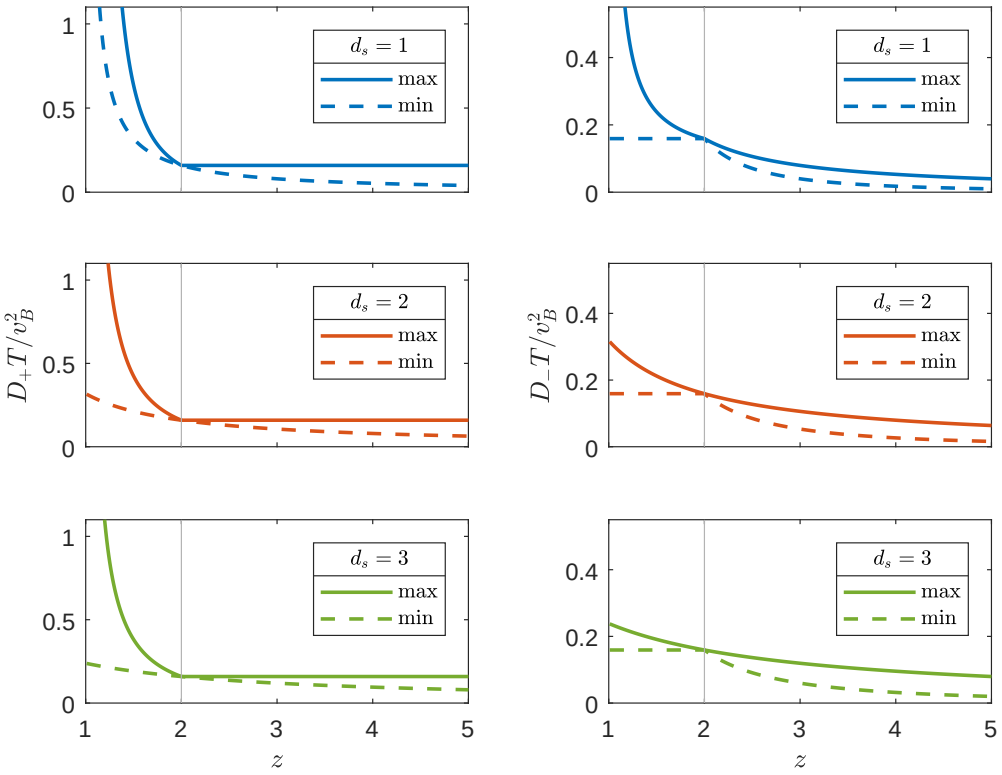

Figure 4.4: The bounds of $D_\pm T/v_B^2$ for $d_s = \{1, 2, 3\}$. The minimum of D_+T/v_B^2 asymptotes to $1/4\pi$ as $z \to \infty$.

which exactly match the purported decoupled forms in [56, 57]. For $z \geq 2$ and $z \geq d_s$, which heads toward the decoupling limit of large z, we find these forms match $\max(D_-T/v_B^2)$ and $\min(D_+T/v_B^2)$ exactly. The limits in which deviations occur are laid bare in Fig. 4.3. For D_-, deviation from this behavior is found when $\tilde{\mu}_2 \gg 1$, the limit in which we expect thermoelectric interactions to be quite strong and so inhibit charge flow. For D_+, deviation is found under either the conditions $\tilde{k} \gg 1$ or $\tilde{\mu}_2 \gg 1$, emphasizing that energy diffusivity is heavily subject to all matter interactions.

A limit of interest is $z \to \infty$. In particular, the bounds indicate clearly that $D_-T/v_B^2 \to 0$, signaling that charge does not diffuse in this limit, only energy. Conventionally, $z \to \infty$ corresponds to localized critical physics; the divergence of the critical length guarantees no dynamic critical behavior can obtain on any appreciable time scale. For our system, we can interpret this to mean charge must follow this type of quantum critical behavior but energy does not. We also notice the saturation of the D_+ diffusion constant for $z \geq 2$, whereupon $1/4\pi \leq D_+T/v_B^2 \leq 1/2\pi$. The upper bound is the typical saturation observed in the SYK model [85]. Intuitively, this characterizes the fact that energy diffusivity must be bounded from below and above, so long

as momentum dissipation is present, regardless of the value of z.

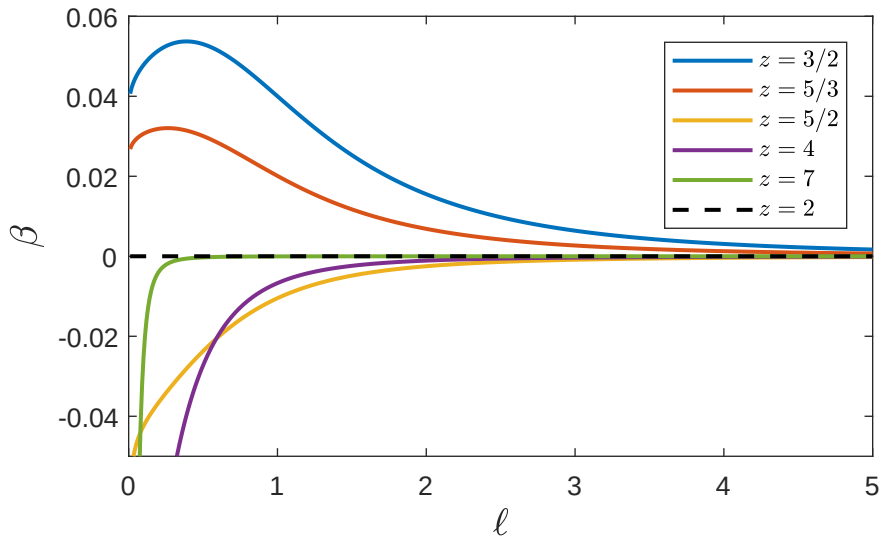

Figure 4.5: Plot of the β-function (Eq. (4.3)) illustrating the universality of the diffusivities as a function of length for varying z, using $\tilde{\mu}_2 = 1.8$ and $d_s = 3$. The qualitative features of β are independent of the chemical potential and the number of spatial dimensions. The universal sign change signifies that the length dependence of the diffusivities is controlled by a fixed point at $z = 2$.

4.9 Summary of Lifshitz Transport

From this detailed treatment of Lifshitz holography, we have been able to derive a series of therodynamic and dynamical response functions. Of particular note is the explicit derivation of both the Bekenstein-Hawking and Smarr-like relationships, made possible by the exact computation of the renormalized thermodynamic potential. Our calculations reveal the universal features of the diffusion constants near $z = 2$ even in the complicated setting in which charge and thermal degrees of freedom are treated on equal footing. The vanishing of the charge diffusion constant in the local critical limit of $z \to \infty$ represents the ultimate deviation from the expected bounds. This limit, of course, is in the extreme case where the matter content of our theory dominates. Since our treament fully incorporates thermodynamics and electrical responses, it should serve as a template for extracting the coterie of transport coefficients relevant to quantum critical matter.

5 Future Work

From this detailed treatment of Lifshitz holography, we have been able to derive a series of thermodynamic and dynamical response functions. Of particular note is the explicit derivation of both the Bekenstein-Hawking and Smarr-like relationships, made possible by the exact computation of the renormalized thermodynamic potential. Our calculations reveal the universal features of the diffusion constants near $z = 2$ even in the complicated setting in which charge and thermal degrees of freedom are treated on equal footing. This universality obtains because of the emergence of a fixed point characterizing the length dependence of the diffusivities at $z = 2$. The vanishing of the charge diffusion constant in the local critical limit of $z \to \infty$ represents the ultimate deviation from the expected bounds. Since our treatment fully incorporates thermodynamics and electrical responses, it should serve as a template for extracting the coterie of transport coefficients relevant to quantum critical matter.

A Appendix

A.1 Full Background Renormalization

For $k \neq 0$ we can have a possibly infinite number of divergent terms in Eq. (4.13). Consider counter-terms

$$I_{\text{c.t.}} = \int_{\partial\mathcal{M}} \sum_{n=0} \left(c_n^{(\text{vol})} \sqrt{-\gamma} + c_n^{(J_1^2)} \frac{J_1^2}{\sqrt{-\gamma} Z_1(\phi)} \right) \left[X(\phi) \sum_{I=1}^{d_s} \left(\hat{\nabla} \chi_I \right)^2 \right]^n , \tag{A.1}$$

whose contributions to our boundary responses are

$$\begin{aligned} \mathbb{T}^a{}_{b|\text{c.t.}} = & \sum_{n=0} \left[X(\phi) \sum_{J=1}^{d_s} \left(\hat{\nabla} \chi_J \right)^2 \right]^{n-1} \\ & \times 2X(\phi) \sum_{I=1}^{d_s} \left[c_n^{(\text{vol})} \sqrt{-\gamma} \left(\frac{1}{2} \delta^a{}_b \left(\hat{\nabla} \chi_I \right)^2 - n \hat{\nabla}^a \chi_I \hat{\nabla}_b \chi_I \right) \right. \\ & \left. + \frac{c_n^{(J_1^2)}}{\sqrt{-\gamma} Z_1(\phi)} \left(J_1^a J_{1,b} \left(\hat{\nabla} \chi_I \right)^2 - n J_1^2 \hat{\nabla}^a \chi_I \hat{\nabla}_b \chi_I - \frac{1}{2} \delta^a{}_b J_1^2 \right) \left(\hat{\nabla} \chi_I \right)^2 \right], \end{aligned} \tag{A.2}$$

$$\mathbb{A}_{1,a|\text{c.t.}} = \sum_{n=0} \left[X(\phi) \sum_{I=1}^{d_s} \left(\hat{\nabla} \chi_I \right)^2 \right]^n \frac{2 c_n^{(J_1^2)} J_{1,a}}{\sqrt{-\gamma} Z_1(\phi)}, \tag{A.3}$$

$$\begin{aligned} \mathbb{O}_{\phi|\text{c.t.}} = & \sum_{n=0} \left[X(\phi) \sum_{I=1}^{d_s} \left(\hat{\nabla} \chi_I \right)^2 \right]^n \\ & \times \left[c_n^{(\text{vol})} \sqrt{-\gamma} \frac{n X'(\phi)}{X(\phi)} + c_n^{(J_1^2)} \frac{J_1^2}{\sqrt{-\gamma} Z_1(\phi)} \left(\frac{n X'(\phi)}{X(\phi)} - \frac{Z_1'(\phi)}{Z_1(\phi)} \right) \right]. \end{aligned} \tag{A.4}$$

In general, we can increment n to cancel out higher order powers involving k^2 terms that bleed over from our established action. The constants are given by

$$c_n^{(\text{vol})} = \vartheta_n^{(\text{vol})} \frac{(2n-1)(z-1) - 2d_s}{(4d_s(d_s - z))^n}, \tag{A.5}$$

$$c_n^{(J_1^2)} = \vartheta_n^{(J_1^2)} \frac{1}{(z + d_s)\left(4d_s(d_s - z)\right)^n}, \tag{A.6}$$

and are determined recursively from $n = 0$ with $\vartheta_n^{(\mathrm{vol})} = \{-1, 1, \frac{1}{2}, \frac{1}{2}, \frac{5}{8}, \frac{7}{8}, \dots\}$ and $\vartheta_n^{(J_1^2)} = \{\frac{1}{2}, \frac{1}{2}, \frac{3}{4}, \frac{5}{4}, \frac{35}{16}, \frac{63}{16}, \dots\}$. This is a specific encoding of the renormalization provided by the Hamilton-Jacobi equations, which expands in a series of functional derivatives [9, 10].

A.2 Killing Vector Conserved Quantity

Here we determine the bulk conserved quantity that will be dual to the heat current as outlined in [34]. Suppose there exists a Killing vector ξ, defined by

$$\mathcal{L}_\xi g_{ab} = \nabla_{(a}\xi_{b)} = 0, \tag{A.7}$$

which of course can correspond to an infinitesimal diffeomorphism. We consider that the Lie derivatives on our physical observable fields vanish, that is

$$\mathcal{L}_\xi F_{q,ab} = \mathcal{L}_\xi \phi = \mathcal{L}_\xi \chi_I = 0. \tag{A.8}$$

The first of these, rewritten, states that

$$\left(i_\xi d + d i_\xi\right) F_q = 0, \tag{A.9}$$

and thus we can assume that $i_\xi F_q$ is an exact form

$$i_\xi F_q = d\theta_q \tag{A.10}$$

for some functions θ_q. This also implies that we can express

$$\mathcal{L}_\xi A_q = d\psi_q \tag{A.11}$$

for some functions ψ_q. These identities will allow us to construct a total derivative by examining

$$\begin{aligned}\nabla_b \nabla^a \xi^b &= R^a{}_b \xi^b, \\ &= \frac{1}{d_s} V(\phi) \xi^a + \frac{1}{2} \sum_{q=1}^{2} \left(\xi^c Z_q(\phi) F_q^{ab} F_{q,cb} - \frac{1}{2d_s} \xi^a Z_q(\phi) F_q^2 \right).\end{aligned} \tag{A.12}$$

This expression can be rearranged as

$$\nabla_b G^{ab} = \frac{1}{d_s} V(\phi) \xi^a, \tag{A.13}$$

where

$$G^{ab} = \nabla^a \xi^b + \frac{1}{2d_s} \sum_{q=1}^{2} Z_q(\phi) \left(\left(\psi_q - d_s \theta_q\right) F_q^{ab} + 2\xi^{[a} F_q^{b]c} A_{q,c} \right). \tag{A.14}$$

To deduce this expression, we use the identities

$$\xi^c Z_q(\phi) F_q^{ab} F_{q,cb} = \nabla_b \left(\theta_q Z_q(\phi) F_q^{ab}\right), \tag{A.15}$$

$$\xi^a Z_q(\phi) F_q^2 = \nabla_b \left(4\xi^{[a} Z_q(\phi) F_q^{b]c} A_{q,c} + 2\psi_q Z_q(\phi) F_q^{ab}\right), \tag{A.16}$$

where the latter of these can be realized from rearranging the Lie derivative $\mathcal{L}_\xi F_{q,ab} = \xi^c \nabla_c F_{q,ab} + F_{q,bc}\nabla_a \xi^c + F_{q,ac}\nabla_b \xi^c = 0$. Now, as long as any components of ξ vanish we can deduce a conserved quantity. By choosing $\xi = \nabla_t$, it is clear that the x^i components then generate conserved quantities, which are dual to the boundary heat currents.

A.3 Renormalization for Currents

With the counter-terms provided in Eq. (4.15), we find that

$$\mathbb{T}^{x^1}_{\ t} = j^{(\epsilon)} \tag{A.17}$$

and as such we would like to construct our boundary theory such that this is the response to our metric variation. Presently, we would find that the boundary variation leaves a source term [34] in the action. This is not a problem for $z = 1$, but otherwise this term is divergent. To attenuate this divergence we can recast the intrinsic metric γ_{ab} as

$$\gamma_{ab} dx^a dx^b = -n^2 \left(dt - \frac{n_i}{n^2} dx^i\right)^2 + \sigma_{ij} dx^i dx^j, \tag{A.18}$$

akin to the ADM formalism but where our boundary spacetime is instead foliated by the normalized timelike covector $\frac{1}{n}\nabla_t$. Then we can consider the fundamental variational objects of our theory to be n, n_i and σ_{ij} instead of the boundary metric. Our variation becomes

$$\delta I = \int_{\partial\mathcal{M}} \left[\left(-\mathbb{T}^{tt} n^2 + \mathbb{T}^{ij}\frac{n_i n_j}{n^2}\right)\frac{\delta n}{n} - \mathbb{T}^i_{\ t}\frac{\delta n_i}{n^2} + \frac{1}{2}\mathbb{T}^{ij}\delta\sigma_{ij} + \cdots\right], \tag{A.19}$$

and now the source term present in the δn_i term decays. Additionally, thanks to our formulation of n_i as a small parameter, the response to the normalized variation of the lapse $\delta n/n$ is exactly $\mathbb{T}^t_{\ t}$. Thus nothing about our static background scheme is modified.

A.4 Linear Time Sources

Linear time sources provide a straightforward scheme for deducing DC response functions. Additionally, through our gauge symmetries they have a

clear interpretation as temperature and chemical potential gradients. We can transform the metric and $U(1)$ fields as

$$g_{ab} \to g_{ab} + \mathcal{L}_\xi g_{ab}, \tag{A.20}$$
$$A_{q,a} \to A_{q,a} + \mathcal{L}_\xi A_{q,a} + \nabla_a \Lambda_q \tag{A.21}$$

where ξ parameterizes an infinitesimal coordinate transformation $x^a \to x^a + \xi^a$ and each Λ_q a $U(1)$ transformation, respectively. For the choices

$$\xi = -tx^1 \frac{\nabla T}{T} \nabla_t, \tag{A.22}$$
$$\Lambda_q = tx^1 \nabla \mu_q, \tag{A.23}$$

our ansatz sources become

$$\delta ds^2 = 2r^{2z} f x^1 \frac{\nabla T}{T} dt^2, \tag{A.24}$$
$$\delta A_q = x^1 \left(\nabla \mu_q - A_{q,t} \frac{\nabla T}{T} \right) dt, \tag{A.25}$$

which are exactly the gradients we would expect for small perturbations of T and μ_q. The form of the temperature fluctuations are determined by perturbing the period of Euclidean time, $1/T$.

A.5 Interpretation of the Lifshitz Boundary

In a traditional asymptotically *AdS* spacetime, a constant radial slice looks identical to Minkowski spacetime. Thus, we have a clean picture of what the boundary spacetime looks like: just that, Minkowski spacetime. However, an asymptotically Lifshitz geometry does not have slices that are so easy to interpret. The asymmetric scaling of time and space mean that a slice looks like Minkowski spacetime with a divergent speed of light. This is no real world interpretation at all. Instead, we can use the Newton-Cartan formalism outlined in [53, 54, 76].

Rather than the boundary metric serving as the fundamental description of spacetime, consider instead a vielbein. What's more, we can encode the nonrelativistic Galilean boost in this model. Consider the intrinsic metric and its inverse to be expressed respectively as

$$\gamma_{ab} = -r^{2z} f \tau_a \tau_b + r^2 \delta_{ij} e^i_a e^j_b, \tag{A.26}$$
$$\gamma^{ab} = -r^{-2z} f^{-1} v^a v^b + r^{-2} \delta^{ij} e^a_i e^b_j, \tag{A.27}$$

where the vielbein obeys

$$v^a \tau_a = 1, \quad e^a_i \tau_a = 0, \quad v^a e^i_a = 0, \quad e^a_j e^i_a = \delta^i_j. \tag{A.28}$$

It's also convenient to define the spatial metric via $h_{ab} = \delta_{ij} e^i_a e^j_b$. The fundamental objects of the theory will be the timelike 1-form τ_a and the inverse spatial metric h^{ab}.

The proposed vielbein is invariant under a Milne boost ψ_a, defined by

$$\begin{aligned} &\tau_a \to \tau_a, \quad v^a \to v^a + h^{ab}\psi_b, \\ &h^{ab} \to h^{ab}, \quad h_{ab} \to h_{ab} - \left(\tau_a P^c_b + \tau_b P^c_a\right)\psi_c + \tau_a \tau_b h^{cd}\psi_c\psi_d, \end{aligned} \tag{A.29}$$

where τ_a and h^{ab} are left invariant and the operator $P^a_b = \delta^a_b - v^a\tau_b$ is a spatial projector. The Milne boost transformation should be familiar! It's a generalized encoding of a Galilean boost for nontrivial spacetimes. Squint your eyes and tilt your head to the side and you'll see it's identical in construction.

At the boundary, the vielbein is given by

$$\tau_a dx^a = dt, \quad e^i_a dx^a = dx^i - v^i dt, \quad v^a\nabla_a = \nabla_t + v^i\nabla_i, \quad e^a_i\nabla_a = \nabla_i, \tag{A.30}$$

where we have included a Galilean boost v^i. Any $U(1)$ fields can be encoded by their tangent space dopplegangers,

$$A_{q,0} = v^a A_{q,a}, \quad A_{q,i} = e^a_i A_{q,a}. \tag{A.31}$$

In this formalism, the variation of the Einstein-Maxwell-dilaton action can be expressed

$$\delta I = \int_{\partial\mathcal{M}} \left(-S^0_a \delta v^a + S^a_i \delta e^i_a + \sum_{q=1}^{2} \left(J^0_q \delta A_{q,0} + J^i_q \delta A_{q,i} \right) + \mathcal{O}_\phi \delta\phi \right), \tag{A.32}$$

where all the fundamental variations are vielbein objects.[1] Converting back, our responses, the stress-energy tensor and currents, are given by

$$T^a{}_b = S^0_b v^a - S^i_b e^a_i, \quad J^a_q = J^0_q v^a + J^i_q e^a_i. \tag{A.33}$$

Before any counter-terms, the forms of stress-energy tensor and currents are

$$T^a{}_b = 2\sqrt{-\gamma}\left(K^{ab} - \gamma^{ab}K\right) + \sum_{q=1}^{2} J^a_q A_{q,b}, \tag{A.34}$$

$$J^a_q = \sqrt{-\gamma} N_b Z_q(\phi) F^{ab}_q. \tag{A.35}$$

Interestingly, this vielbein concoction modifies the form of the stress-energy tensor! Indeed, it is actually asymmetric in general, which can accommodate torsion. In general, because the vielbein is $O(1)$ by construction, we are guaranteed a stable boundary variation.

[1] Of course, we need only one pair from the vielbein thanks to the constraints (A.28).

References

[1] J. Maldacena. The Large N limit of superconformal Field theories and supergravity. *Adv. Theor. Math. Phys.*, 2:231, 1998.

[2] Edward Witten. Anti-de Sitter space and holography. *Adv. Theor. Math. Phys.*, 2:253–291, 1998.

[3] Thomas Faulkner, Nabil Iqbal, Hong Liu, John McGreevy, and David Vegh. Strange metal transport realized by gauge/gravity duality. *Science*, 329(5995):1043–1047, 2010.

[4] Sean A. Hartnoll, Christopher P. Herzog, and Gary T. Horowitz. Holographic superconductors. *Journal of High Energy Physics*, 2008(12):015, 2008.

[5] Gary T. Horowitz, Jorge E. Santos, and Benson Way. Holographic josephson junctions. *Phys. Rev. Lett.*, 106:221601, Jun 2011.

[6] Mohammad Edalati, Robert G. Leigh, and Philip W. Phillips. Dynamically generated mott gap from holography. *Phys. Rev. Lett.*, 106:091602, Mar 2011.

[7] Yunseok Seo, Geunho Song, Philip Kim, Subir Sachdev, and Sang-Jin Sin. Holography of the dirac fluid in graphene with two currents. *Phys. Rev. Lett.*, 118:036601, Jan 2017.

[8] Robert M Wald. *General relativity*. Chicago Univ. Press, Chicago, IL, 1984.

[9] Ioannis Papadimitriou. Holographic renormalization of general dilaton-axion gravity. *Journal of High Energy Physics*, 2011(8):119, Aug 2011.

[10] Wissam Chemissany and Ioannis Papadimitriou. Lifshitz holography: the whole shebang. *Journal of High Energy Physics*, 2015(1):52, Jan 2015.

[11] Thomas Faulkner, Hong Liu, John McGreevy, and David Vegh. Emergent quantum criticality, fermi surfaces, and ads_2. *Phys. Rev. D*, 83:125002, Jun 2011.

[12] Sean A Hartnoll. Lectures on holographic methods for condensed matter physics. *Classical and Quantum Gravity*, 26(22):224002, 2009.

[13] Andrea Amoretti, Alessandro Braggio, Nicola Maggiore, Nicodemo Magnoli, and Daniele Musso. Thermo-electric transport in gauge/gravity models with momentum dissipation. *Journal of High Energy Physics*, 2014(9):160, Sep 2014.

[14] Alexander Altland and Ben D. Simons. *Condensed Matter Field Theory*. Cambridge University Press, 2 edition, 2010.

[15] Matthew Headrick, Sam Kitchen, and Toby Wiseman. A new approach to static numerical relativity and its application to KaluzaKlein black holes. *Classical and Quantum Gravity*, 27(3):035002, 2010.

[16] Allan Adams, Paul M. Chesler, and Hong Liu. Holographic turbulence. *Phys. Rev. Lett.*, 112:151602, Apr 2014.

[17] L. Trefethen. *Spectral Methods in MATLAB*. Society for Industrial and Applied Mathematics, 2000.

[18] G. T. Horowitz, J. E. Santos, and D. Tong. Optical conductivity with holographic lattices. *Journal of High Energy Physics*, 7:168, July 2012.

[19] Andrew Lucas. Conductivity of a strange metal: from holography to memory functions. *Journal of High Energy Physics*, 2015(3):71, Mar 2015.

[20] D. van der Marel, H. J. A. Molegraaf, J. Zaanen, Z. Nussinov, F. Carbone, A. Damascelli, H. Eisaki, M. Greven, P. H. Kes, and M. Li. Quantum critical behaviour in a high-T_c superconductor. *Nature*, 425(6955):271–274, 2003.

[21] A. El Azrak, R. Nahoum, N. Bontemps, M. Guilloux-Viry, C. Thivet, A. Perrin, S. Labdi, Z. Z. Li, and H. Raffy. Infrared properties of $YBa_2Cu_3O_7$ and $Bi_2Sr_2Ca_{n-1}Cu_nO_{2n+4}$ thin films. *Phys. Rev. B*, 49:9846–9856, Apr 1994.

[22] J Hwang, T Timusk, and G D Gu. Doping dependent optical properties of $Bi_2Sr_2CaCu_2O_{8+\delta}$. *Journal of Physics: Condensed Matter*, 19(12):125208, 2007.

[23] Z. Schlesinger, R. T. Collins, F. Holtzberg, C. Feild, S. H. Blanton, U. Welp, G. W. Crabtree, Y. Fang, and J. Z. Liu. Superconducting energy gap and normal-state conductivity of a single-domain $YBa_2Cu_3O_7$ crystal. *Phys. Rev. Lett.*, 65:801–804, Aug 1990.

[24] P. W. Anderson. Infrared conductivity of cuprate metals: Detailed fit using Luttinger-liquid theory. *Phys. Rev. B*, 55:11785–11788, May 1997.

[25] Masao Ogata and P. W. Anderson. Transport properties in the Tomonaga-Luttinger liquid. *Phys. Rev. Lett.*, 70:3087–3090, May 1993.

[26] Elihu Abrahams and C. M. Varma. What angle-resolved photoemission experiments tell about the microscopic theory for high-temperature superconductors. *Proceedings of the National Academy of Sciences*, 97(11):5714–5716, 2000.

[27] S. Uchida, T. Ido, H. Takagi, T. Arima, Y. Tokura, and S. Tajima. Optical spectra of $La2 - xSrxCuO4$: Effect of carrier doping on the electronic structure of the $CuO2$ plane. *Phys. Rev. B*, 43(10):7942–7954, Apr 1991.

[28] Y. S. Lee, Kouji Segawa, Z. Q. Li, W. J. Padilla, M. Dumm, S. V. Dordevic, C. C. Homes, Yoichi Ando, and D. N. Basov. Electrodynamics of the nodal metal state in weakly doped high-T_c cuprates. *Physical Review B (Condensed Matter and Materials Physics)*, (5):054529–13.

[29] Philip Phillips. *Colloquium* : Identifying the propagating charge modes in doped Mott insulators. *Rev. Mod. Phys.*, 82:1719–1742, May 2010.

[30] A. Donos and J. P. Gauntlett. Holographic Q-lattices. *Journal of High Energy Physics*, 4:40, April 2014.

[31] M. Rangamani, M. Rozali, and D. Smyth. Spatial Modulation and Conductivities in Effective Holographic Theories. *ArXiv e-prints*, May 2015.

[32] Sidney Coleman. Q-balls. *Nuclear Physics B*, 262(2):263 – 283, 1985.

[33] Brandon W. Langley, Garrett Vanacore, and Philip W. Phillips. Absence of power-law mid-infrared conductivity in gravitational crystals. *Journal of High Energy Physics*, 2015(10):163, Oct 2015.

[34] Aristomenis Donos and Jerome P. Gauntlett. Thermoelectric dc conductivities from black hole horizons. *Journal of High Energy Physics*, 2014(11):81, Nov 2014.

[35] Aristomenis Donos and JeromeP. Gauntlett. The thermoelectric properties of inhomogeneous holographic lattices. *Journal of High Energy Physics*, 2015(1), 2015.

[36] William Witczak-Krempa and Subir Sachdev. Quasinormal modes of quantum criticality. *Phys. Rev. B*, 86:235115, Dec 2012.

[37] Edward Witten. SL(2,Z) action on three-dimensional conformal field theories with Abelian symmetry. pages 1173–1200, 2003.

[38] K. Limtragool and P. Phillips. Power-law Optical Conductivity in the Cuprates from Unparticle Stuff. *ArXiv e-prints*, June 2015.

[39] Óscar J. C. Dias, Gary T. Horowitz, Nabil Iqbal, and Jorge E. Santos. Vortices in holographic superfluids and superconductors as conformal defects. *Journal of High Energy Physics*, 2014(4):96, Apr 2014.

[40] Antonio Bianconi. Lifshitz transitions in multi-band hubbard models for topological superconductivity in complex quantum matter. *Journal of Superconductivity and Novel Magnetism*, 31(3):603–610, Mar 2018.

[41] M. R. Norman, Jie Lin, and A. J. Millis. Lifshitz transition in underdoped cuprates. *Phys. Rev. B*, 81:180513, May 2010.

[42] X. Shi, Z-Q Han, X-L Peng, P. Richard, T. Qian, X-X Wu, M-W Qiu, S. C. Wang, J. P. Hu, Y-J Sun, and H. Ding. Enhanced superconductivity accompanying a lifshitz transition in electron-doped fese monolayer. *Nature Communications*, 8:14988 EP –, 04 2017.

[43] G. E. Volovik. Topological lifshitz transitions. *Low Temperature Physics*, 43(1):47–55, 2017.

[44] Shamit Kachru, Xiao Liu, and Michael Mulligan. Gravity duals of lifshitz-like fixed points. *Phys. Rev. D*, 78:106005, Nov 2008.

[45] Petr Hořava. Quantum gravity at a lifshitz point. *Phys. Rev. D*, 79:084008, Apr 2009.

[46] Koushik Balasubramanian and John McGreevy. The particle number in galilean holography. *Journal of High Energy Physics*, 2011(1):137, Jan 2011.

[47] Elias Kiritsis. Lorentz violation, gravity, dissipation and holography. *Journal of High Energy Physics*, 2013(1):30, Jan 2013.

[48] Kristan Jensen. On the coupling of galilean-invariant field theories to curved spacetime. *SciPost Phys.*, 5:11, 2018.

[49] B. Goutéraux and E. Kiritsis. Generalized holographic quantum criticality at finite density. *Journal of High Energy Physics*, 2011(12):36, Dec 2011.

[50] ZhongYing Fan. Holographic superconductors with hyperscaling violation. *Journal of High Energy Physics*, 2013(9):48, Sep 2013.

[51] B. Goutéraux. Charge transport in holography with momentum dissipation. *Journal of High Energy Physics*, 2014(4):181, Apr 2014.

[52] Javier Tarrio. Asymptotically lifshitz black holes in einstein-maxwell-dilaton theories. *Fortschritte der Physik*, 60(910):1098–1104.

[53] Elias Kiritsis and Yoshinori Matsuo. Charge-hyperscaling violating lifshitz hydrodynamics from black-holes. *Journal of High Energy Physics*, 2015(12):1–51, Dec 2015.

[54] Elias Kiritsis and Yoshinori Matsuo. Hyperscaling-violating lifshitz hydrodynamics from black-holes: part ii. *Journal of High Energy Physics*, 2017(3):41, Mar 2017.

[55] Ioannis Papadimitriou. Hyperscaling violating lifshitz holography. *Nuclear and Particle Physics Proceedings*, 273-275:1487 – 1493, 2016. 37th International Conference on High Energy Physics (ICHEP).

[56] Mike Blake. Universal charge diffusion and the butterfly effect in holographic theories. *Phys. Rev. Lett.*, 117:091601, Aug 2016.

[57] Mike Blake, Richard A. Davison, and Subir Sachdev. Thermal diffusivity and chaos in metals without quasiparticles. *Phys. Rev. D*, 96:106008, Nov 2017.

[58] E. Abrahams, P. W. Anderson, D. C. Licciardello, and T. V. Ramakrishnan. Scaling theory of localization: Absence of quantum diffusion in two dimensions. *Phys. Rev. Lett.*, 42:673–676, Mar 1979.

[59] Da-Wei Pang. Conductivity and diffusion constant in lifshitz backgrounds. *Journal of High Energy Physics*, 2010(1):120, Jan 2010.

[60] Xian-Hui Ge, Sang-Jin Sin, Yu Tian, Shao-Feng Wu, and Shang-Yu Wu. Charged btz-like black hole solutions and the diffusivity-butterfly velocity relation. *Journal of High Energy Physics*, 2018(1):68, Jan 2018.

[61] Sean A. Hartnoll. Theory of universal incoherent metallic transport. *Nature Physics*, 11:54–61, Dec 2014.

[62] Thomas Hartman, Sean A. Hartnoll, and Raghu Mahajan. Upper bound on diffusivity. *Phys. Rev. Lett.*, 119:141601, Oct 2017.

[63] Davide Cassani and Anton F. Faedo. Constructing lifshitz solutions from ads. *Journal of High Energy Physics*, 2011(5):13, May 2011.

[64] Tomás Andrade and Simon F Ross. Boundary conditions for metric fluctuations in lifshitz. *Classical and Quantum Gravity*, 30(19):195017, 2013.

[65] Ioannis Papadimitriou. Hyperscaling violating lifshitz holography. *Nuclear and Particle Physics Proceedings*, 273-275:1487 – 1493, 2016. 37th International Conference on High Energy Physics (ICHEP).

[66] Vijay Balasubramanian and Per Kraus. A stress tensor for anti-de sitter gravity. *Communications in Mathematical Physics*, 208(2):413–428, Dec 1999.

[67] Wissam Chemissany, David Geissbhler, Jelle Hartong, and Blaise Rollier. Holographic renormalization for z = 2 lifshitz spacetimes from ads. *Classical and Quantum Gravity*, 29(23):235017, 2012.

[68] Ville Keränen and Larus Thorlacius. Thermal correlators in holographic models with lifshitz scaling. *Classical and Quantum Gravity*, 29(19):194009, 2012.

[69] Marika Taylor. Lifshitz holography. *Classical and Quantum Gravity*, 33(3):033001, 2016.

[70] S. Cremonini, Hai-Shan Liu, H. Lü, and C.N. Pope. Dc conductivities from non-relativistic scaling geometries with momentum dissipation. *Journal of High Energy Physics*, 2017(4):9, Apr 2017.

[71] Sera Cremonini, Mirjam Cvetič, and Ioannis Papadimitriou. Thermoelectric dc conductivities in hyperscaling violating lifshitz theories. *Journal of High Energy Physics*, 2018(4):99, Apr 2018.

[72] Mohsen Alishahiha, Eoin Ó Colgáin, and Hossein Yavartanoo. Charged black branes with hyperscaling violating factor. *Journal of High Energy Physics*, 2012(11):137, Nov 2012.

[73] Xiao-Mei Kuang and Jian-Pin Wu. Analytical shear viscosity in hyperscaling violating black brane. *Physics Letters B*, 773:422 – 427, 2017.

[74] Balt C. van Rees. Holographic renormalization for irrelevant operators and multi-trace counterterms. *Journal of High Energy Physics*, 2011(8):93, Aug 2011.

[75] Igal Arav, Yaron Oz, and Avia Raviv-Moshe. Lifshitz anomalies, ward identities and split dimensional regularization. *Journal of High Energy Physics*, 2017(3):88, Mar 2017.

[76] Jelle Hartong, Elias Kiritsis, and Niels A. Obers. Field theory on newton-cartan backgrounds and symmetries of the lifshitz vacuum. *Journal of High Energy Physics*, 2015(8):6, Aug 2015.

[77] Tomás Andrade and Benjamin Withers. A simple holographic model of momentum relaxation. *Journal of High Energy Physics*, 2014(5):101, May 2014.

[78] Julian Sonner. On universality of charge transport in ads/cft. *Journal of High Energy Physics*, 2013(7):145, Jul 2013.

[79] Tevian Dray and Gerard 't Hooft. The gravitational shock wave of a massless particle. *Nuclear Physics B*, 253:173 – 188, 1985.

[80] Konstadinos Sfetsos. On gravitational shock waves in curved spacetimes. *Nuclear Physics B*, 436(3):721 – 745, 1995.

[81] Alan P Reynolds and Simon F Ross. Butterflies with rotation and charge. *Classical and Quantum Gravity*, 33(21):215008, 2016.

[82] Stephen H. Shenker and Douglas Stanford. Black holes and the butterfly effect. *Journal of High Energy Physics*, 2014(3):67, Mar 2014.

[83] David Tong and Kenny Wong. Fluctuation and dissipation at a quantum critical point. *Phys. Rev. Lett.*, 110:061602, Feb 2013.

[84] M. Reza Mohammadi Mozaffar and Ali Mollabashi. Holographic quantum critical points in lifshitz space-time. *Journal of High Energy Physics*, 2013(4):81, Apr 2013.

[85] Richard A. Davison, Wenbo Fu, Antoine Georges, Yingfei Gu, Kristan Jensen, and Subir Sachdev. Thermoelectric transport in disordered metals without quasiparticles: The sachdev-ye-kitaev models and holography. *Phys. Rev. B*, 95:155131, Apr 2017.